AD-A164 105 UNSTEADY SOLUTION OF THE BOUNDARY LAYER EQUATIONS WITH APPLICATION TO SPA..(U) AIR FORCE INST OF TECH WRIGHT-PATTERSON AFB OH SCHOOL OF ENGI.. K J LANGE 1/2

UNCLASSIFIED JUN 85 AFIT/GAE/ENY/84D-11 F/G 20/13 NL

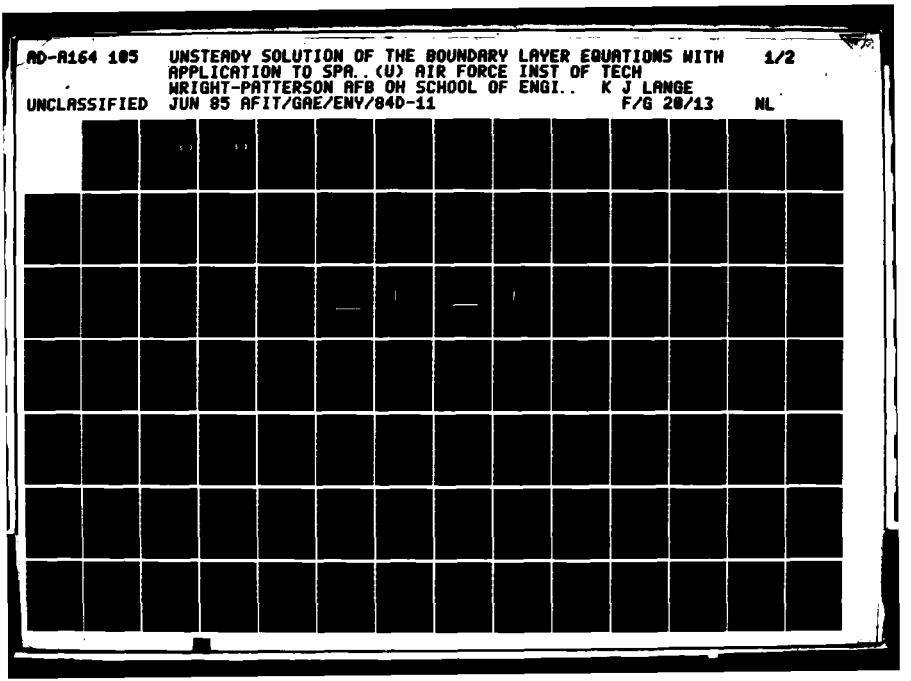

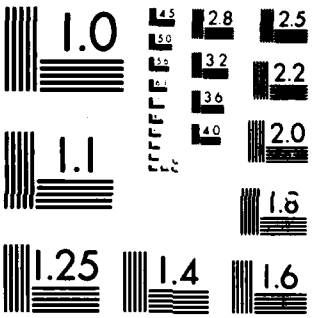

MICROCOPY RESOLUTION TEST CHART
NATIONAL BUREAU OF STANDARDS 1963 A

(1)

UNSTEADY SOLUTION OF THE BOUNDARY LAYER EQUATIONS WITH APPLICATION TO SPACE SHUTTLE TILES

THESIS

Karen J. Lange
Captain, USAF

DEPARTMENT OF THE AIR FORCE
AIR UNIVERSITY
AIR FORCE INSTITUTE OF TECHNOLOGY

Wright-Patterson Air Force Base, Ohio

(1)

AFIT/GAE/ENY/84D-11

UNSTEADY SOLUTION OF THE BOUNDARY LAYER EQUATIONS WITH APPLICATION TO SPACE SHUTTLE TILES

THESIS

Karen J. Lange
Captain, USAF

AFIT/GAE/ENY/84D-11

AFIT/GAE/ENY/84D-11

UNSTEADY SOLUTION OF THE BOUNDARY LAYER EQUATIONS WITH APPLICATION TO SPACE SHUTTLE TILES

THESIS

Presented to the Faculty of the School of Engineering

of the Air Force Institute of Technology

Air University

In Partial Fulfillment of the

Requirements for the Degree of

Master of Science in Aeronautical Engineering

Karen J. Lange, B.S.
Captain, USAF

June 1985

Approved for public release; distribution unlimited

ACKNOWLEDGMENTS

I would like to recognize the contributions of the following individuals, whose guidance and support helped me complete this project.

First, I want to thank Maj. James K. Hodge for his long hours of assistance and understanding during the many weeks that I was struggling to get positive results from my computer program.

Secondly, I wish to express my appreciation to Dr. James Hitchcock, who motivated me to pursue heat transfer by the quality of his guidance and his wisdom in the classroom. His classes were very interesting and I enjoyed them immensely.

Last, but not least, I want to thank my husband, Joel and my dog, Beau, for their many long months of devotion and understanding without which I could not have finished this project.

Contents

List of Figures

List of Tables

List of Symbols

a	Speed of sound
Cp	Specific heat capacity at constant pressure
H	Total enthalpy
h	Heat transfer coefficient
h_{iso}	Heat transfer coefficient for an isothermal wall
h_{ref}	Reference heat transfer coefficient
h_x	Local heat transfer coefficient
$h_{.9}$	Heat transfer coefficient with .9 recovery factor
I	Number of spatial node points in X direction
i	Node point in X direction
J	Number of spatial node points in y direction
j	Node point in y direction
k	Conductivity
L	Plate length
M	Mach number
M_∞	Freestream Mach number
Nu_x	Local Nusselt number
P	Pressure
P_o	Stagnation pressure
Pr	Prandtl number
q	Heat rate
q_o	Heat rate at the wall
R	Gas constant
r	Recovery factor
RC	Time constant

Re	Reynolds number
Re_x	Local Reynolds number
T	Temperature
T_{aw}	Adiabatic Wall temperature
T_e	Boundary layer edge temperature
T_w	Wall temperature
T_o	Stagnation temperature
T_∞	Freestream temperature
T*	Reference temperature
t	Time
U	Dorodnitsyn's transformation of streamwise flow velocity
u	Streamwise flow velocity
V	Dorodnitsyn's transformation of normal flow velocity
v	Normal flow velocity
X	Dorodnitsyn's transformation of streamwise spatial coordinate
x	Streamwise spatial coordinate
Y	Dorodnitsyn's transformation of normal spatial coordinate
y	Normal spatial coordinate
α	Deflection angle of experimental plate
β	Wave angle
δ	Boundary layer thickness
γ	Specific heat ratio
θ	Wedge angle
η	Transformed Y in the computational plane
μ	Viscosity
μ_e	Boundary layer edge viscosity

μ_∞ Freestream Viscosity

ρ Density

ρ_e Boundary layer edge density

ρ_∞ Freestream density

ξ Transformed X in the computational plane

ζ Streamwise location of wall temperature step

Superscripts

n Time level

s Iteration level

* Reference temperature conditions

' Dimensional Quantity

Subscripts

e Boundary layer edge condition

i,j Spatial node point

∞ Freestream condition

Abstract

Wind tunnel tests were conducted on Space Shuttle Orbiter insulating articles. The data was processed by a heat estimation program, revealing a large discrepancy in magnitude of the heat transfer coefficient over the Space Shuttle tile when compared to that yielded by flat plate theory and thin skin test results. An initial suggestion for the cause of this discrepancy was the nonisothermal wall effect. Understanding this effect was the main objective of this project.

In order to investigate these effects, an unsteady compressible boundary layer code, THESIS, was developed. First the boundary layer equations were transformed using the Dorodnitsyn transformation to allow the equations to be solved similar to incompressible equations. Then, the equations were then transformed to the computational plane and approximated by finite differences. Optimized successive over-relaxation is then used to solve the difference equations. The grid used for this program is optimized based on the Blasius solution, but the program is not limited to this because it has a generalized grid.

Upon running this program, leading edge startup problems arose. Therefore, a similarity solution is assumed at the leading edge which corrected the problem.

The program was verified with an incompressible case which was in good agreement with the Blasius solution, and a compressible case with an isothermal wall which agreed well with approximate theory. The isothermal case showed the solution was dependent on the grid. The steady state and transient nonisothermal wall cases displayed the same trend as the approximate nonisothermal solution. All cases had the same

dramatic decrease in the heat transfer coefficient and the subsequent recovery in the streamwise direction. The most significant results came from pitching the plate with a nonisothermal wall. A large lag due to the nonisothermal wall effects exists. These results indicate that the nonisothermal wall effects may be affecting the wind tunnel results.

UNSTEADY SOLUTION OF THE BOUNDARY LAYER EQUATIONS WITH APPLICATION TO SPACE SHUTTLE TILES

I. INTRODUCTION

The Space Shuttle has completed numerous missions in a relatively short time and has become an important tool in the study and understanding of space. The unique feature of the shuttle is its reuseability. The Thermal Protection System (TPS) protects the shuttle from extreme temperatures upon reentry into the atmosphere and enables it to be reused. Understanding how the TPS responds to the temperature flucuations is important for future applications such as designing new hypersonic vehicles. Studies can be accomplished through many means such as actual flights, wind tunnels, and computers.

Background

Flight test maneuvers were simulated in a twenty inch hypersonic wind tunnel to verify a technique used to estimate heating rate and thermal parameters from Space Shuttle thermocouple data. The tests were conducted by the Air Force Wright Aeronautical Laboratory at Wright-Patterson AFB, Ohio. Three types of materials, a thin skin stainless steel plate, and two TPS panels, a high-temperature reuseable surface insulation (HRSI), and a flexible reuseable surface insulation (FRSI), were flush mounted on a test plate with a wedge-shape leading edge as shown in Figure 1. The wedge was 1.25 feet by 7 inches wide, and a 6

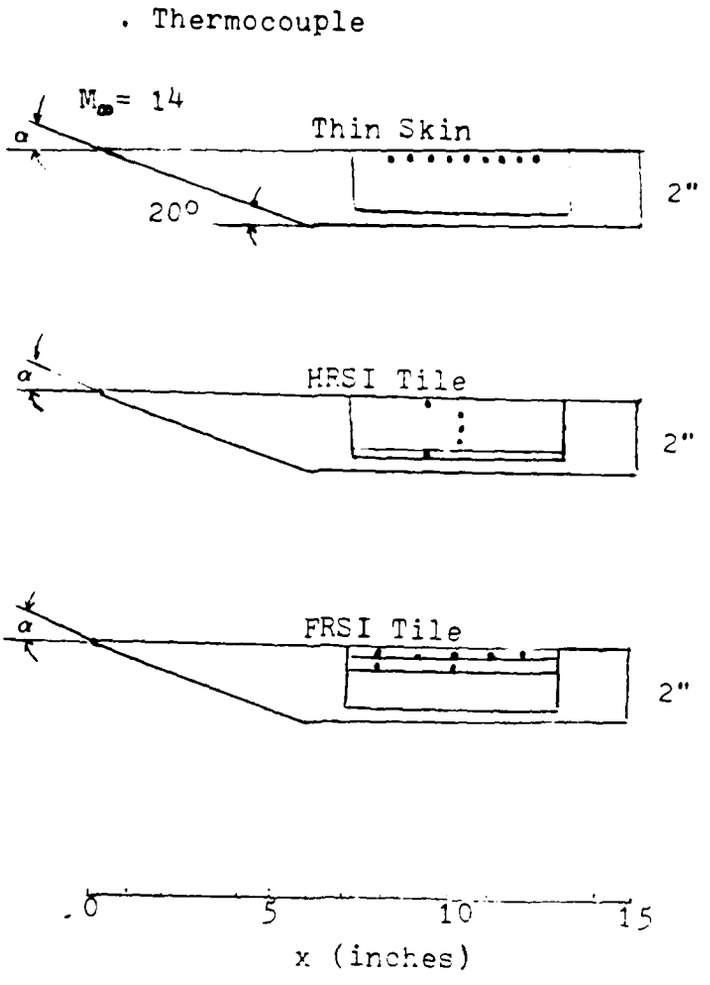

Figure 1 Thin Skin, HRSI, or FRSI, Panels in Wedge Test Article

inch by six inch panel interfaced with the stainless steel surface at a streamwise distance of 7 inches from the leading edge or at x/L = .467. Different thermocouple instrumentation was installed in each panel. The deflection angle (α) was held at a constant angle or varied temporally between 3 degrees and 14 degrees during a wind tunnel run. The wedge was pitched at a constant pitch rate of 2 degrees/second to selected deflection angles and held for a prescribed time.

The conditions in the test section were known from the test section Mach number of 14.237, the stagnation temperature of 2020 degrees R, and the stagnation pressure of 1600 pounds per square inch. The air was assumed to be a perfect gas with a specific heat ratio (γ) of 1.4.

Fifty nine tests were run. The first 26 were with a HRSI test article, 27-45 were with a FRSI test article, and the last 14 test runs were with the thin skin article which simulated an isothermal wall. The thin skin results indicate a good agreement with the isothermal wall predictions but the HRSI and FRSI panels differed markedly from Eckert flat plate theory. The main difference between the TPS panels and the thin skin stainless steel panel was the thermal properties. The TPS panels had a much lower conductivity so the surface temperature increased much more rapidly than the stainless steel. Therefore, the tile was much hotter than the stainless steel wedge, causing a temperature discontinuity. This nonisothermal wall was indicated by the results as the cause of an additional thermocouple lag during the pitching maneuvers. (7:5-7) It also causes a large decrease or increase in laminar heating depending on the direction of the temperature jump.

The results of the wind tunnel tests show that nonisothermal effects should not be neglected for vehicles with laminar flow that have numerous interfaces of different low heat capacity materials. Understanding the effects will be important to understanding the thermocouple data from the Space Shuttle and in future hypersonic vehicle design.

Objectives and Approach

The nonisothermal wall is caused by the transient response of the wall temperature which is caused by the limited duration test and by the motion of the plate. Understanding these nonisothermal wall effects and the heating rate is important to understanding how the TPS responds. One method used to accomplish this is wind tunnel tests. Another method is a two-dimensional computer program using the transient compressible boundary layer equations. Ideally, the computer program would include the solution of the flow through a shock wave and the determination of the heat rate with both convection and conduction included. Ultimately, it would be able to match a full wind tunnel profile so the numerical results could be compared to the wind tunnel results.

A two-dimensional computer program with the transient heat transfer boundary layer equations is written using an implicit finite difference technique. A pitching flat plate will model the wind tunnel wedge. Using the same free stream conditions as the wind tunnel, shock theory is used to determine the flow field behind the shock wave. The first checkout of the computer program is an incompressible steady state flat plate with an isothermal wall. The results should match the Blasius profile. To further verify the program, an isothermal wall is run to

steady state using the same conditions as the thin skin stainless steel panel in the wind tunnel tests. This is completed at deflection angles of 3 degrees, 10 degrees, and 14 degrees. The heat transfer coefficient ratio (h/h_{ref}) should compare well with Eckert's flat plate theory. To investigate the nonisothermal wall case, temperature increases of 170 degrees R for the FRSI panel and 270 degrees R for the HRSI panel are placed at x/L = .467 with a deflection angle (α) of 14 degrees. The results should indicate a large initial decrease in the heat transfer coefficient ratio. Moving down the plate, the ratio should increase and level off. To further study the nonisothermal effects, transient cases are run.

There are two types of transient cases. The first case is at a constant deflection angle of 14 degrees with the wall temperature changing with time by

$$Tw^n = (1 - e^{-t/RC})\Delta Tw + Tw^{n-1} \qquad (1)$$

where Tw^n and Tw^{n-1} are the wall temperature at the present and previous time, respectively, ΔTw is the temperature step, RC is the time constant, and t is the time. The results should converge on the same solution as the steady state nonisothermal wall case explained above. The second transient case pitches the plate from 14 degrees to 3 degrees and back to 14 degrees with both isothermal and nonisothermal walls. These cases will show the capability of the program and will enhance the knowledge of nonisothermal wall effects.

II. Theory

Governing Equations

The unsteady compressible boundary layer equations were solved numerically for both an isothermal and a nonisothermal wall.

The Navier-Stokes equations for laminar flow are simplified by assuming that gradients in the streamwise direction are small in comparison with normal gradients. The normal velocity component is also small. Terms of order δ/L compared to unity have been ignored. The resulting boundary layer equations (8:17-38) in conservative form are:

continuity
$$\frac{\partial \rho'}{\partial t'} + \frac{\partial \rho' u'}{\partial x'} + \frac{\partial \rho' v'}{\partial y'} = \emptyset \tag{2}$$

x-momentum
$$\frac{\partial \rho' u'}{\partial t'} + \frac{\partial \rho' u^{2'}}{\partial x'} + \frac{\partial \rho' v' u'}{\partial y'} = -\frac{\partial P'}{\partial x'} + \frac{\partial}{\partial y'}\left(\mu' \frac{\partial u'}{\partial y'}\right) \tag{3}$$

y-momentum
$$\frac{\partial P'}{\partial y'} = \emptyset \tag{4}$$

energy
$$\frac{\partial \rho' H'}{\partial t'} + \frac{\partial \rho' u' H}{\partial x'} + \frac{\partial \rho' v' H'}{\partial y'} = \frac{\partial P'}{\partial t'} - \frac{\partial q'}{\partial y'} + \frac{\partial}{\partial y'}\left(u' \mu' \frac{\partial u'}{\partial y'}\right) \tag{5}$$

and are subject to boundary conditions at the edge of the boundary layer and at the wall. The equations are nondimensionalized using these factors

$$x = \frac{x'}{L'} \quad y = \frac{y'}{L'} \quad t = \frac{t'}{L'/u'_\infty} \quad u = \frac{u'}{U'_\infty} \quad v = \frac{v'}{U'_\infty}$$
$$\mu = \frac{\mu'}{\mu'_\infty} \quad \rho = \frac{\rho'}{\rho'_\infty} \quad H = \frac{H'}{U'^2_\infty} \quad T = \frac{C_p' T'}{U'^2_\infty} \quad P = \frac{P'}{\rho'_\infty U'^2_\infty} \tag{6}$$

and become

$$\text{continuity} \quad \frac{\partial \rho}{\partial t} + \frac{\partial \rho u}{\partial x} + \frac{\partial \rho v}{\partial y} = 0 \tag{7}$$

$$\text{x-momentum} \quad \frac{\partial \rho u}{\partial t} + \frac{\partial \rho u^2}{\partial x} + \frac{\partial \rho uv}{\partial y} = -\frac{\partial P}{\partial x} + \frac{\partial}{\partial y}\left(\frac{\mu}{Re}\frac{\partial u}{\partial y}\right) \tag{8}$$

$$\text{y-momentum} \quad \frac{\partial P}{\partial y} = 0 \tag{9}$$

$$\text{energy} \quad \frac{\partial \rho H}{\partial t} + \frac{\partial \rho uH}{\partial x} + \frac{\partial \rho vH}{\partial y} = \frac{\partial P}{\partial t} + \frac{\partial}{\partial y}\left(\frac{\mu}{RePr}\frac{\partial H}{\partial y}\right) + \frac{\partial}{\partial y}\left(\frac{\mu\,(1-\frac{1}{Pr})}{Re}\frac{\partial U^2/2}{\partial y}\right) \tag{10}$$

In order to solve the unsteady compressible boundary layer equations in a form similar to the incompressible boundary layer equations, the Dorodnitsyn transformation (9:2-4) is used. This transformation is

$$X = x \qquad Y = \int_0^y \rho \, dy \qquad t = t \qquad H = H$$

$$U = u \qquad V = \rho v + \frac{\partial Y}{\partial t} + u\frac{\partial Y}{\partial x} \tag{11}$$

where Y is scaled with the density. The nondimensional governing equations become

$$\text{continuity} \quad \frac{\partial U}{\partial X} + \frac{\partial V}{\partial Y} = 0 \tag{12}$$

$$\text{x-momentum} \quad \frac{\partial U}{\partial t} + U\frac{\partial U}{\partial X} + V\frac{\partial U}{\partial Y} = -\frac{1}{\rho}\frac{\partial P}{\partial X} + \frac{\partial}{\partial Y}\left(\frac{\mu\rho}{Re}\frac{\partial U}{\partial Y}\right) \tag{13}$$

$$\text{y-momentum} \quad \frac{\partial \rho}{\partial Y} = 0 \tag{14}$$

$$\text{energy} \quad \frac{\partial H}{\partial t} + \frac{U\partial H}{\partial X} + \frac{V\partial H}{\partial Y} = \frac{1}{\rho}\frac{\partial P}{\partial t} + \frac{\partial}{\partial Y}\left(\frac{\mu\rho}{RePr}\frac{\partial H}{\partial Y}\right) + \frac{\partial}{\partial Y}\left(\frac{\mu\rho\left(1-\frac{1}{Pr}\right)}{Re}\frac{\partial U^2/2}{\partial Y}\right) \quad (15)$$

The equations look like the incompressible equations with the density imbedded in the viscous terms and the pressure term. For detailed information on transforming the boundary layer equations, see Appendix A.

The density (ρ') is calculated from the perfect gas equation of state

$$P' = \rho' R' T' \quad (18)$$

where R is the gas constant and P' and T' are the pressure and temperature respectively. Since the boundary layer is assumed to be thin, the pressure at the edge of the boundary layer is transmitted without change to the surface. Therefore, the pressure is known everywhere in the boundary layer. Also, the temperature is known from the solution of the energy equation. The only unknown is density which is then solved by

$$\rho' = \frac{P'}{RT'} \quad (19)$$

which nondimensionally is

$$\rho = \frac{\gamma}{\gamma-1}\frac{P}{T} \quad (20)$$

Low Temperature Viscosity

The standard relationship used to calculate viscosity (μ) is that given by Sutherland's Law

$$\mu' = \frac{2.27 \times 10^{-8}\ T^{3/2}}{T' + 198.6}\ \frac{\text{lb sec}}{\text{ft}^2} \qquad (21)$$

According to Fiore (5), this may not be valid for hypersonic wind tunnel applications. In hypersonic tunnels, the freestream temperature generally falls in a range between T_∞ = 30 degrees R and T_∞ = 200 degrees R which is outside the demonstrated range of applicability of Sutherland's law. An alternate method to calculate viscosity is

$$\mu' = \frac{2.32 \times 10^{-8}\ T^{1/2}}{1 + \frac{220}{T' \times 10^{9/T'}}}\ \frac{\text{lb sec}}{\text{ft}^2} \qquad (22)$$

This equation provides good correlation to experimental data at low temperatures and corresponds well with viscosity calculations by Sutherland's Law at temperatures above T_∞ = 300 degrees R (2:13-18).

Heat Transfer Coefficient

Heat transfer over a flat plate can be calculated by Eckert theory, assuming that the flow medium is an ideal, single component gas with no dissociation and has constant properties, independent of temperature and pressure. Also, the surface temperature is assumed constant. Using these assumptions, the Nusselt Number for laminar flow over a flat plate (8:134-139) is

$$Nu_x = 0.332\ Pr^{1/3}\ Re_x^{1/2} \qquad (23)$$

Pr is the Prandtl Number and is defined as

$$Pr = \frac{cp'\,\mu'}{k'}$$

where c_p is the specific heat at constant pressure of the fluid, k is the conductivity, and μ is the fluid viscosity. Re_x is the local Reynold's Number defined by

$$Re_x = \frac{\rho'_e \, u'_e \, x'}{\mu'_e} \tag{24}$$

where the subscript e denotes boundary layer edge conditions. Using this definition of Nusselt number,

$$Nu_x = \frac{h_x \, x'}{k} \tag{25}$$

the heat transfer coefficient for an isothermal wall on a flat wedge (h_{iso}) for laminar flow is given by

$$h_{iso} = .332 \, cp' \sqrt{\frac{\mu'_e \, \rho'_e \, u'_e}{x'}} \Big/ Pr^{2/3} \tag{26}$$

This h_{iso} is independent of wall temperature, but the properties are not constant. The viscosity and density vary with temperature across a boundary layer. Therefore, Eckert's reference temperature (4:10-13)

$$T^* = T'_e + .5(T'_w - T'_e) + .22(T'_{aw} - T'_e) \tag{27}$$

is used as an approximation and

$$h_{iso} = .332 \, cp^{*'} \sqrt{\frac{\mu^* \, \rho^* \, u'_e}{x'}} \Big/ Pr^{2/3} \tag{28}$$

where the * indicates the condition at the reference temperature.

The heat transfer coefficient can be calculated numerically at the wall by

$$h_{.9} = q'_o/(.9T'_{o\infty} - T'_w) \tag{29}$$

where q_o is the heat rate and is equal to

$$q'_o = -k' \frac{\partial T'}{\partial y'}\Big)_{y=0} \tag{30}$$

The temperature gradient at the wall is determined from the solution to the boundary layer equations. The adiabatic wall recovery factor is always assumed to be .9 even though it usually is defined as $\sqrt{Pr}$. Using $\sqrt{Pr}$ as the recovery factor will only change the magnitude of the heat transfer coefficient by the factor $\frac{.9T'_o - T'_w}{\sqrt{Pr}T'_o - T'_w}$ which will usually be small for high speed flow.

A ratio of the heat transfer coefficient, $h_{.9}$ to a reference heat transfer coefficient at zero deflection angle, h_{ref}, is determined where the reference heat transfer coefficient is

$$h_{ref} = .332\, cp' \sqrt{\frac{\mu_\infty' \rho_\infty' u_\infty'}{x'}} \Big/ Pr^{2/3} \tag{31}$$

The conditions in front of the shock wave are considered the freestream conditions and are constant at any deflection angle. Thus, $h_{.9}$ is nondimensionalized by a constant which is scaled by $\sqrt{x}$.

For a nonisothermal wall on a flat wedge with a wall temperature jump from T_1' to T_2' at ζ, the heat transfer coefficient for laminar flow is given by (8:134-139)

$$h_{.9} = h_{iso}\left[(T'_{aw}-T'_1) + (1-\frac{\zeta}{x^r})^{3/4})^{-1/3}\ (T'_1-T'_2)\right] /(.9T'_{aw}-T'_w) \quad (32)$$

Oblique Shock Theory

The edge conditions of the boundary layer change as the plate is pitched from 3 degrees to 14 degrees. It is necessary to know these edge conditions; hence, they are calculated using oblique shock wave theory assuming adiabatic flow of a perfect gas (11:84-88). The first task is to calculate the Mach number after the shock, M_2. In order to do this, the shock wave angle, β, is calculated by iteration using

$$\tan\theta = 2\cot\beta\left[\frac{M_1^2\sin^2\beta - 1}{M_1^2(\gamma+\cos 2\beta)+2}\right] \quad (33)$$

where M_1 is the freestream Mach number, γ is the specific heat ratio, and θ is the wedge angle. Once β is known, the Mach number is calculated using

$$M_2 = \left\{\frac{\left[1+\frac{\gamma-1}{2}M_1^2\sin^2\beta\right]}{\left[\gamma M_1^2\sin^2\beta - \frac{\gamma-1}{2}\right]}\right\}^{1/2} \quad (34)$$

Using this Mach number, the temperature and pressure behind the shock wave are determined by the following equations

$$\frac{T'_o}{T'_2} = 1 + \frac{\gamma-1}{2}M_2 \quad (35)$$

$$P'_2 = P'_1 \left[1 + \frac{2\gamma}{\gamma-1} (M_1^2 \sin^2 \beta - 1) \right] \tag{36}$$

where T'_o is the stagnation temperature.

The velocity is also known because the Mach number and the speed of sound, a', is known as

$$a' = \sqrt{\gamma RT'} \tag{37}$$

where R is the gas constant for air.

III. Finite Difference Solution

A two dimensional computer program is developed using the transient compressible boundary layer equations. The equations are transformed first with a Dorodnitsyn transformation and then transformed into a computational plane. The convective terms are differenced using second order upwind differencing and the viscous terms are second order central differenced. The time terms use a first order backward difference. The differencing is done implicitly and successive over-relaxation is used to solve the momentum and energy equations. The continuity equation is solved by integration using the trapezoidal rule. In the program, a flat plate simulates the wind tunnel wedge.

Grid

The grid generation is an important aspect of setting up any finite difference solution. In this case, the computational domain is 1.25 feet in the x'-direction and approximately 10 times the boundary layer thickness (δ) in the y'-direction. Both x' and y' are nondimensionalized by the length of the plate, L, so x goes from 0 to 1 and y goes from 0 to approximately $\frac{10\delta}{L}$. The computational domain has 1830 grid points or 61 points in the streamwise direction and 30 points in the normal direction. These numbers can be varied to specify a finer or coarser grid.

An optimized grid based on a Blasius solution at a Reynold's number of $2X10^6$ is used as the basis of this program's grid. It was optimized to minimize truncation error in velocity gradients. To optimize a grid based on a Blasius solution, the velocity profile is determined and plotted for a specific location. Since similarity of velocity profiles

exist in an incompressible boundary layer, any location can be chosen, in this case, x equal to 1.Ø. A constant Δu of .1 was chosen. At each increment of .1, the y value was determined as illustrated in Figure 2. Outside the boundary layer another method which minimizes the change in step size is used to choose y because no Δu exists. The y values used in the program are given in Table I. When transformed to the computational grid, the plot of η versus u would be a diagonal line as shown in Figure 3. Therefore, the truncation terms, $u_{\eta\eta}$, $u_{\eta\eta\eta}$, u_{η}, $H_{\eta\eta}$ and $H_{\eta\eta\eta}$ would all equal Ø in the boundary layer for Pr=1.

This optimized Blasius grid is modified for a Reynold's number of $9x10^{5}$ which matches the wind tunnel condition. It is then scaled by the $\sqrt{x}$ and divided by the Prandtl number to allow for the thickness of the thermal layer. In the streamwise direction, the node points are equally spaced. Every X location is specified in the domain and, therefore, the X value does not change in the Y direction. These X, Y pair combinations specify an initial grid in the Dorodnitsyn plane which is fixed. Since this grid is based on an incompressible solution, it must be scaled to account for the change in the boundary layer due to compressibility by a factor. A factor of 1.Ø was used for the grid transformation in this project. This is now the fixed grid. Since density changes with both temperature and time the grid in the physical plane also changes due to the Dorodnitsyn transformation equation from the fixed grid to the physical grid.

$$y = \int_{o}^{Y} \frac{1}{\rho}\, dY \qquad (38)$$

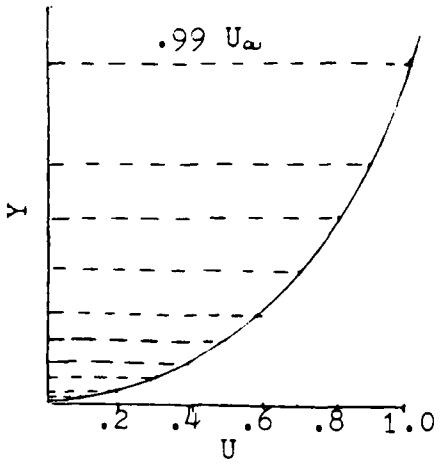

Figure 2 Illustration of Y Value Determination for the Optimized Blasius Grid

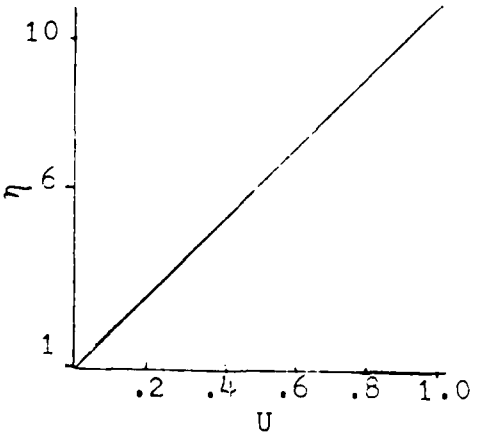

Figure 3 η versus Velocity in the Transformed Plane

Table I

Y Values of the Optimized Blasius Grid

η	Y
1	0.0000
2	.000248
3	.0005
4	.000756
5	.001024
6	.001316
7	.00166
8	.002
9	.002671
10	.003402
11	.004342
12	.005548
13	.007099
14	.009092
15	.01165
16	.014945
17	.019174
18	.024609
19	.031593
20	.040568
21	.0521
22	.06692
23	.085963
24	.11043
25	.14187
26	.18226
27	.23414
28	.30076
29	.3862
30	.496

Comparing Fig 4 and Fig 4b, the fixed grid, and Fig 5 and Fig 5b, the physical grid at steady state, the density effect can be seen.

Using the fixed grid, a transformation can be made to a rectangular computational grid. This grid is in the ξ-η plane where η is in the streamwise direction and η is perpendicular to ξ. The metrics ξ_X, ξ_Y, η_X, and η_Y appear in the differential equations and can be solved from the expressions

$$\begin{aligned} \xi_X &= Y_\eta/J \\ \xi_Y &= -X_\eta/J \\ \eta_X &= -Y_\xi/J \\ \eta_Y &= X_\xi/J \\ J &= X_\xi Y_\eta - Y_\xi X_\eta \end{aligned} \tag{39}$$

Since X is not changing in the η direction, X_η is Ø. This eliminates all ξ_Y terms in the differential equations and the other metrics become

$$\begin{aligned} \xi_X &= 1/X_\xi \\ \eta_Y &= 1/Y_\eta \\ \eta_X &= -\frac{Y_\xi}{X_\xi Y_\eta} \end{aligned} \tag{40}$$

The terms X_ξ and Y_η are determined using finite differences. The Y_ξ is determined analytically which is discussed in the section on metrics.

A unique feature of this program is that the grid used can be easily replaced by another grid. The derivatives are calculated in the program so the only replacement is the generation of the fixed grid. This is based on the assumption that X does not change as you move in

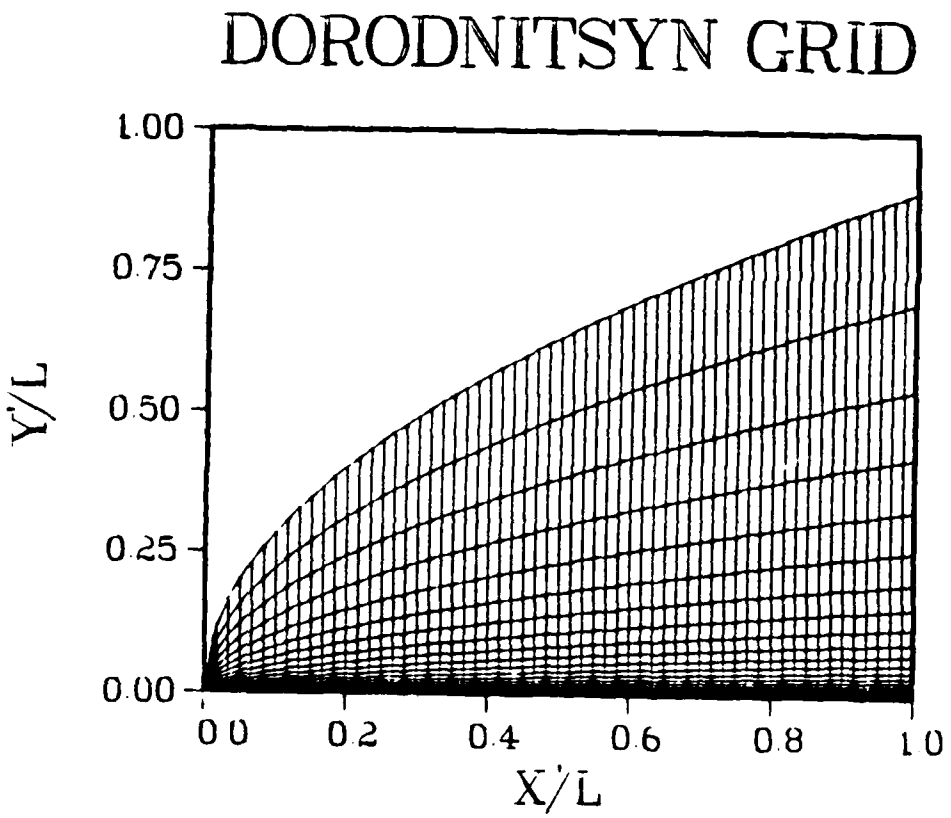

Figure 4a Fixed Grid

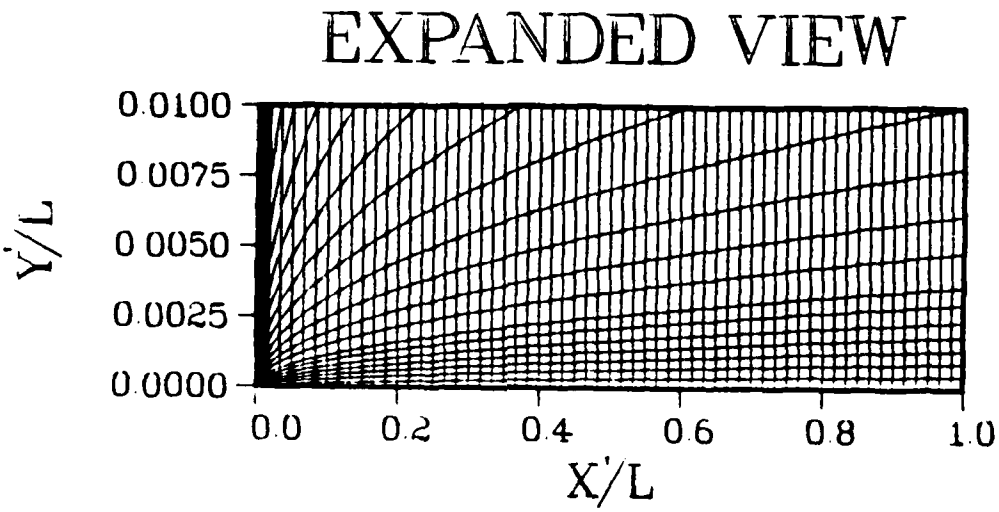

Figure 4b Expanded View of Fixed Grid

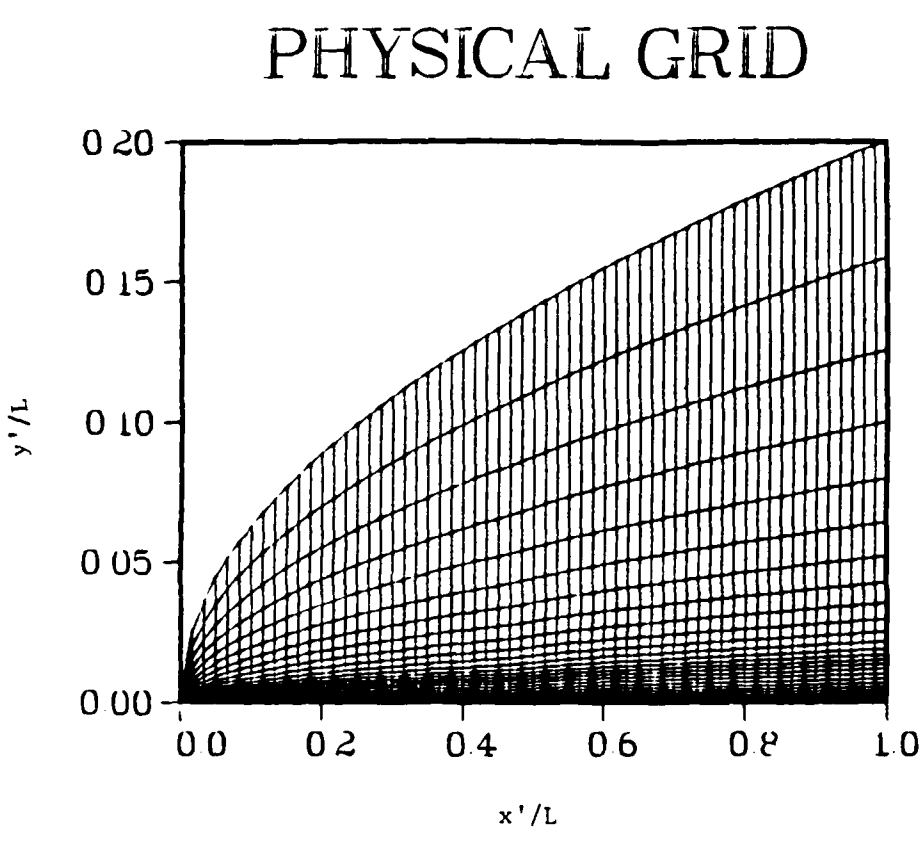

Figure 5a Physical Grid at steady state

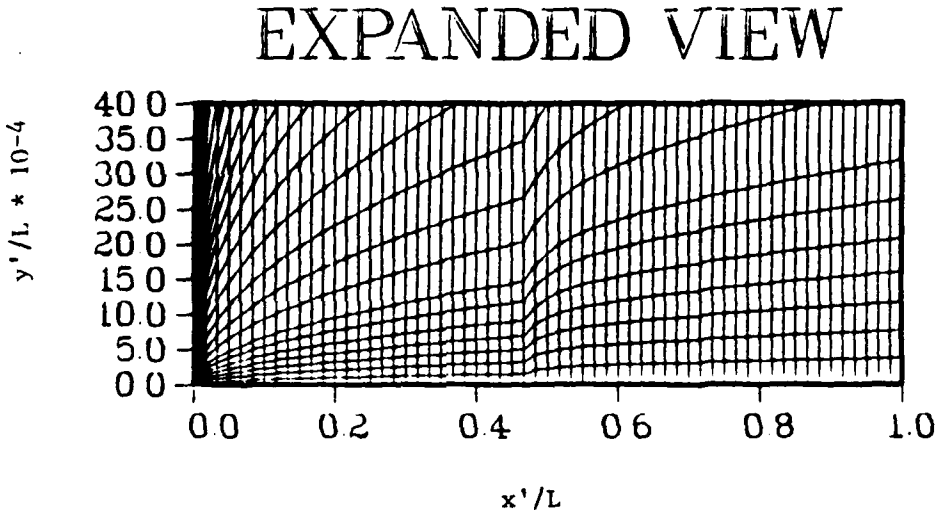

Figure 5b Expanded View of the Physical Grid at steady state

the Y direction. If X does change in the Y direction, then X_η is not zero, and additional terms would have to be added to the differential equations. If X_η is not zero, a variation from the normal boundary layer assumptions would have to be implemented.

Numerical Method

The nondimensional transient two-dimensional boundary layer equations are solved numerically by using an implicit finite difference scheme because it is unconditionally stable according to linear theory. First the Dorodnitsyn transformation transforms the governing equations, Eqs 12 through 15, and then they are transformed from the X - Y plane to the ξ - η computational plane. The equations become

Continuity
$$\xi_X U_\xi + \eta_X U_\eta + \eta_Y V_\eta = 0 \tag{41}$$

X-Momentum
$$U_t + U(U_\xi \xi_X + U_\eta \eta_X) + VU_\eta \eta_Y = \frac{1}{Re}\left[\mu\rho(U_\eta \eta_Y)\right]_\eta \eta_Y \tag{42}$$

Energy
$$H_t + U(H_\xi \xi_X + H_\eta \eta_X) + VH_\eta \eta_Y = \frac{1}{\rho} P_t + \left[\frac{\mu\rho}{RePr} H_\eta \eta_Y\right]_\eta \eta_Y + \left[\frac{\mu\rho(1-\frac{1}{Pr})}{2Re} \eta_Y \left(U^2/2\right)_\eta\right]_\eta \eta_Y \tag{43}$$

The momentum and energy equations are solved for U and H respectively using SOR and then the continuity equation is solved to give V.

Momentum and Energy Equations. The momentum and energy equations must first be finite differenced and some assumptions must be made. On a stationary plate, the pressure gradients are zero since inviscid oblique shock theory is assumed. In the momentum equation, Eq 42, the dP/dX term has been assumed to be zero for all cases. For a pitching

plate, the transients in the hypersonic flow or supersonic edge flow have a much shorter time constant than the thermal response of the TPS surface and can be neglected (7:5). For example, the HRSI tile has a time constant of three seconds and the transient time constant is .00026 sec. Also, no curvature is being assumed. The equations would need to be rederived to account for curvature.

Once the equations are transformed to the $\xi - \eta$ plane, the first order derivatives in the momentum and energy equations, Eqs 42 and 43, are differenced using three point upwind differencing. This differencing scheme guarantees diagonal dominance and is second order accurate in the computational plane. The time derivative is differenced using two point backward which implies the scheme is only first order accurate in time. The second derivatives, such as the viscous terms $U_{\eta\eta}$, $H_{\eta\eta}$, and $T_{\eta\eta}$, are approximated with second order accurate central differencing. The like terms are then combined. The equations are written for U_{ij}^{n} and H_{ij}^{n} and become

$$\text{Momentum} \quad U_{ij}^{n} = \Big\{ U_{ij}^{n-1} + 2\xi_X U\Delta t U_{i-1j}^{n} - .5\,\xi_X U\Delta t U_{i-2j}^{n} +$$

$$\left[2\eta_X U\Delta t + 2\eta_Y V\Delta t + \frac{\eta_Y \Delta t}{Re}\left((\rho\mu)_{j+1/2}\,\eta_Y\right) \right] U_{ij-1}^{n} - \tag{44}$$

$$[.5\eta_X U\Delta t + .5\eta_Y V\Delta t]\, U_{ij-2}^{n} + \frac{\eta_Y \Delta t}{Re}\left((\rho\mu)_{j+1/2}\,\eta_Y\right) U_{ij+1}^{n} \Big\} / UCOEF$$

$$UCOEF = 1 + \frac{3\xi_X\, U\Delta t}{2} + \frac{3\eta_X U\Delta t}{2} + \frac{3\eta_Y V\Delta t}{2} + \frac{\eta_Y \Delta t(\rho\mu_{j+1/2}\eta_Y + \rho\mu_{j-1/2}\,\eta_Y)}{Re}$$

$$\text{Energy} \qquad H_{ij}^{n} = \Big\{ H_{ij}^{n-1} + 2\xi_X U\Delta t\, H_{i-1j}^{n} - .5\xi_X U\Delta t\, H_{i-2j}^{n} +$$

$$[2\eta_X U\Delta t + 2\eta_Y V\Delta t + \frac{\eta_Y \Delta t}{RePr}((\rho\mu)_{j-1/2}\eta_Y)]\, H_{ij-1}^{n} -$$

$$[.5\eta_X U\Delta t + .5\eta_Y V\Delta t]\, H_{ij-2}^{n} + \frac{\eta_V \Delta t}{RePr}((\rho\mu)_{j+1/2}\eta_Y)\, H_{ij+1}^{n} +$$

$$\frac{1}{\rho}\, dP + \frac{(1-\frac{1}{Pr})\eta_Y\, \Delta t}{2\, Re}\Big[(\rho\mu)_{j+1/2}^{2n}\eta_Y U_{ij+1} - ((\rho\mu)_{j+1/2}^{2n}\eta_Y + (\rho\mu)_{j-1/2}^{2n}\eta_Y)U_{ij} +$$

$$(\rho\mu)_{j-1/2}^{2n}\eta_Y U_{ij-1}\Big]\Big\} \,/UCOEF \qquad (45)$$

$$UCOEF = 1 + \frac{3\xi_X U\Delta t}{2} + \frac{3\eta_X U\Delta t}{2} + \frac{3\eta_Y V\Delta t}{2} + \frac{\eta_Y \Delta t(\rho\mu_{j+1/2}\eta_Y + \rho\mu_{j-1/2}\eta_Y)}{RePr} \qquad (46)$$

Where i and j define the location in the ξ-η plane and n is the time level. The notation for $\rho\mu_{j+1/2}$ and $\rho\mu_{j-1/2}$ defines an average value of density time viscosity where

$$\rho\mu_{j+1/2} = (\rho\mu_{j+1} + \rho\mu_j)/2 \qquad (47)$$
$$\rho\mu_{j-1/2} = (\rho\mu_j + \rho\mu_{j-1})/2$$

The momentum equation is a nonlinear equation and the energy equation depends on the velocity calculated by the momentum equation. To linearize the equations for the first iteration, the coefficients could be lagged "in time" or "in space." The coefficients in this program are based on the solution for U, V, and H at the previous time and same location for the first iteration, and subsequently on values

from the previous iteration. Also, the temperature value in the energy equation is lagged in time for the first iteration due to its dependence on H and U.

Metrics. Imbedded in the coefficients are the metrics ξ_X, η_X, and η_Y. These quantities can be calculated using Eq 40. A first order central difference is used to determine X_ξ. Since the points in the streamwise direction are equally spaced, X_ξ is a constant which is equal to the delta x. The inverse of X_ξ is ξ_X and is therefore also a constant. Two differencing schemes are used to find Y_η, the inverse of η_Y, depending on the η_Y location in the equation. For η_Y inside the viscous terms, such as $\left[\frac{\mu\rho}{Re}\eta_Y U_\eta\right]_\eta$ and $\left[\frac{\mu\rho}{Re}\eta_Y H_\eta\right]_\eta$, the Y_η is differenced the same direction as the $\rho\mu$ term. For instance, the Y_η term is a first order forward difference for $\rho\mu_{j+1/2}$ and a first order backward difference for $\rho\mu_{j-1/2}$. When the complete term is differenced, the overall accuracy is second order. In all other places, Y_η is solved using a second order central difference.

The derivative Y_ξ needs to be calculated to determine η_X. It is calculated analytically. Since the grid is scaled by the Blasius transformation in the X-direction,

$$\eta_b = Y\sqrt{\frac{Re}{x}} \tag{48}$$

is used, along with the fact that x is equal to ξ times d_X, to calculate Y_ξ. This implies that

$$Y = \frac{\eta_b\sqrt{\xi dX}}{\sqrt{Re}} \tag{49}$$

and

$$dY = \frac{1}{2} \frac{\eta_b \sqrt{dX}\ \partial\xi}{\sqrt{Re}\ \sqrt{\xi}} \tag{50}$$

Now, replacing η_b with Eq 48 and canceling like terms

$$Y_\xi = \frac{.5Y}{\xi} \tag{51}$$

where ξ=i-1. Therefore, Y becomes

$$Y_\xi = \frac{.5Y}{(i-1)} \tag{52}$$

If a different grid is used, another method for calculating Y_ξ would have to be used. The method used should be developed with care.

Initially Y_ξ was calculated using a central difference with a backward difference at the end of the domain. A large amount of leading edge error was induced with this method. For instance, at i=2, the analytical Y_ξ is .000099437, and the central difference is .000200479 for a dX of .016667. Even for a smaller dX, error is induced. Downstream of the leading edge, the central difference is accurate. Therefore, the grid could be evaluated numerically downstream and analytically near the leading edge of the flat plate.

Once the momentum and energy equations are linearized and the metrics calculated, the equations are written as

$$\text{Momentum} \qquad {}^{s+1}_{n}U_{ij} = \left\{ {}^{n-1}_{n}U_{ij} + \frac{2\Delta t\, {}^{s}_{n}U_{ij}}{X_\xi}\, {}^{s+1}_{n}U_{i-1j} - \frac{.5\Delta t\, {}^{s}_{n}U_{ij}}{X_\xi}\, {}^{s+1}_{n}U_{i-2j} + \right.$$

$$\Delta t \left[2\, {}^{s}_{n}U_{ij}\, \eta_x + \frac{2\, {}^{s}_{n}V_{ij}}{Y} + \frac{2}{(Y_{ij+1} - Y_{ij-1})Re} \frac{\rho\mu_{j-1/2}}{(Y_{ij} - Y_{ij-1})} \right] {}^{s}_{n}U_{ij-1} -$$

$$\xi$$

$$.5\Delta t \left[{}^{s}_{n}U_{ij}\, \eta_x + \frac{{}^{s}_{n}V_{ij}}{Y_\xi} \right] {}^{s}_{n}U_{ij-2} + \frac{2\Delta t}{(Y_{ij+1} - Y_{ij-1})Re} \frac{\rho\mu_{j+1/2}}{(Y_{ij+1} - Y_{ij})}\, {}^{n}U_{ij+1} \Big\} / UCOEF \quad (53)$$

$$UCOEF = 1 + 1.5\, {}^{s}_{n}U_{ij}\, \Delta t + 1.5\, {}^{s}_{n}U_{ij}\, \eta_x\, \Delta t + \frac{1.5\, {}^{s}_{n}V_{ij}\, \Delta t}{X_\xi} + \frac{1.5\, {}^{s}_{n}V_{ij}\, \Delta t}{Y_\eta} +$$

$$\frac{2\Delta t}{(Y_{ij+1} - Y_{ij-1})Re} \left(\rho\mu_{j+1/2} \frac{}{(Y_{j+1} - Y_j)} + \rho\mu_{j-1/2} \frac{}{(Y_j - Y_{j-1})} \right)$$

$$\text{Energy} \qquad {}^{s+1}_{n}H_{ij} = \left\{ {}^{n-1}_{n}H_{ij} + \frac{2\Delta t\, {}^{s}_{n}U_{ij}}{X_\xi}\, {}^{s+1}_{n}H_{i-1j} - \frac{.5\Delta t\, {}^{s}_{n}U_{ij}}{X_\xi}\, {}^{s+1}_{n}H_{i-2j} + \right.$$

$$\Delta t \left[2\, {}^{s}_{n}U_{ij}\, \eta_x + \frac{2\, {}^{s}_{n}V_{ij}}{Y_\eta} + \frac{2}{(Y_{ij+1} - Y_{ij-1})Re} \frac{\rho\mu_{j-1/2}}{(Y_{ij} - Y_{ij-1})} \right] {}^{s}_{n}H_{ij-1} -$$

$$.5\ \Delta t \left[U_{ij}^{s_n}\ \eta_X + \frac{V_{ij}^{s_n}}{Y_\eta} \right] H_{ij-2}^{s_n} + \frac{2\ \Delta t}{(Y_{ij+1} - Y_{ij-1})Re} \frac{\rho\mu_{j+1/2}}{(Y_{ij+1} - Y_{ij})} H_{ij+1}^{s_n} + \frac{1}{\rho} dP +$$

$$\frac{2\ (1-\frac{1}{Pr})\ \Delta t}{(Y_{j+1}-Y_{ij-1})\ Re} \left[\frac{\rho\mu_{j+1/2}}{(Y_{ij+1}-Y_{ij})} \frac{U_{ij+1}^{2n_s} - \left(\frac{\rho\mu_{j+1/2}}{(Y_{j+1}-Y_j)} + \frac{\rho\mu_{j-1/2}}{(Y_j-Y_{j-1})} \right) U_{ij}^{2n_s}}{2} + \right.$$

$$\left. \frac{\rho\mu_{j-1/2}}{(Y_j-Y_{j-1})} U/2_{ij-1}^{2n_s} \right] \Bigg\} /UCOEF \qquad (54)$$

$$UCOEF = 1 + 1.5 \frac{U_{ij}^{s_n}}{X_\xi} \Delta t + 1.5\ U_{ij}^{s_n}\ \eta_X\ \Delta t + 1.5 \frac{V_{ij}^{s_n}}{Y_\eta} \Delta t +$$

$$\frac{2\Delta t}{(Y_{ij+1}-Y_{ij-1})RePr} \left(\frac{\rho\mu_{j+1/2}}{(Y_{j+1}-Y_j)} + \frac{\rho\mu_{j-1/2}}{(Y_j - Y_{j-1})} \right) \qquad (55)$$

Where

$$X_\xi = (X_{i+1j} - X_{i-1j})/2$$

$$Y_\eta = (Y_{ij+1} - Y_{ij-1})/2 \qquad (56)$$

$$\eta_X = .5Y/[(i-1)X_\xi Y_\eta]$$

s is the iteration level

These equations are programmed. At the i=2 and/or j=2, a two point backward difference is used on the convective terms if necessary. Then an optimized successive over-relaxation technique is used.

Optimized Successive Over-Relaxation. Optimized successive over-relaxation (SOR) is a technique which is used in an attempt to accelerate the iterative procedure (1:132-133). The arbitrary corrections to the intermediate values of the unknowns are

$$U_{ij}^{s+1'} = \omega\, U_{ij}^{s+1} + (1-\omega)\, U_{ij}^{s'} \qquad (57)$$

$$H_{ij}^{s+1'} = \omega\, H_{ij}^{s+1} + (1-\omega)\, H_{ij}^{s'}$$

where U_{ij}^{s+1} is the most recently calculated value of U_{ij}, $U_{ij}^{s'}$ is the value from the previous iteration adjusted by the application of equation 57. The term $U_{ij}^{s+1'}$ is the newly adjusted or "better guess" for U_{ij}. The formula is applied immediately at each point after $U_{ij}^{s+1'}$ is obtained and U_{ij}^{s+1} replaces U_{ij}^{s+1}. The same iterpretation is used for the H equation. In the computer program, U is iterated once and then H is iterated once. This is repeated until U and H are converged.

Omega (ω) is the relaxation parameter and is between zero and two. Outside the boundary layer, ω is one. An optimized ω, ω_{opt}, is calculated for the locations inside the boundary layer. The ω_{opt} is not easily defineable for a three point backward scheme but the two point backward scheme is defined. This is used in helping to define ω_{opt} for

the three point backward scheme (6). Since the boundary conditions are not taken into account, ω_{opt} is not a true optimum. The U velocity equation is put in the form of

$$AU_{ij-1} + BU_{ij} + CU_{ij+1} = U_{ij-2} + U_{i-1j} + U_{i-2j} + \text{All other terms} \quad (58)$$

Then a maximum eigenvalue, λ_k, for Jacobi iteration is determined locally using the A, B, and C coefficients where

$$\lambda_{k_{max}} = \frac{-2\sqrt{AC}}{B} \cos\frac{\pi}{JMAX+1} \quad (59)$$

and, therefore

$$\lambda_{k_{max}} = -2\sqrt{\left(\frac{2U_{ij}\Delta t\eta_x}{\overline{Y_\eta}} + \frac{2\Delta tV_{ij}}{\overline{ReY_\eta}} + \frac{\Delta t}{\overline{ReY_\eta}}\frac{\rho\mu_{j-1/2}}{(Y_j-Y_{j-1})}\right)\left(\frac{\Delta t}{\overline{ReY_\eta}}\frac{\rho\mu_{j+1/2}}{(Y_{j+1}-Y_j)}\right)}\cos\frac{\pi}{JMAX+1} \quad (60)$$
$$\frac{}{1+1.5\frac{U_{ij}\Delta t}{X_\xi} + 1.5U_{ij}\eta_x\Delta t + 1.5\frac{V_{ij}\Delta t}{Y_\eta} + \frac{\Delta t}{Y_\eta Re}\left(\frac{\rho\mu_{j+1/2}}{Y_{j+1}-Y_j} + \frac{\rho\mu_{j-1/2}}{Y_j-Y_{j-1}}\right)}$$

As an approximation, the two circled 2's are replaced with 1's (6). The Δt can be divided out and the λ_k become

$$\lambda_{k_{max}} = -2\sqrt{\left(\frac{2U_{ij}\eta_x}{\overline{Y_\eta}} + \frac{V_{ij}}{\overline{Y_\eta}} + \frac{1}{\overline{Y_\eta Re}}\frac{\rho\mu_{j-1/2}}{(Y_j-Y_{j-1})}\right)\left(\frac{1}{\overline{Y_\eta Re}}\frac{\rho\mu_{j+1/2}}{(Y_{j+1}-Y_j)}\right)}\cos\frac{\pi}{JMAX+1} \quad (61)$$
$$\frac{}{\frac{1}{\Delta t} + 1.5\frac{U_{ij}}{X_\xi} + 1.5U_{ij}\eta_x + 1.5\frac{V_{ij}}{Y_\eta} + \frac{1}{Y_\eta Re}\left(\frac{\rho\mu_{j+1/2}}{Y_{j+1}-Y_j} + \frac{\rho\mu_{j-1/2}}{Y_j-Y_{j-1}}\right)}$$

and

$$\omega_{opt} = \frac{2}{1+\sqrt{1-\lambda_k^2}} \quad (62)$$

For a real Jacobi eigenvalue, the λ_k is limited to be approximately less than .995, i.e. ω_{opt} is approximately less than 1.85. The ω_{opt} is recalculated in the program after a specified number of time iterations. The ω_{opt} should be used in the program because it helps reduce computation time. In some problems, it can reduce the computation time by a factor of 30 which is significant (1:132-133).

Once the updated values of U and H are calculated for every j location, the V velocity can be calculated from the continuity equation.

Continuity Equation. The continuity equation is used to calculate the V velocity. First, the equation is transformed to the ξ-η plane, Eq 41, and the V_η is solved for

$$V_\eta = \frac{-Y_\eta}{\overline{X_\xi}} U_\xi + \frac{Y_\xi}{\overline{X_\xi}} U_\eta \tag{63}$$

Now, the equation is integrated to find V using the trapezoidal rule

$$V^n_{ij} - V^n_{ij-1} = \frac{-Y_\eta}{\overline{X_\xi}} \left(\frac{U_{\xi\ ij} + U_{\xi\ ij-1}}{2} \right) + \frac{Y_\xi}{\overline{X_\xi}} \left(\frac{U_{\eta\ ij} + U_{\eta\ ij-1}}{2} \right) \tag{64}$$

The U_ξ are finite differenced with a second-order three point upwind difference. The $\frac{U_{\eta\ ij} + U_{\eta\ ij-1}}{2}$ looks like $U_{\eta\ ij-1/2}$ and is differenced with a central difference about j-1/2. Like terms are combined, and the differenced equation becomes

$$V^n_{ij} = V^n_{ij-1} + \left(\frac{-3\ Y_\eta}{4\ X_\xi} + \frac{Y_\xi}{\overline{X_\xi}} \right) U^n_{ij} + \frac{Y_\eta}{\overline{X_\xi}} U^n_{i-1j} - \frac{Y_\eta}{4X_\xi} U^n_{i-2j} +$$

$$\left(\frac{-3\,Y_\eta - Y_\xi}{4\,X_\xi} \quad \frac{}{X_\xi}\right) U^n_{ij-1} + \frac{Y_\eta}{X_\xi} U^n_{i-1j-1} - \frac{Y_\eta}{4X_\xi} U^n_{i-2j-1} \qquad (65)$$

Once V is calculated, the iteration is complete. The U, H, and V equations are iterated until the convergence criteria is met. Upon convergence, the heat rate at the wall can be calculated for that i-location.

Heat Rate. The heat rate at the wall, q_o, is defined by Eq 30. This equation must be tranformed to the Dorodnitsyn plane before it can be differenced. After it is transformed, the equation becomes

$$q'_o = -k'\rho'_{wall} \left(\frac{\partial T'}{\partial Y'}\right)_{Y=o} \qquad (66)$$

where k is the conductivity and is calculated by

$$k' = \frac{\mu' Cp'}{Pr} \qquad (67)$$

The derivative $\partial T/\partial Y$ is transformed to the ξ-η plane and a three point windward difference is used for second order accuracy in the ξ-η plane. Since q is a dimensioned quantity, the T and Y must be dimensioned and the equation becomes

$$q_o = \frac{\mu'}{Pr} \frac{\rho'_{wall}\, U'^2_\infty}{L'\Delta Y}\left(\frac{-3T_{i1} + 4T_{i2} - T_{i3}}{2}\right) \qquad (68)$$

where

$$\Delta Y = (-3Y_{i1} + 4Y_{i2} - Y_{i3}) / 2 \qquad (69)$$

Now the heat transfer coefficient is calculated by

$$h_{.9} = q'_o/(.9\ T'_{aw} - T'_{wall}) \qquad (70)$$

where .9 is the recovery factor instead of $\sqrt{Pr}$. Now this heat transfer coefficient can be divided by the reference heat transfer coefficient as defined by Eq 31.

Upon completion of this step, the program can march in the i direction and the solution procedure is repeated at this new location. Finally, when the end of the plate is reached, the program goes to the beginning of the flat plate and starts again.

Boundary Conditions

In order to completely define this problem, the initial condition and the wall and edge boundary conditions must be specified.

Wall-Boundary Conditions. The wall boundary conditions are no slip conditions which means U(i,1) = o and V(i,1) = o. The wall temperature depends on the case being run. For an isothermal case, the wall temperature is constant at 530 degrees R. Several nonisothermal cases with a temperature step at x/L of .466667 were run. Again, this temperature step depends on the case. Some of the cases had a temperature step of 170 degrees R, increasing the wall temperature from 530 degrees R to 700 degrees R to simulate the FRSI wind tunnel tests, and others had a temperature step of 270 degrees R, increasing the wall temperature to 800 degrees R to simulate the HRSI wind tunnel tests. In addition to these nonisothermal cases, the wall temperature was varied in time from 530 degrees R to 800 degrees R using Equation 1. Finally, the wall temperature on a HRSI tile was varied in time from 530 degrees

to a radiation equilibrium temperature where

$$T'_{eq} = \left(\frac{q'}{\sigma\epsilon}\right)^{.25}$$

and σ is the Stefan-Boltzmann constant and ϵ is the tile emissivity.

The above conditions may not be an accurate calculation of the small region at the leading edge (12) and would indicate lower heating near the knife blade leading edge than the exact answer. The heating near the leading edge would also be affected by a shock-boundary layer interaction at the lower deflection angles. The full or parabolized Navier-Stokes equations would have to be solved at each deflection angle in order to resolve the interaction.

Edge Boundary Conditions. The boundary conditions at the outer edge were approximated by oblique shock theory. Oblique shock theory assumes inviscid flow in a perfect gas. The only pressure gradients in the flow are assumed to be across the oblique shock. Therefore, the edge conditions were based on the conditions behind the oblique shock. If the plate is stationary, the edge conditions do not change. As the plate is pitched, the edge conditions are recalculated for each new angle using Eqs 33 to 37. Instead of solving the equations at each angle, the program interpolates from Table II which is the result of the equations at each deflection angle.

Initial Conditions. To begin the calculations, an initial U and V velocity and total enthalpy must be known. The V velocity was assumed to be zero everywhere. Inside the boundary layer, the U velocity is calculated using the cubic given as

$$\frac{u}{u'_\infty} = \frac{u'}{u'_\infty} = \frac{u'}{u'_\infty}\left[1.5\left(\frac{y'}{\delta'}\right) - .5\left(\frac{y'}{\delta'}\right)^3\right] \tag{71}$$

where

$$\delta = \frac{5.2\sqrt{x^n}}{\sqrt{Re}} \tag{72}$$

for incompressible flow and y is in the physical plane and not the transformed plane. This equation is used because it gives a zero second derivative at the wall and gives a reasonably good velocity profile through the boundary layer (1Ø). The same cubic equation is used to determine the total enthalpy profile, but it is based on the thermal boundary layer thickness δ_T. The equation for enthalpy is

$$\frac{H}{U'^2_\infty} = \frac{H'}{U'^2_\infty} = \frac{H'_w}{U'^2_\infty} + \frac{(H'_e - H'_w)}{U'^2_\infty}\left[1.5\left(\frac{y'}{\delta'_T}\right) - .5\left(\frac{y'}{\delta'_T}\right)^3\right] \tag{73}$$

where $\delta_T = \delta/Pr$.

Outside the boundary layer, U and H are equal to the edge conditions.

Table II

Oblique Shock Table

θ degrees	Mach	Velocity	Temp	Pressure
3	12.203376	4843.7962	65.62	1.3063
4	11.541259	4834.5371	73.08	1.7262
5	10.886080	4823.7297	81.78	2.2334
6	10.245773	4811.1933	91.84	2.8322
7	9.630664	4796.8408	103.33	3.5250
8	9.046685	4780.5741	116.30	4.3135
9	8.498054	4762.3358	130.80	5.1985
10	7.986783	4742.0933	146.83	6.1801
11	7.512550	4719.8062	164.39	7.2581
12	7.0741	4695.4522	183.49	8.4319
13	6.6693	4669.00	204.12	9.7010
14	6.2690	4639.60	227.99	11.060

IV. Results

To investigate the heat transfer on a wedge, different cases were run using the unsteady boundary layer code developed in this project. The program is verified using incompressible and compressible cases. Both cases are steady state solutions, each having an isothermal wall. The incompressible solution is compared to the Blasius solution (13:142) and the compressible solution is compared to approximate isothermal Eckert theory and another numerical solution at three angles, 3 degrees, 10 degrees, and 14 degrees. After the cases are verified, steady state solutions with a nonisothermal wall are run and compared to theory and experimental data. In addition to the steady state solutions, transient cases are investigated. The transient cases change the wall temperature of the tile as a function of time at a constant of 14 degrees. Equation (1) is used with a time constant of 10 seconds to change the wall temperature; in another case, the change depends on both the heat rate and the time constant. Finally, the plate is pitched with an isothermal wall in one case and a nonisothermal wall in another case from 14 degrees to 3 degrees and back to 14 degrees.

Program Verification

In order to use the program, THESIS, developed in this project, the program must be verified. The first step towards this goal is running an incompressible case. In this case, M_e is equal to .05 which is also equal to M_∞ with a wall temperature of 530 degrees R. Since the density is essentially constant, the Dorodnitsyn transformation is negated and only the incompressible boundary layer equations are verified. In Figure 6, the numerical solution is compared to the

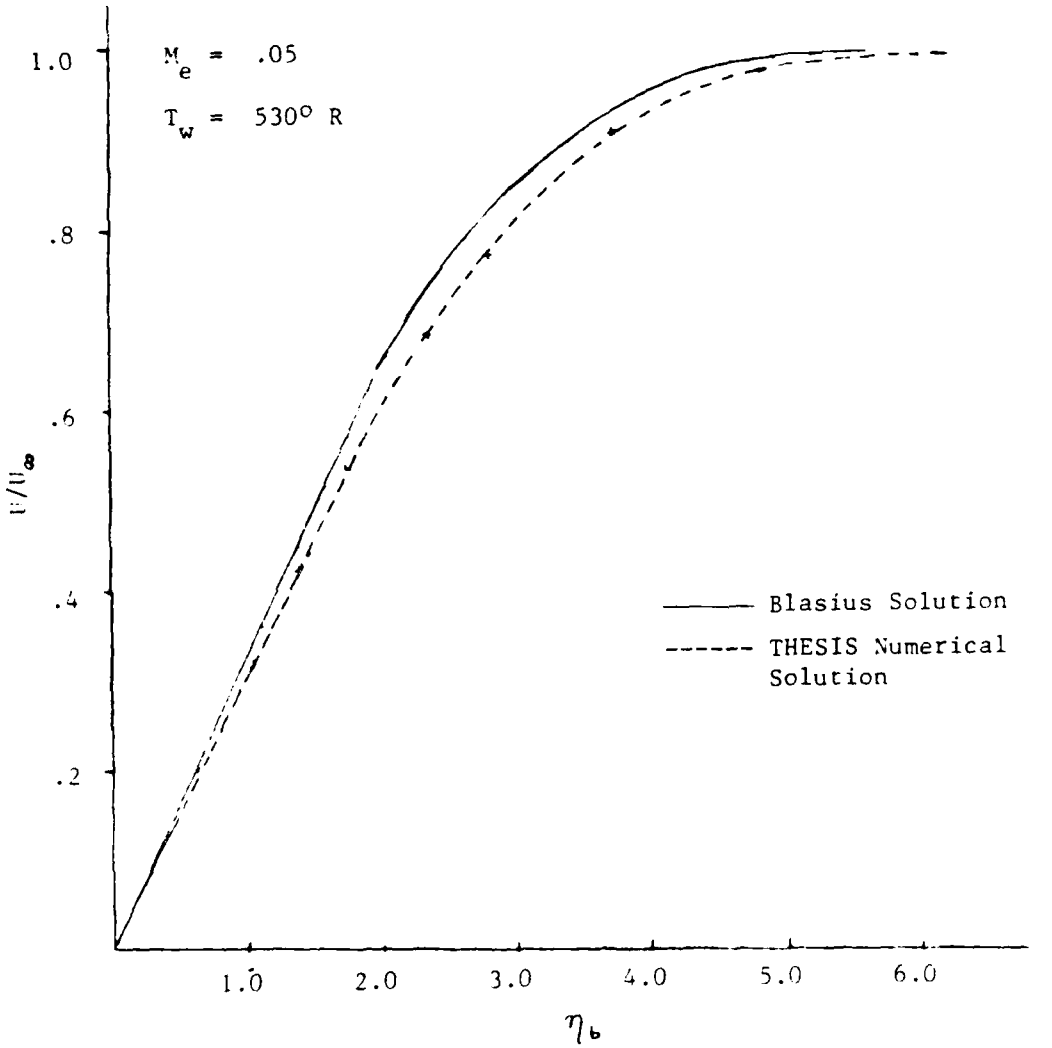

Figure 6 Comparison of Blasius Solution with the Numerical Solution

Blasius solution (13:42). The velocity ratio, u/u_∞, is .99 at η_b equal to 5.64 for the Blasius solution and 6.14 for the numerical solution. The two curves compare well with the max error being five percent.

To verify the Dorodnitsyn transformed equations, a compressible case is solved using the thin skin wind tunnel test as a model. This case is an isothermal wall at 530 degrees R and M_∞ of 14.237. The T_o and P_o are 2020 degrees R and 1600 psia respectively. These conditions are used in each case for angles of 14 degrees, 10 degrees and 3 degrees, and the boundary layer edge conditions are adjusted according to oblique shock theory.

Due to compressibility effects, the grid used in the incompressible case must be adjusted to get enough grid points in the boundary layer to take into account the temperature inversion and get an accurate solution. This grid is adjusted by multiplying the Y location by a grid factor. The smaller the grid factor, the more points inside the boundary layer. Table III shows the relationship of the grid factor to the h/h_{ref} for the three angles. A grid factor of 1.0 is used for this work, realizing that this is still a relatively coarse grid.

Once the grid is modified, a solution for the compressible case can be determined but the result will have a large error due to the large gradients at the leading edge and the coarse grid. A unique way of taking care of this leading edge problem is to assume a zero gradient at the leading edge. This implies that U(1,j) is equal to U(2,j), H(1,j) is equal to H(2,j), and V(1,j) is equal to V(2,j). This assumption could be used in other problems that do not have similarity solutions because the dx could be made sufficiently small to make the assumption

Table III

Grid Factor Effects on h/h_{ref}

grid factor	h/h_{ref}		
	3 degrees	10 degrees	14 degrees
.1	1.4484	3.1334	4.1709
.5	1.44375	3.1342	4.1729
1.0	1.42639	3.1262	4.16815
3.0	1.28286	3.0467	4.1042
5.0	1.09215	2.9089	3.99679
approximate isothermal theory	1.65	3.55	4.6552
other numerical solution	1.55	3.35	4.45

valid. When this assumption is used, the results for the isothermal compressible case were constant as the approximate isothermal Eckert theory predicted.

Upon the resolution of the grid and the leading edge error, the steady state solution for the three angles was calculated. To avoid any start up problems, the 14 degrees steady state solution was used as the 10 degrees initial conditions and the 10 degrees steady state solution was used as the 3 degrees initial conditions. The results are compared in Figure 7 to the approximate analytical solution, to another steady numerical boundary layer solution (2), and to thin skin wedge data from the wind tunnel. As is shown, the h/h_{ref} results from THESIS are lower than both the approximate theory by approximately 10 percent and the numerical solution by about 6 percent at 14 degrees and 10 degrees and lower at 3 degrees. An explanation for this difference goes back to Table III, which shows that the solution depends on the grid and ultimately the grid factor. Six times as many grid points were used in the other steady boundary layer solution. The thin skin data varies more than the difference in the predicted solutions, which can be for several reasons. Variation in the thin skin heating data along the panel can be due to small nonisothermal wall effects and thermal expansion of the thin skin panel. In addition, a jet of air from the tunnel start up before model injection was increasing the temperature on the downstream part of all panels, and caused lower heating at the rear of the panel (7:5). Some variation may also be due to shock interaction with the viscous boundary layer.

ISOTHERMAL

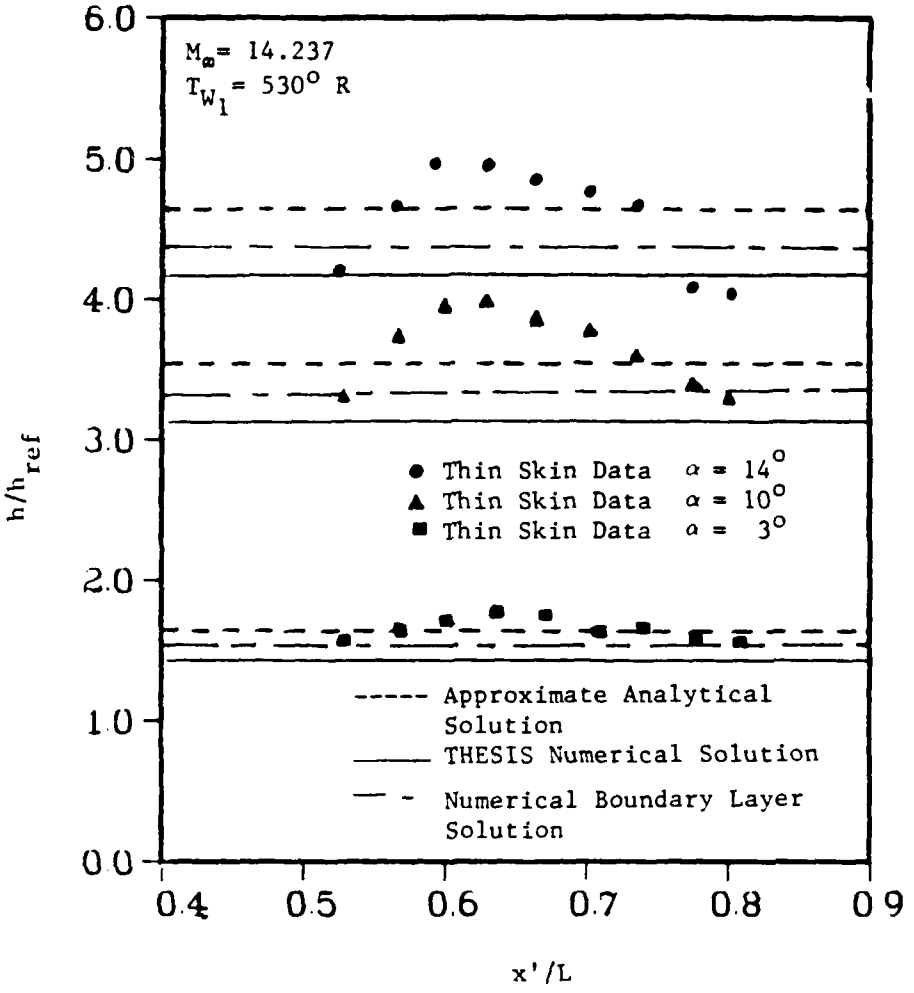

Figure 7 Thin Skin Wedge Heating Comparison with Predictions for Isothermal Wall

Even though the numerical solutions from THESIS are grid dependent, the results compare well with both the approximate isothermal Eckert theory and another steady numerical solution. This implies that the Dorodnitsyn transformed boundary layer equations are correct.

Nonisothermal Cases

To begin the investigation of nonisothermal wall effects, some steady state solutions are calculated and compared to approximate analytic solutions and HRSI and FRSI wind tunnel data. The free stream conditions are the same as the isothermal case with a M_∞ of 14.237, P_o of 1600 psia, and T_o of 2020 degrees R, but in these cases, a temperature step is given at a streamwise location of .46667. In order to compare wind tunnel data to the numerical results for the HRSI panel, a temperature step of 270 degrees R is given, making the wall temperature jump from 530 degrees R to 800 degrees R. The solution of the boundary layer equations at 14 degrees deflection is shown in Figure 8. (Versus streamwise distance.) The approximate nonisothermal solution given by equation 32 demonstrates the dramatic decrease in the heat transfer coefficient just downstream of the temperature jump, and the subsequent slow recovery. The numerical boundary layer solution shows the same trend, but at a slightly lower heating magnitude similar to other predictions (7:6). The only available surface thermocouple data show an even lower magnitude and slower recovery of the boundary layer (7:6). For completeness, solutions of the boundary layer equations at 10 and 3 degree deflection angles and the same temperature step are shown in

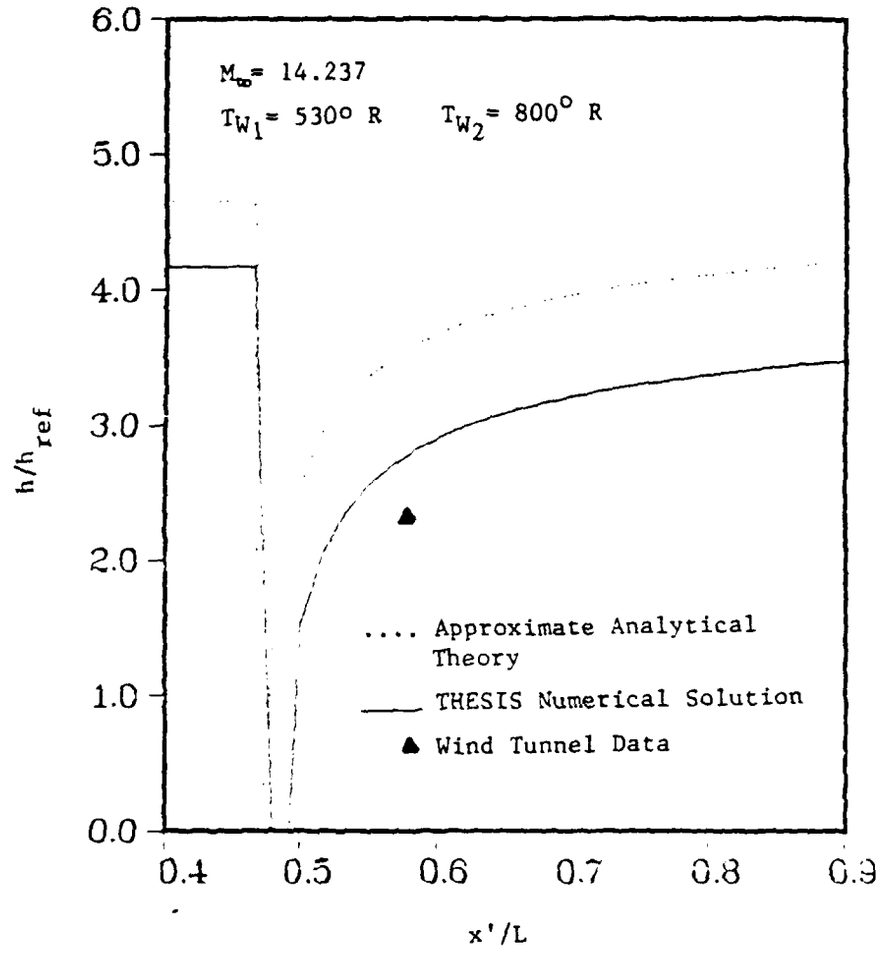

Figure 8 Nonisothermal Wall Solution at 14 Degrees with a HRSI Wall Temperature of 800 Degrees R

Figures 9 and 10 respectively. No wind tunnel results are available for these two solutions. At 3 and 10 degrees, the heating magnitude is slightly lower than the approximate nonisothermal solution.

To compare with FRSI wind tunnel data, a steady state nonisothermal wall case at a 14 degree deflection was run with a temperature step of 170 degrees R making the wall temperature jump from 530 degrees R to 700 degrees R. The results, shown in Figure 11, show the same dramatic decrease in heat transfer coefficient downstream of the jump for both the approximate nonisothermal solution and the THESIS numerical solution, but are still higher than wind tunnel results except at the end of the plate which is lower. The boundary layer appears not to recover as fast as the predictions near the interface, but does recover downstream reasonably close to predicted heating (7:6).

In all of the steady state nonisothermal cases, the numerical results compared well with the approximate nonisothermal solution but were consistently higher than the wind tunnel data.

Transient Cases

Understanding how the transient effects influence the heating rate is important for interpreting the overall results. To investigate these effects, the wall temperature is increased as a function of time by equation 1 from 530 degrees R to 800 degrees R. The deflection angle is held constant at 14 degrees. The 14 degree steady state solution for the isothermal wall is used as the initial condition and the freestream conditions are the same as the steady state nonisothermal wall case. The physical time step is .1 second and the convergence criteria are specified as 1.0 e-6. In Equation 1, the temperature is dependent on

NONISOTHERMAL

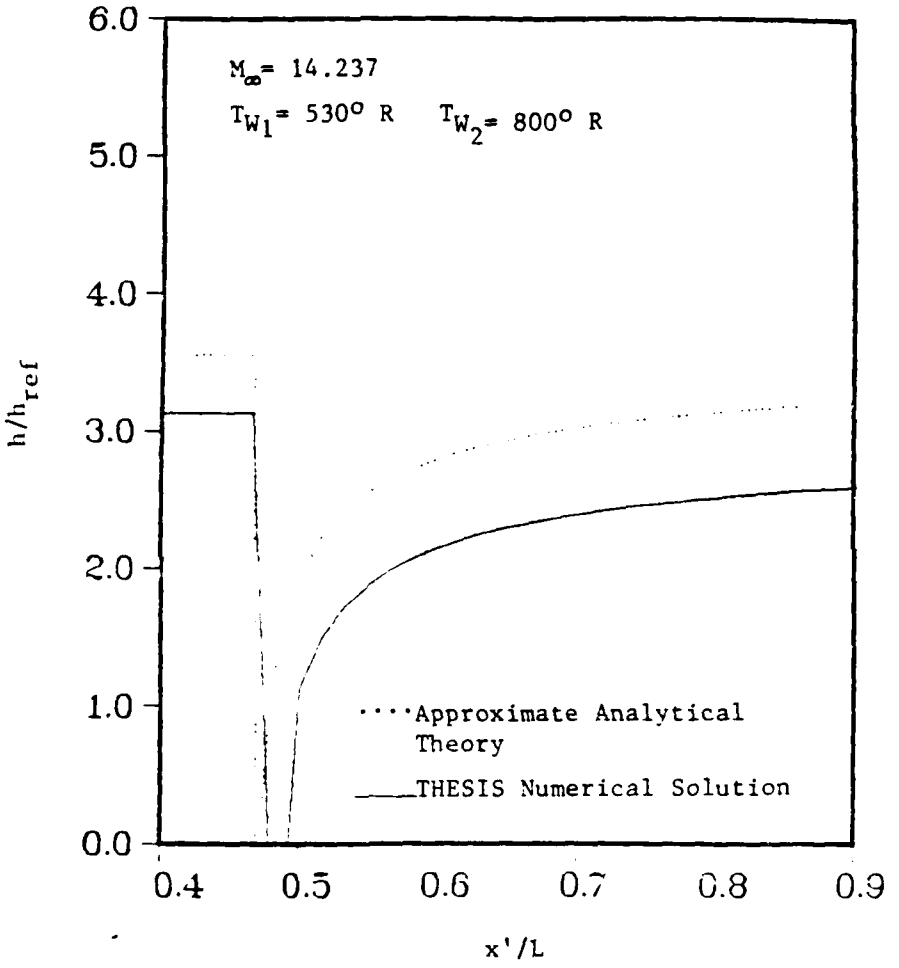

Figure 9 Nonisothermal Wall Solution at 10 Degrees with a HRSI Wall Temperature of 800 Degrees R

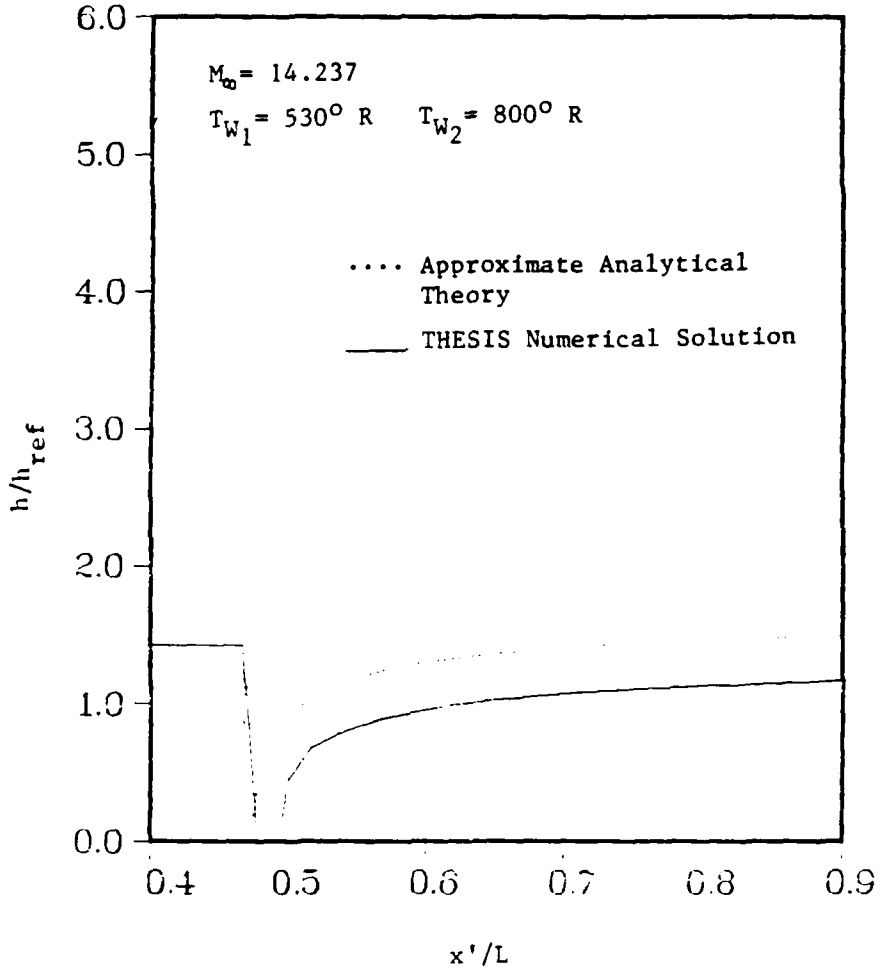

Figure 10 Nonisothermal Wall Solution at 3 Degrees with a HRSI Wall Temperature of 800 Degrees R

NONISOTHERMAL

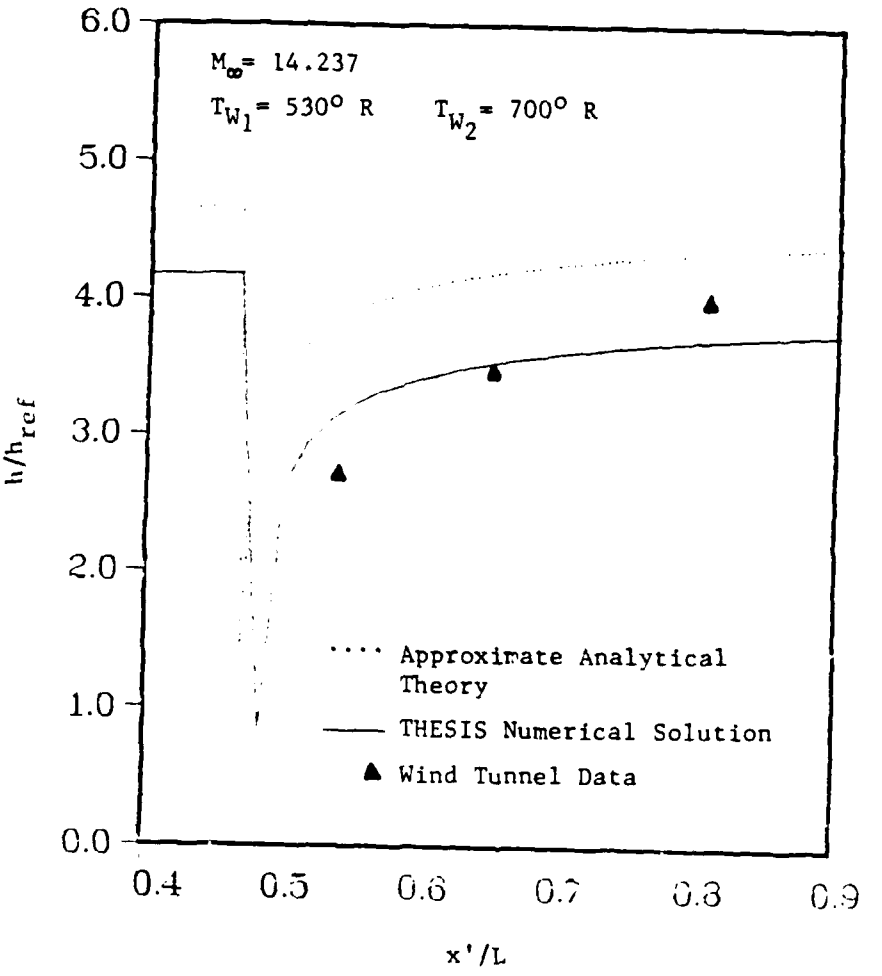

Figure 11 Nonisothermal Wall Solution at 14 Degrees with a FRSI Wall Temperature of 700 Degrees R

both time and a time constant. A time constant of 30 seconds is used to simulate the conduction into the FRSI material. As the solution marches in time the wall temperature is changed. The solution, shown in Figure 12, converges as time increases.

To determine if a lag in the h/h_{ref} occurred due to the change in wall temperatures, some additional steady state isothermal wall problems were run. At a streamwise location of .5, the wall temperature at 10 seconds is recorded to be 635.5. This wall temperature was input for an isothermal case to determine the isothermal heat transfer coefficient ratio. The isothermal h/h_{ref} ratio is 3.26207 and the transient h/h_{ref} ratio is 3.2578 which indicates that a lag exists with this large Δt of .05.

To make this transient case more realistic, the wall temperature is coupled to the heat rate into the wall and, as time increases, an equilibrium wall temperature will be reached. The equation used to calculate the wall temperature is

$$T'w = T'w\, e^{-\Delta t'/RC'} + (1-e^{-\Delta t'/RC'})T'eq \qquad (74)$$

where

$$T'eq = \left(\frac{q'}{\epsilon\sigma}\right)^{1/4} \qquad (75)$$

where ϵ is .85, σ is the Stephen Boltzman constant 4.761×10^{-13}, and dt is .05 seconds. A time constant of 10 seconds is used in this case to simulate the lag due to conduction into a HRSI panel. An assumption is made here that the heat rate into the panel equals the radiation heat rate. This is a good assumption for shuttle flight but not for the wind tunnel; therefore, the equilibrium wall temperature in this case can be higher than in the wind tunnel. The solution of h/h_{ref} at 5, 10, 15,

and 20 seconds and steady state versus streamwise distance are shown in Figure 13. As referenced earlier, the equilibrium temperature is approximately 900 degrees R at the end of the plate, which is higher than the 800 degrees R in the wind tunnel. This solution is used for the initial conditions of the nonisothermal pitching plate case.

Pitching Plate Cases

Pitching the plate with the wall temperature as a function of both the heat rate and time is the most realistic case. A pitching plate with an isothermal wall is examined. Using an isothermal pitching plate, the error due to the first order time difference is investigated. The wall temperature is constant at 530 degrees R and the freestream conditions are the same as the isothermal cases. The plate is pitched at 2 degrees per second and the edge conditions are changed accordingly with interpolation of oblique shock tables. The first Δt is .1 seconds with a maximum of 5 iterations to converge, then the Δt is halved to .05 with a maximum of 5 iterations to converge. Finally, a Δt of .025 is run with maximum iteration limits of 5 and 10.

The h/h_{ref} ratios are compared at Time steps of .1, .05, and .025 at an α of 12 degrees and an X/L location of .5. The h/h_{ref} is 3.45645 at Δt of .1, 3.5351 at Δt of .05 and 3.5887 at Δt of .025 which is less than 2 percent error between Δt of .05 and .025. Furthermore, the Δt of .025 had less than 1 percent error between 5 and 10 iterations. This implies that the unsteady terms could have been ignored without picking up more than 1% error if a small enough time step is used and the solution is a steady state solution at each angle. With this in mind, a Γ function (8:150) could have been used to solve for the heat rate by

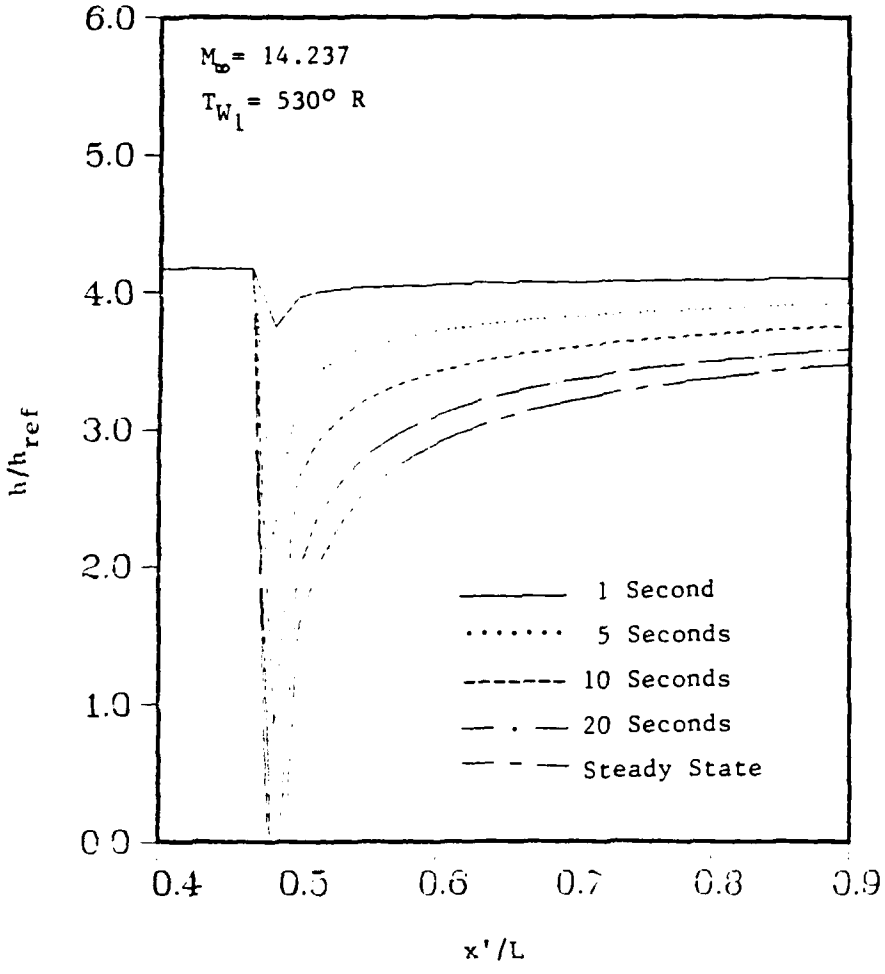

Figure 12 Transient Nonisothermal Wall Solutions at 14 Degrees

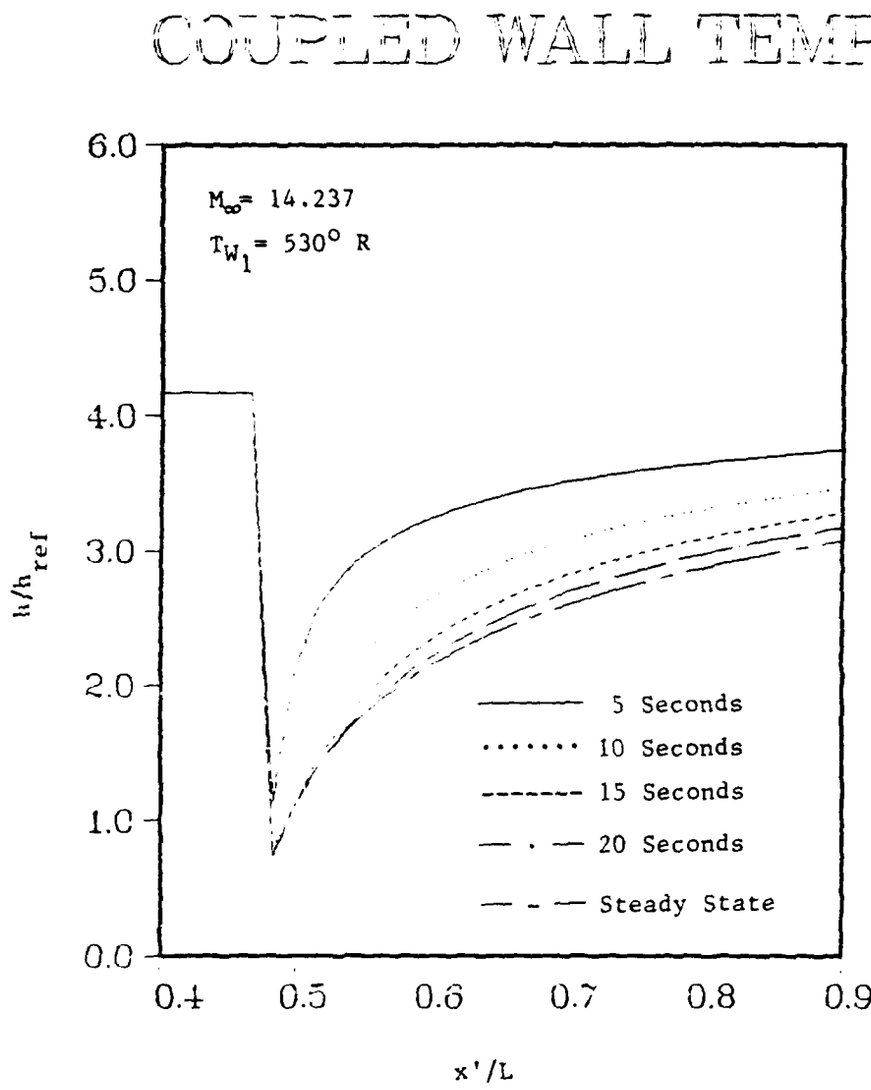

Figure 13 Comparison of Transient Nonisothermal Solutions with the Wall Temperature a Function of the Heating Rate

$$q = .332 \frac{k}{x'} Pr^{1/3} Re^{1/2} \left(\Sigma nBr \frac{4}{x} x^{\cdot n} \beta_n + A \right) \quad (76)$$

where

$$\beta = \frac{\Gamma(4/3n)\ \Gamma(2/3)}{\Gamma(4/3n + 2/3)} \quad (77)$$

Finally, note the h/h_{ref} is lower at the leading edge and recovers to a constant at the end of the plate. The response is faster at the leading edge because the boundary layer is thinner and it takes less time for energy to diffuse across the boundary layer. It also takes less time near the leading edge for energy to convect downstream from any changes upstream.

Pitching the plate with a nonisothermal wall emulates pitching the plate in the wind tunnel and the push over pull up maneuver used by the Space Shuttle (7). The wall temperature is a function of time and heat rate where Equations 74 to 75 apply. The time constant is changed to 3 seconds to emulate the material response of the HRSI tile during a small maneuver and the converged solution of the transient wall temperature as a function of heat rate is used as initial conditions. As before, the plate is pitched at 2 degrees per second with a deflection angle time history shown in Figure 14. Starting at equilibrium, the plate is pitched from 14 degrees to 3 degrees and held for 5 seconds. Then it is pitched back up to 14 degrees and held for another 5 seconds. This solution has some very interesting results. Figures 15 and 16 are plots of the h/h_{ref} and wall temperature, respectively, versus streamwise location for 14, 9, and 3 degrees as the plate is pitched up and 3, 9, and 14 degrees as it is pitched down. Both Figures show a lag in the

wall response, particularly at the end of the plate, which is reasonable. A small transient effect can be seen in Figure 15 near the leading edge. In addition, Figure 15 shows the same trend as previously discussed in the nonisothermal wall cases. However, at the interface, the h/h_{ref} are about the same for all angles before they changed. Furthermore, in many of the previous cases, a temperature step was assumed and Figure 16 is a good illustration that the assumption was an acceptable one.

In addition to these two plots, the h/h_{ref} and wall temperature time histories and the h/h_{ref} versus the deflection angle are plotted for five streamwise locations, .Ø16667, .466667, .483333, .566667, and .983333. The first point, .Ø16667, is right at the leading edge of the plate and Figures 17, 18, and 19 are the above mentioned plots for this location. Figure 17 shows that the h/h_{ref} decreases as the plate is pitched to 3 degrees and increases as it pitches back down to 14 degrees due to the change in the heat rate. At the 5 second hold at both 3 degrees and 14 degrees the solution is at steady state almost immediately, but the unsteady terms in the equations do affect the results at about 1Ø.5 and 16 seconds. Figure 18 shows the temperature is a constant 53Ø degrees R to simulate the steel wind tunnel model throughout the plate pitching, which implies that there are no wall effects at this location. The h/h_{ref} versus the deflection angle, Figure 19, indicates a small hysteresis. This could have numerical error due to the large gradients in the boundary layer at the leading edge and the coarse grid.

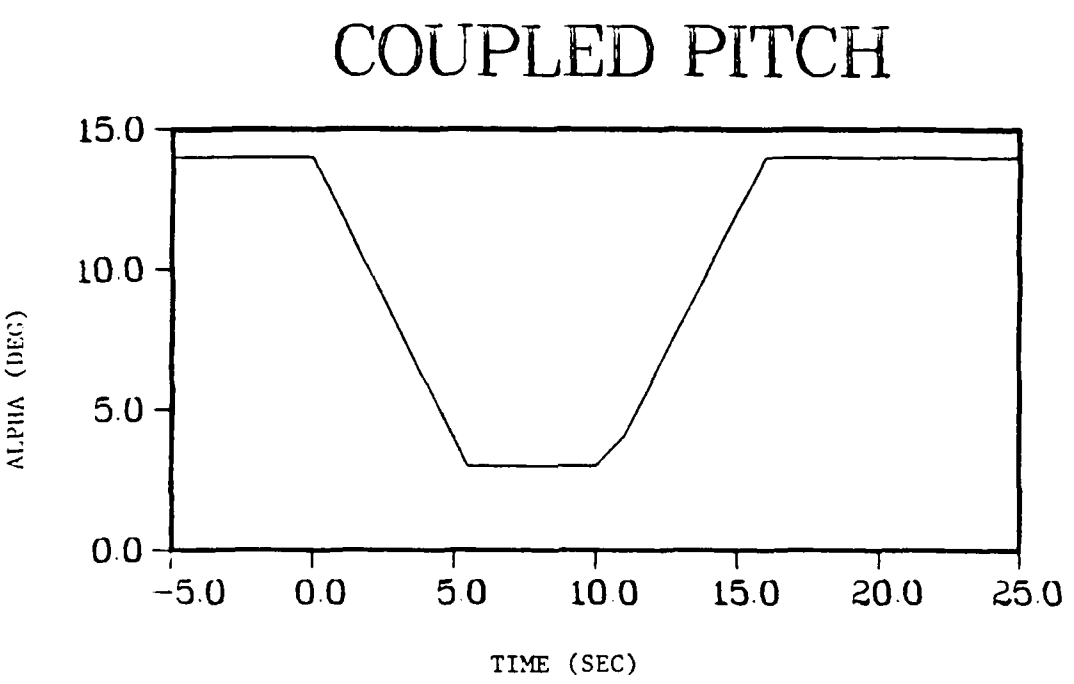

Figure 14 Deflection Angle Time History

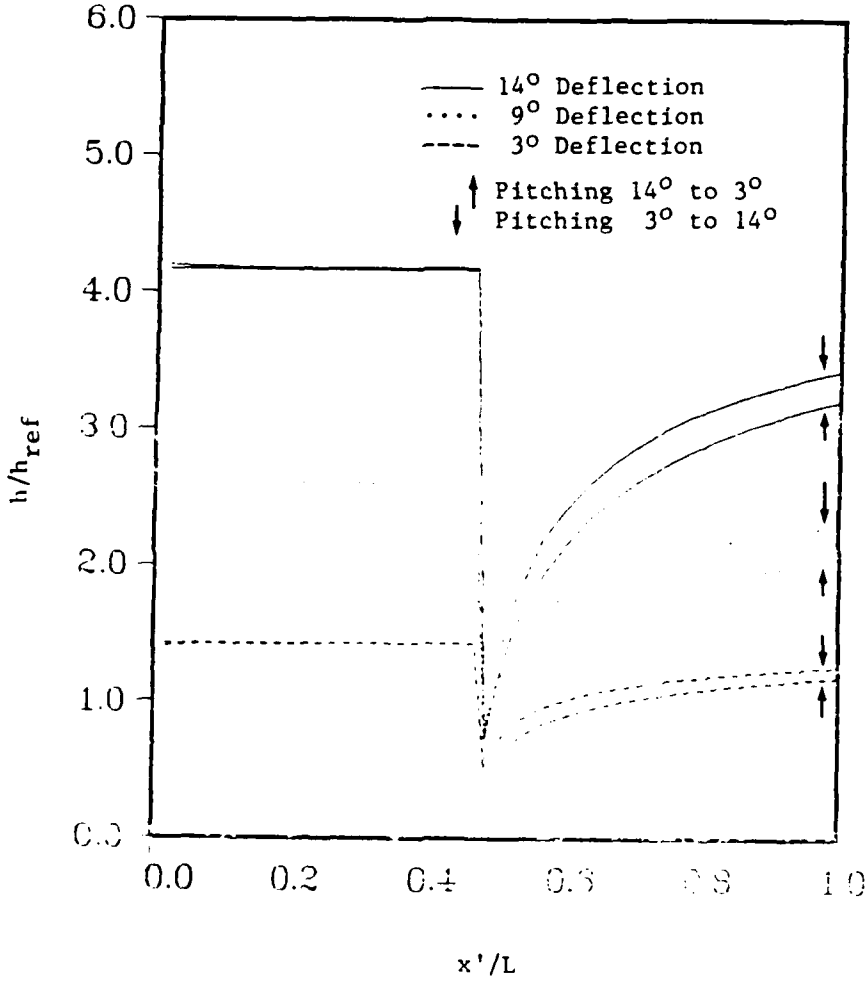

Figure 15 Comparison of Nonisothermal Pitching Plate Solutions for 14 Degrees, 9 Degrees, and 3 Degrees

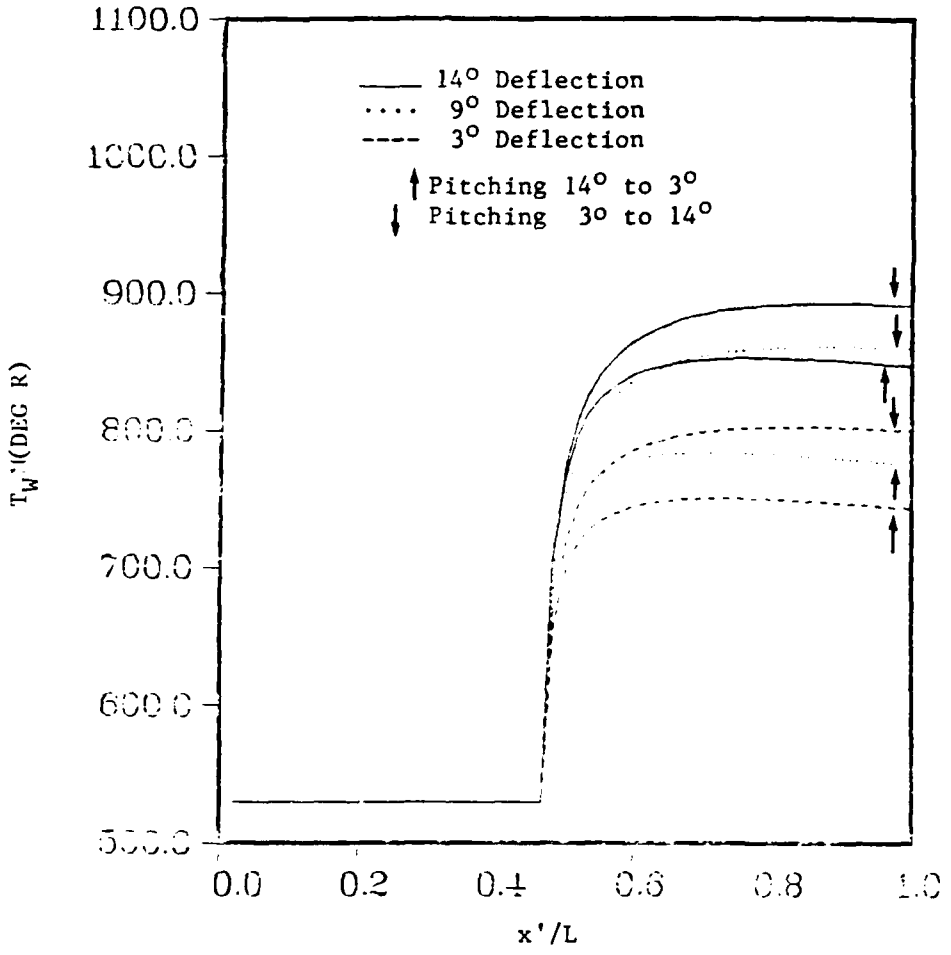

Figure 16 Comparison of the Wall temperatures for the Nonisothermal Pitching Plate for 14 Degrees, 9 Degrees, and 3 Degrees

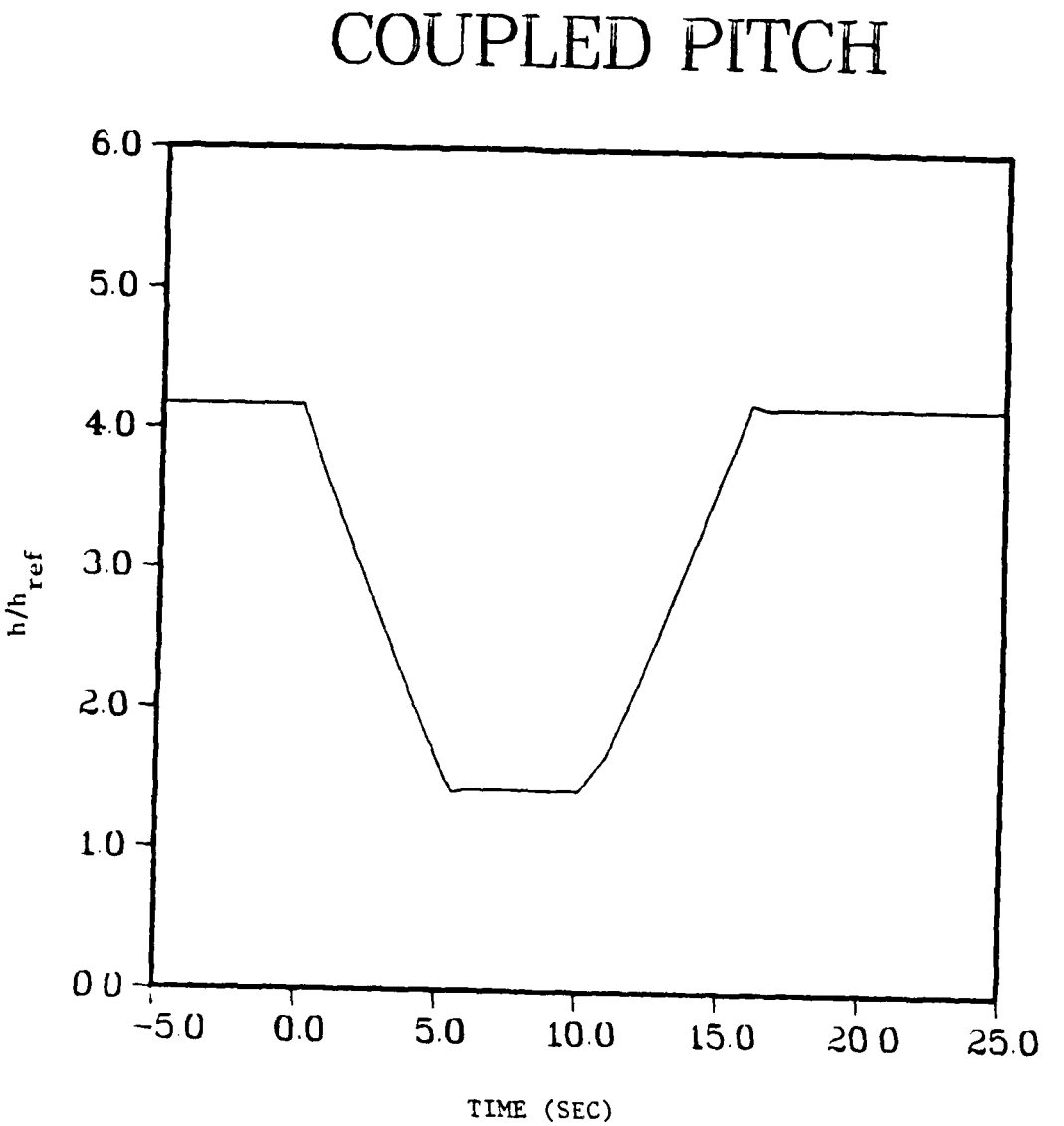

Figure 17 h/href Time History for x/L Location of .Ø16667

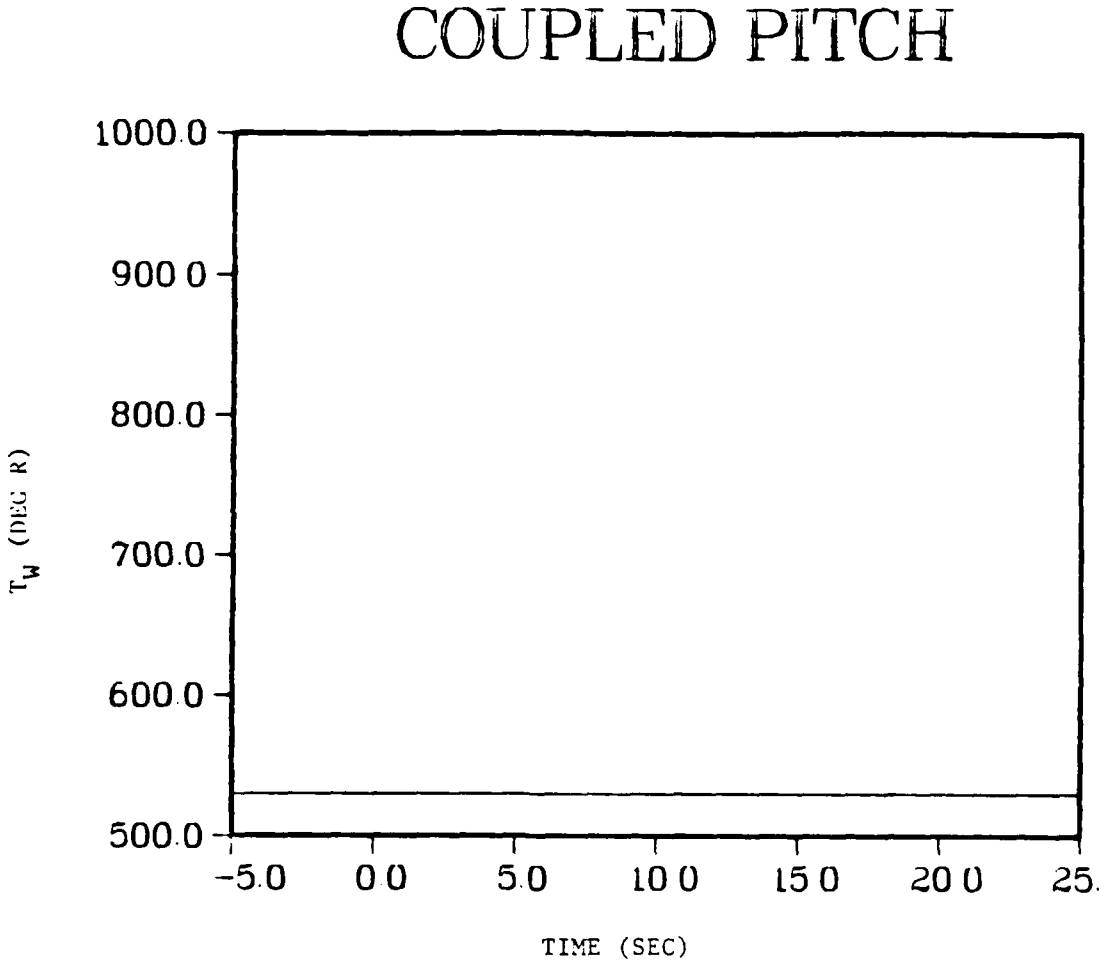

Figure 18 Wall Temperature Time history for the streamwise Location of .016667

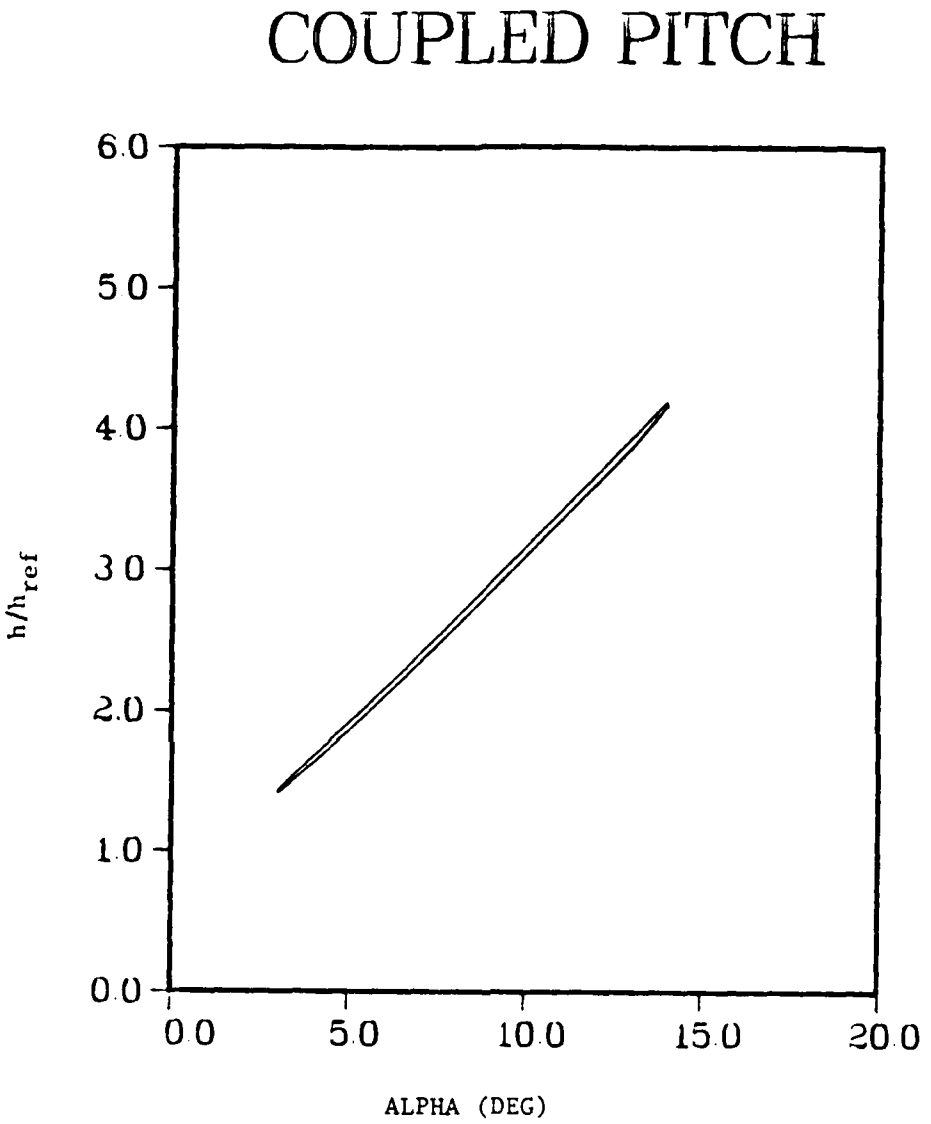

Figure 19 h/href versus Deflection Angle for x/L Location of .Ø16667

At the interface of the panel, .46667 location, Figures 20, 21, and 22 look very similar to the .016667 location. Since conduction through the plate is not accounted for in this project, the wall temperature remains at 530 degrees R, Figure 21, even though it is next to a higher or lower temperature depending on the direction of the pitch. Furthermore, the hysteresis, Figure 22, is less than at the leading edge but that is to be expected since the boundary layer gradients have decreased. Therefore this hysteresis is probably caused by the error due to the coarse grid and some unsteady effects.

For the first location after the interface of the panel, .483333, the h/h_{ref} changes very little as the plate is pitched, Figure 23. The equilibrium h/h_{ref} is much lower than the previous location because the wall temperature is about 200 degrees higher, Figure 24. Hysteresis also exists at this location, Fig 25.

Further down the plate, at location .56667, the results are much more dramatic, Figures 26, 27, and 28. As the plate is pitched the h/h_{ref} decreases. When the deflection angle first reaches 3 degrees, the wall temperature is higher than the equilibrium wall temperature because of a lag. While the plate remains at 3 degrees for 5 seconds, the wall temperature decreases and, in turn, the h/h_{ref} increases until equilibrium is reached. The five second hold was not quite long enough to reach equilibrium. The same phenomenon happens as the plate is pitched back to 14 degrees, only in reverse. When the plate reaches 14 degrees the wall temperature is lower and then rises to equilibrium during the following five seconds. As the temperature rises, the h/h_{ref} decreases. Some unsteady effects, noticed in the solution of the

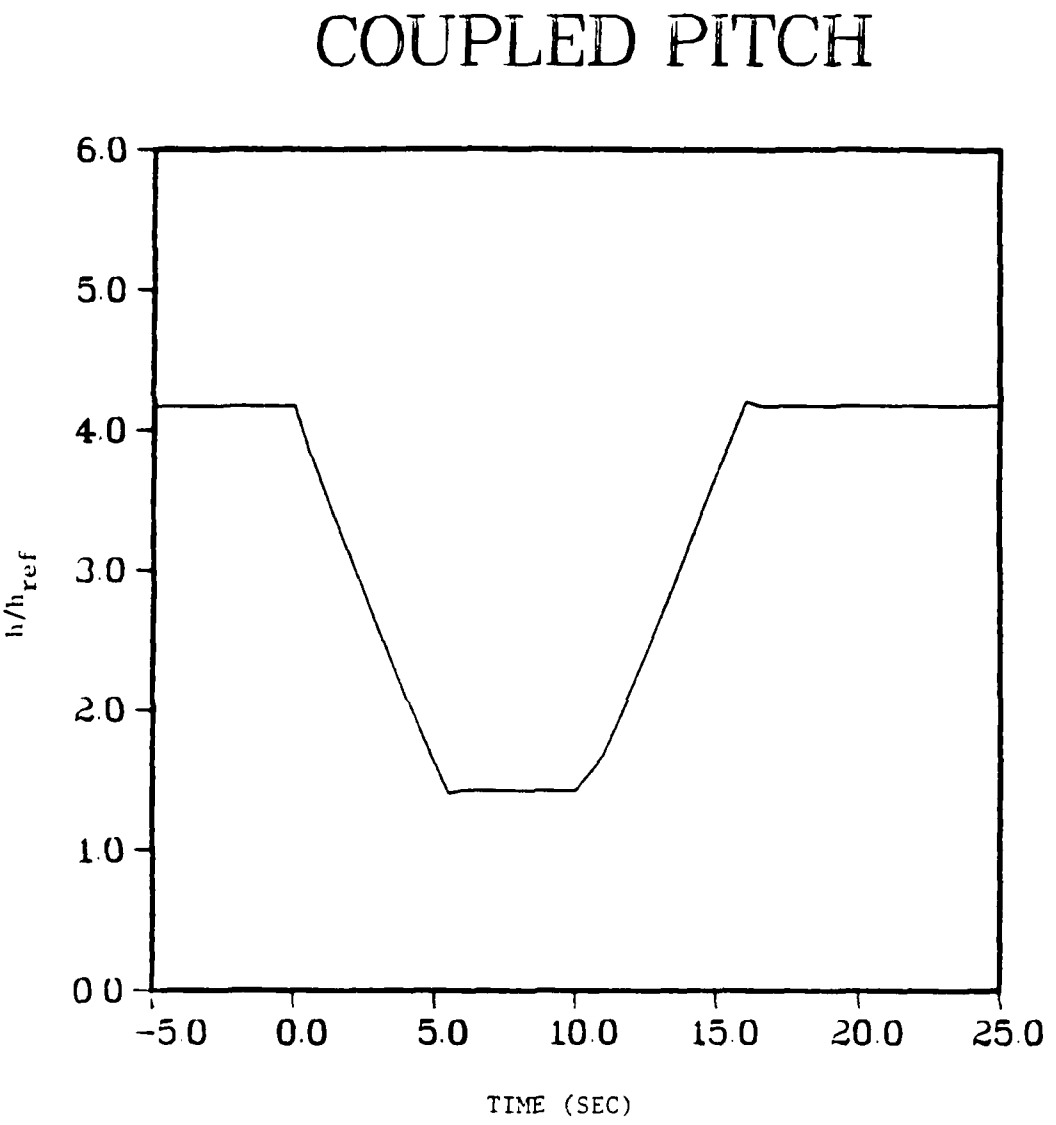

Figure 20 h/href Time History for x/L Location of .466667

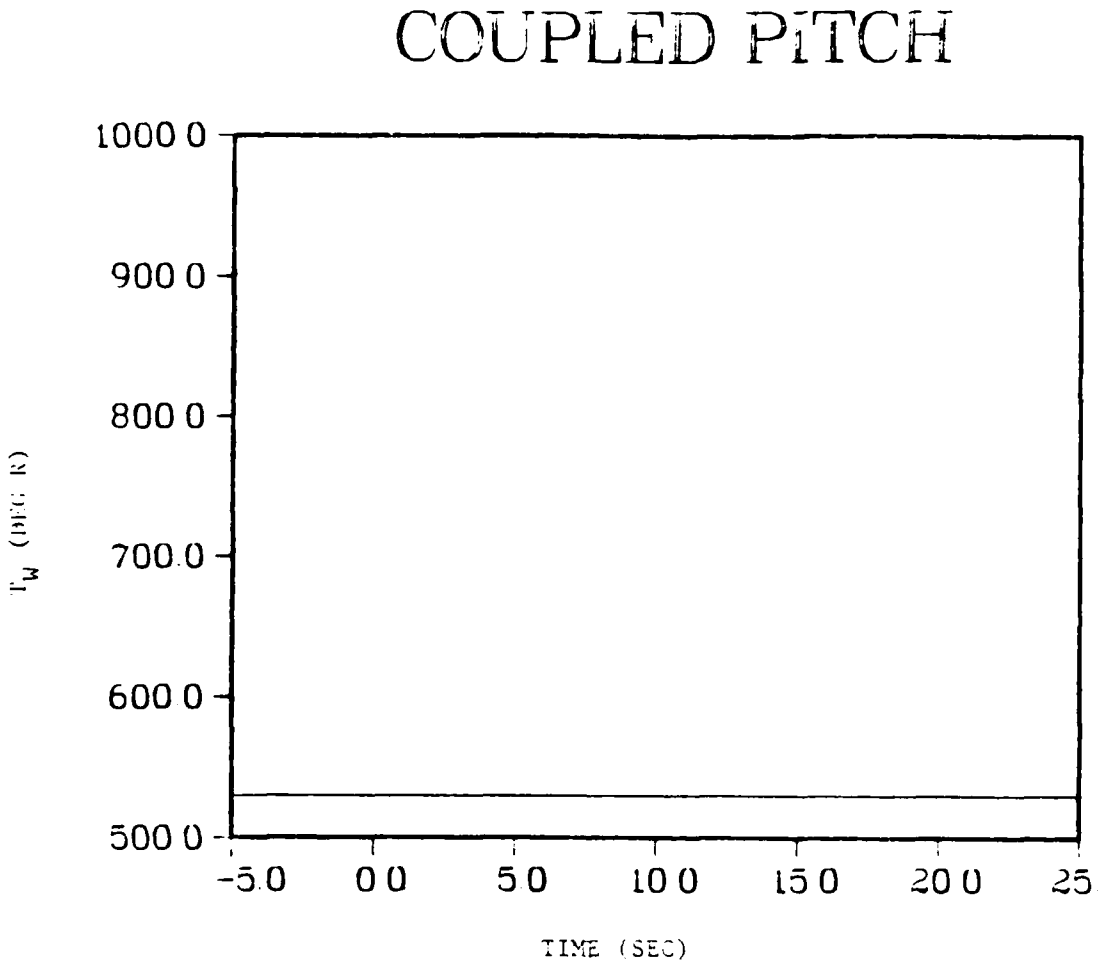

Figure 21 Wall Temperature Time History for x/L Location of .466667

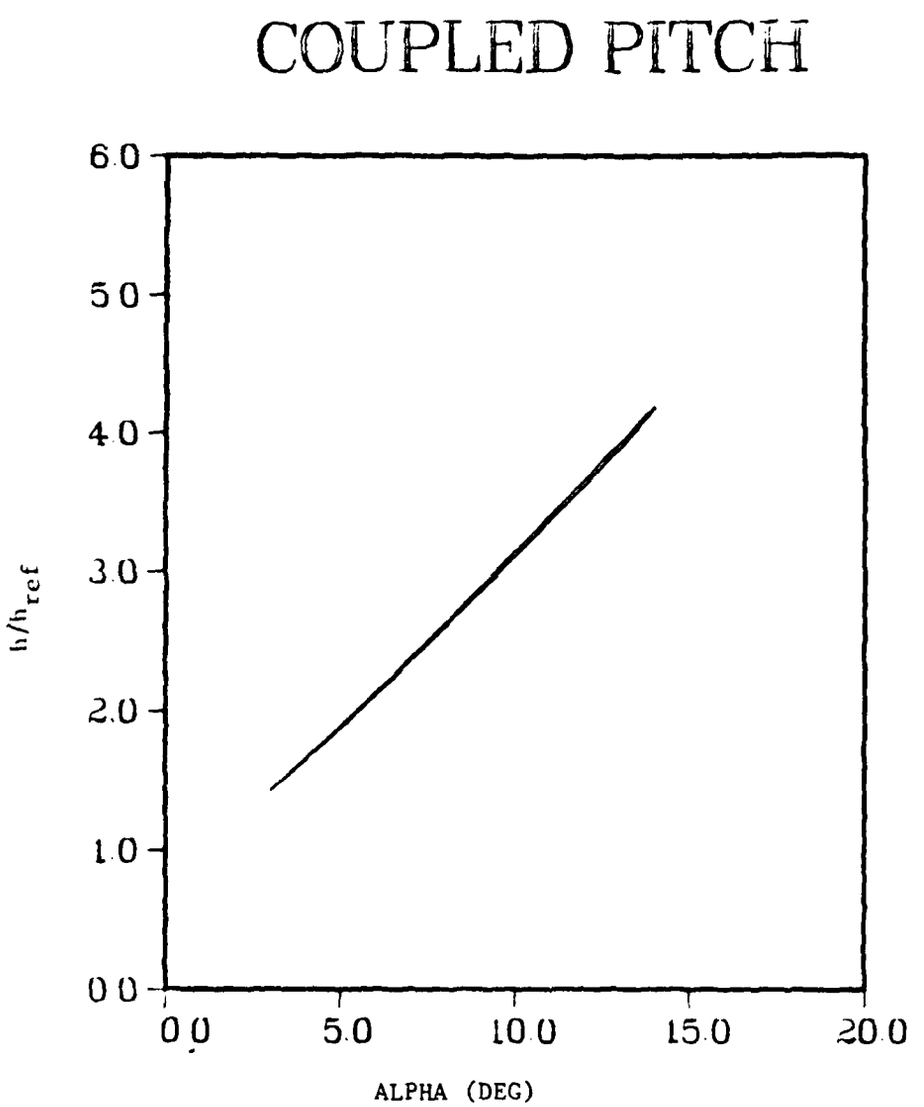

Figure 22 h/href versus Deflection Angle for x/L Location of .466667

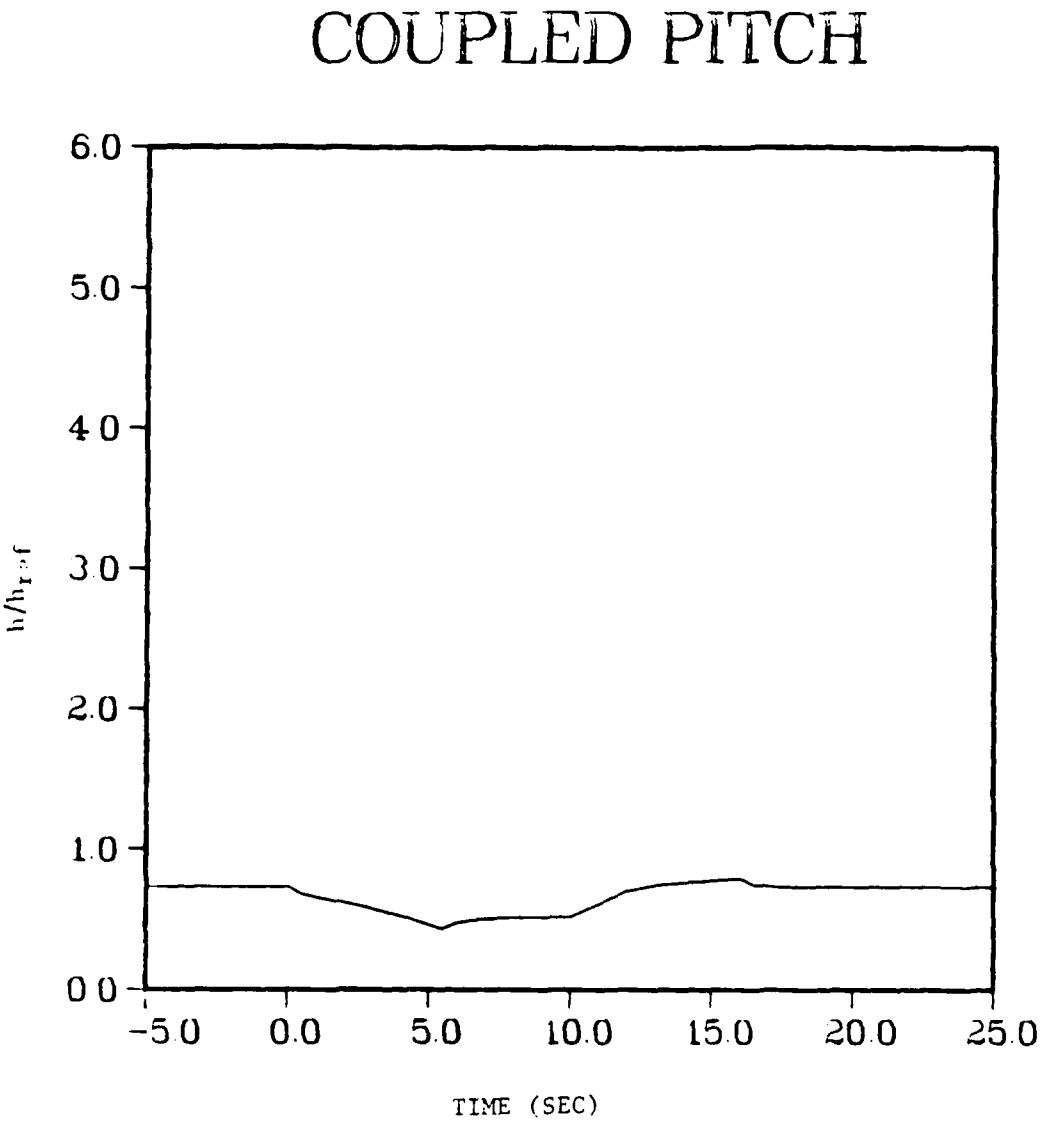

Figure 23 h/href Time History for x/L Location of .483333

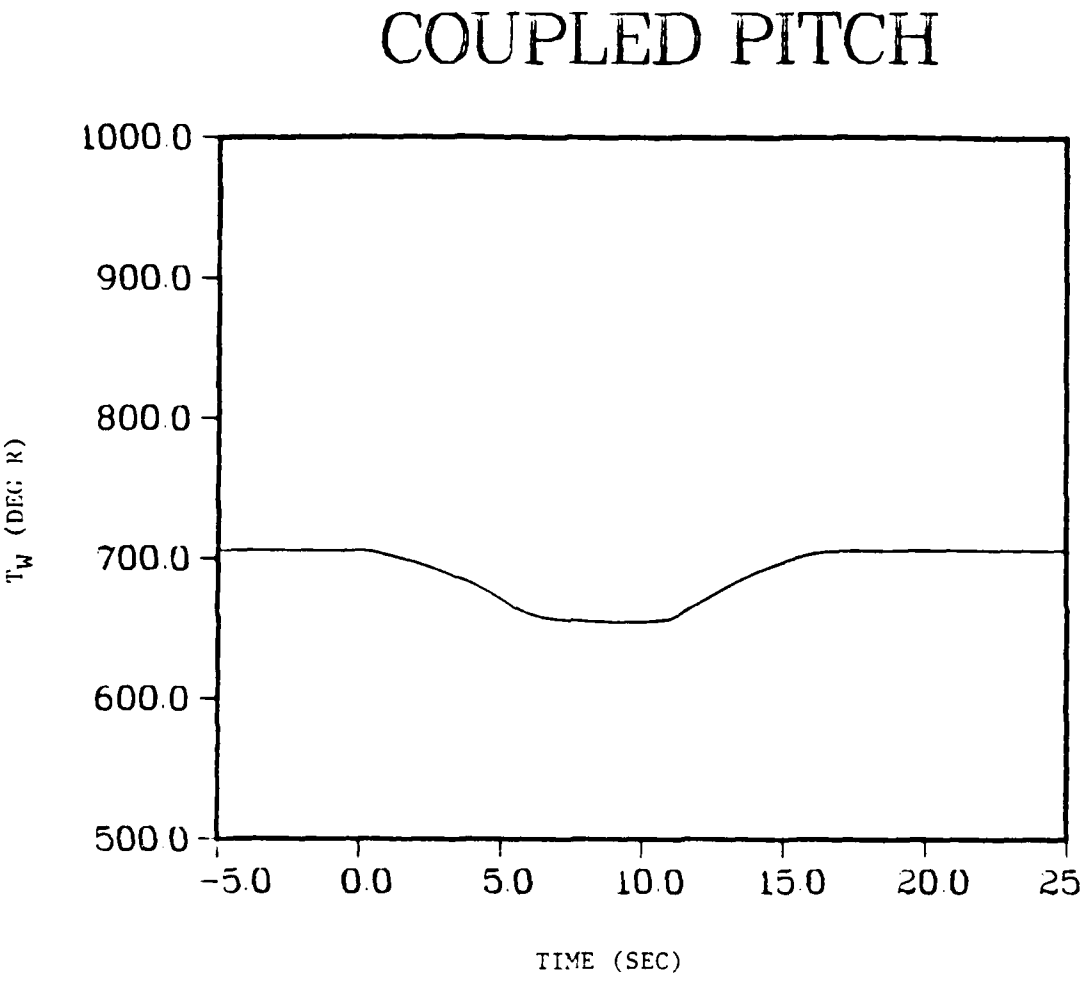

Figure 24 Wall Temperature Time History for x/L Location of .483333

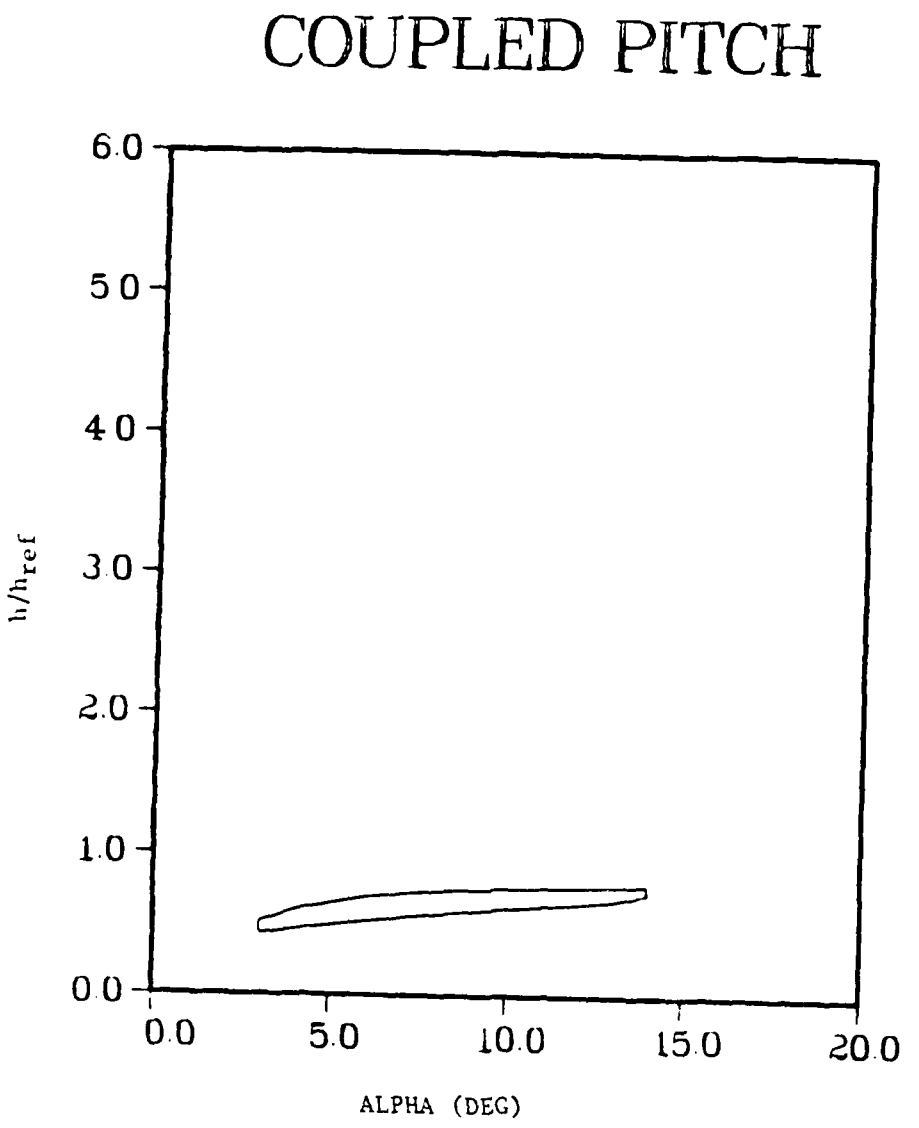

Figure 25 h/href versus Deflection Angle for x/L Location of .483333

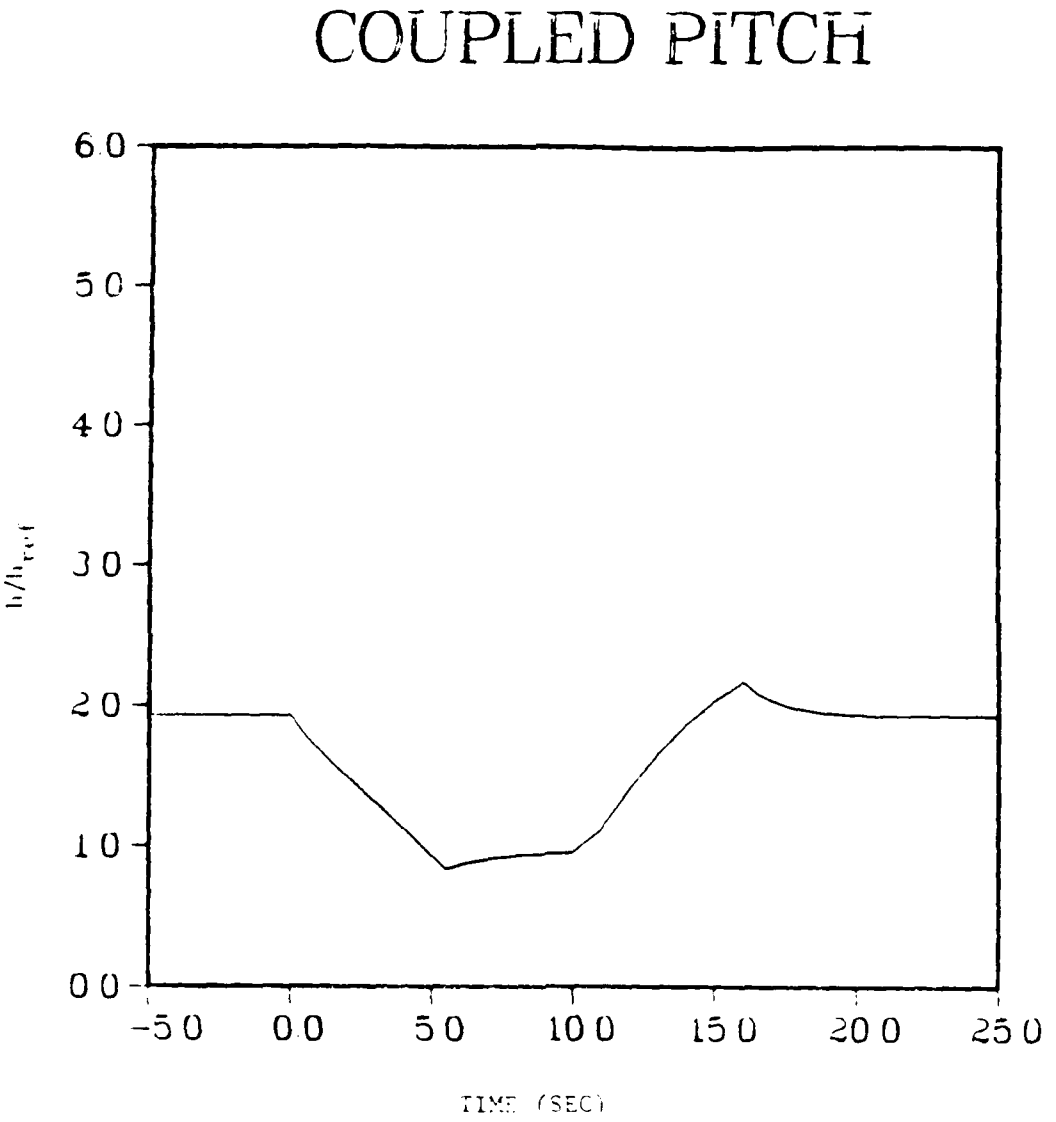

Figure 26 h/href Time History for x/L Location of .566667

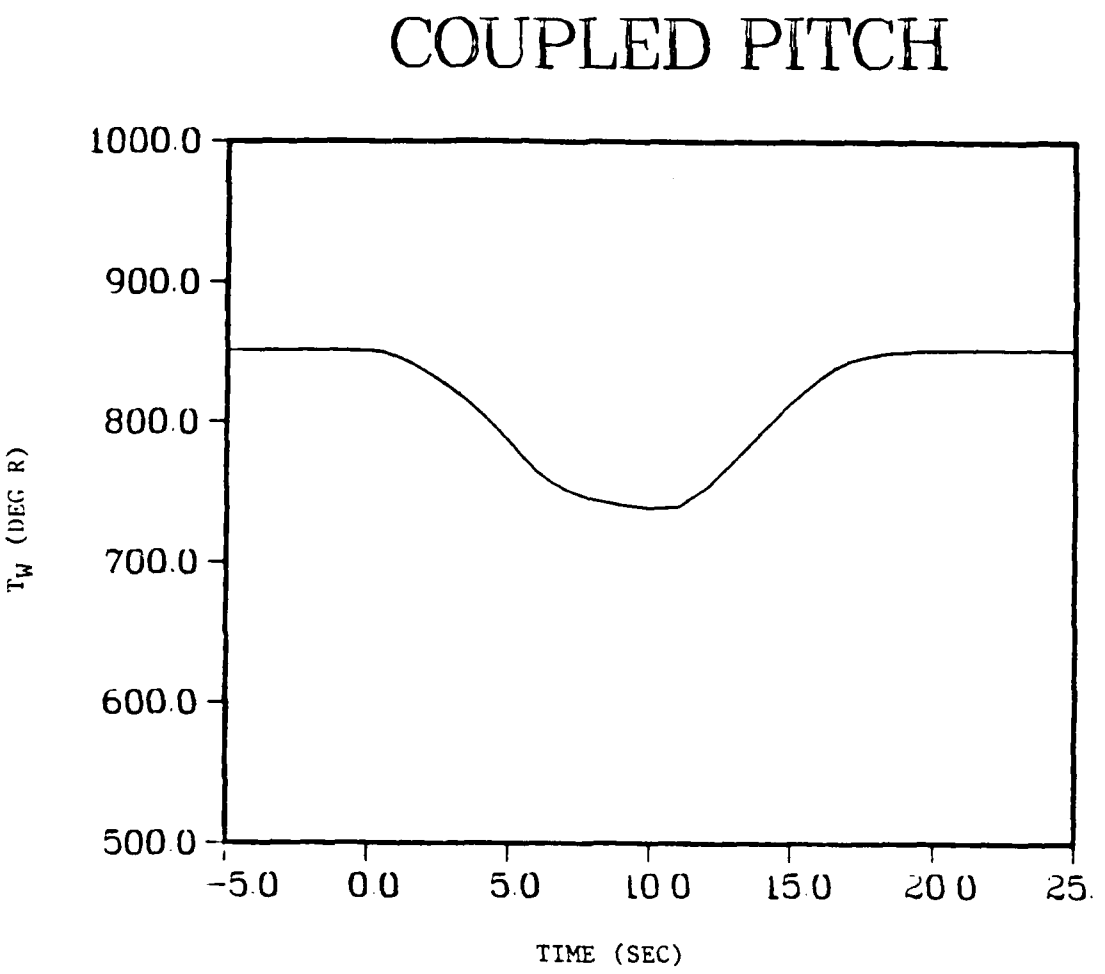

Figure 27 Wall Temperature Time History for x/L Location of .566667

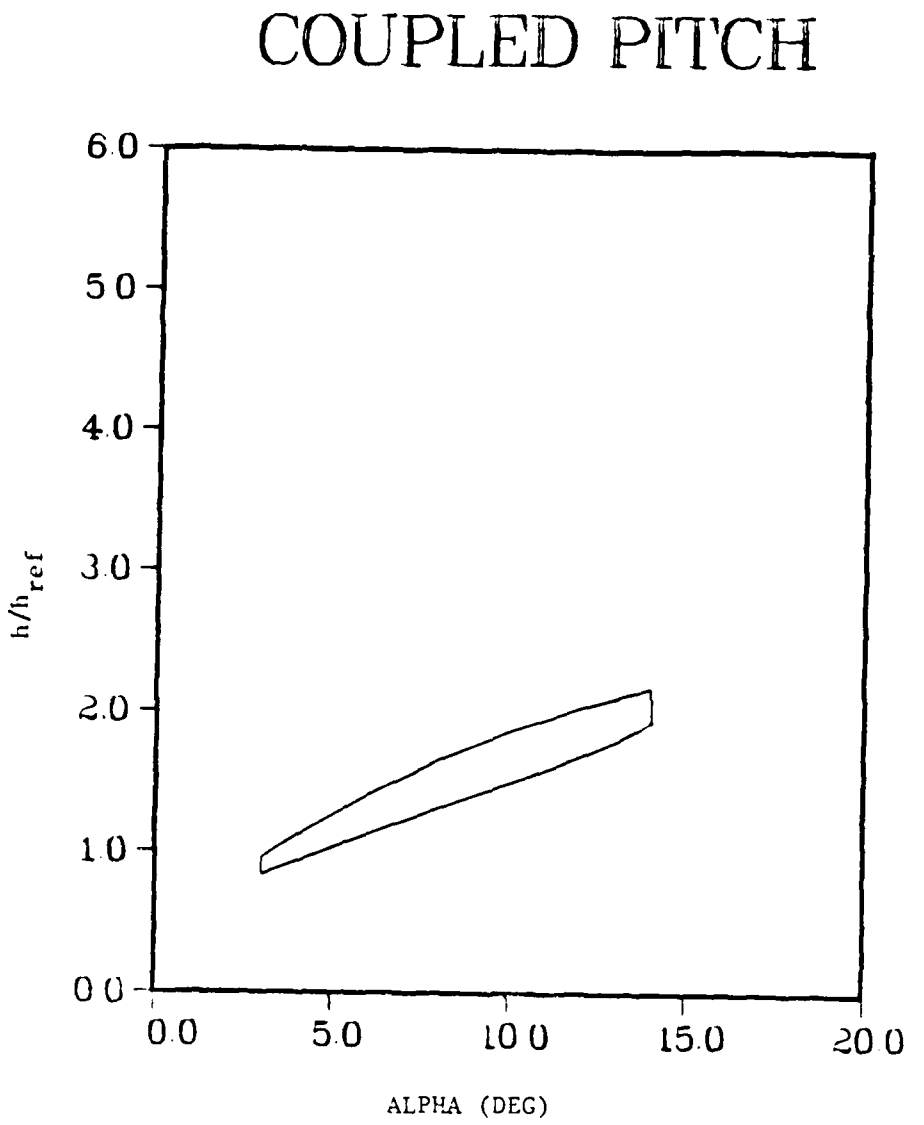

Figure 28 h/href versus Deflection Angle for x/L Location of .566667

leading edge of the plate, may be incorporated in this solution but it is impossible to separate them. Finally, the results show a large hysteresis at this location, which indicates a large time lag. This lag is mainly due to the large temperature gradients at this location and possibly some error due to the coarse grid.

Finally, near the end of the plate at a streamwise location of .983333, Figures 29, 30, and 31, the solution has relatively recovered. Figure 29 looks much like Figure 17 only at a lower heating rate. Some nonisothermal wall effects on Figure 29 are still noticeable at the 3 degrees and 14 degrees five second hold and are caused for the same reasons previously described. When h/h_{ref} is plotted versus the deflection angle, Figure 31, a lag due to nonisothermal effects still exists but less than at the previous location.

In conclusion, this pitching plate case with the wall temperature, as a function of the heat rate, does show a time lag due to nonisothermal wall effects. As the plate pitches the wall temperature lags and when the plate is held at a constant angle, the wall temperature changes until it reaches equilibrium which also causes the h/h_{ref} to change.

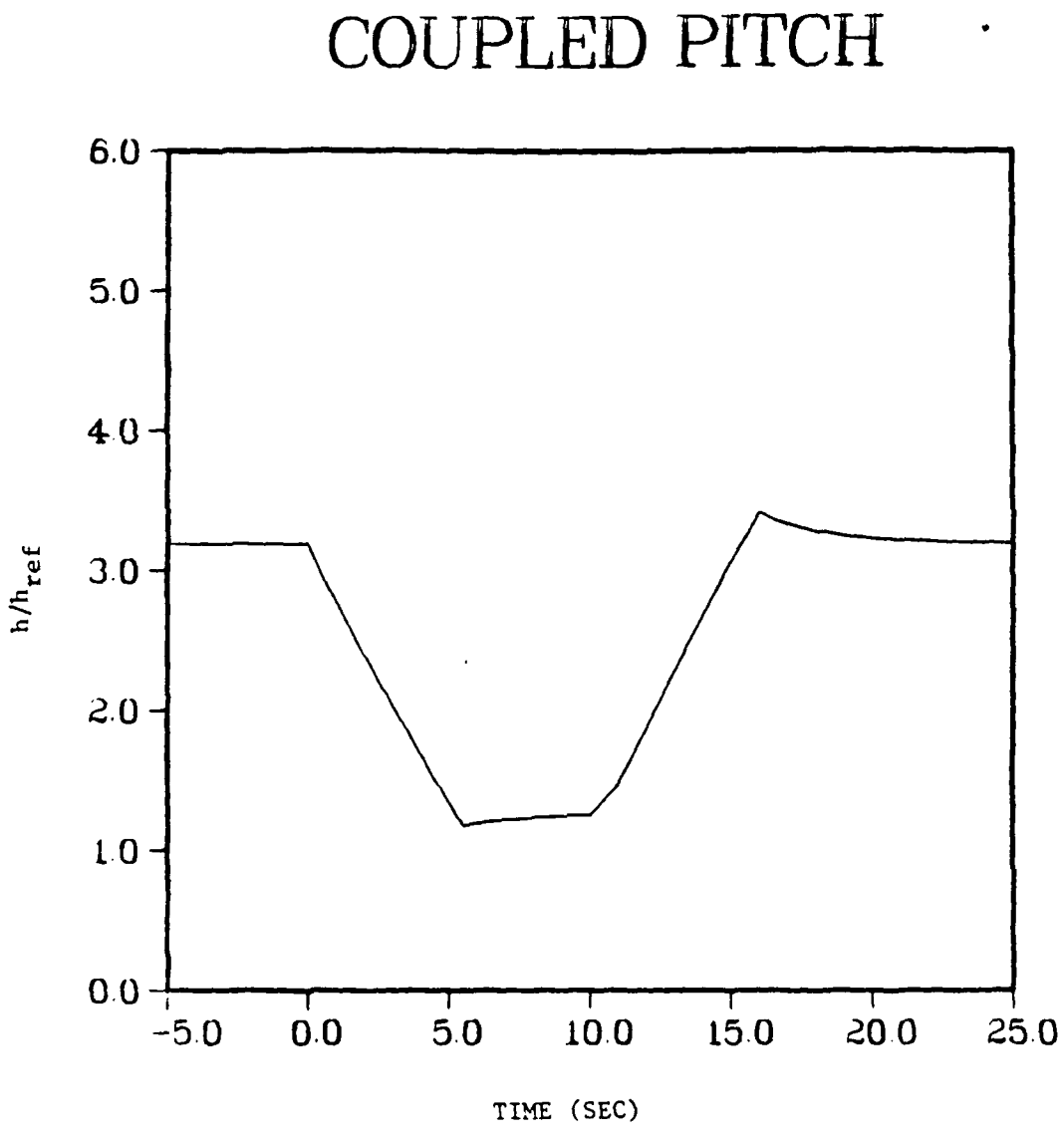

Figure 29 h/href Time History for x/L Location of .983333

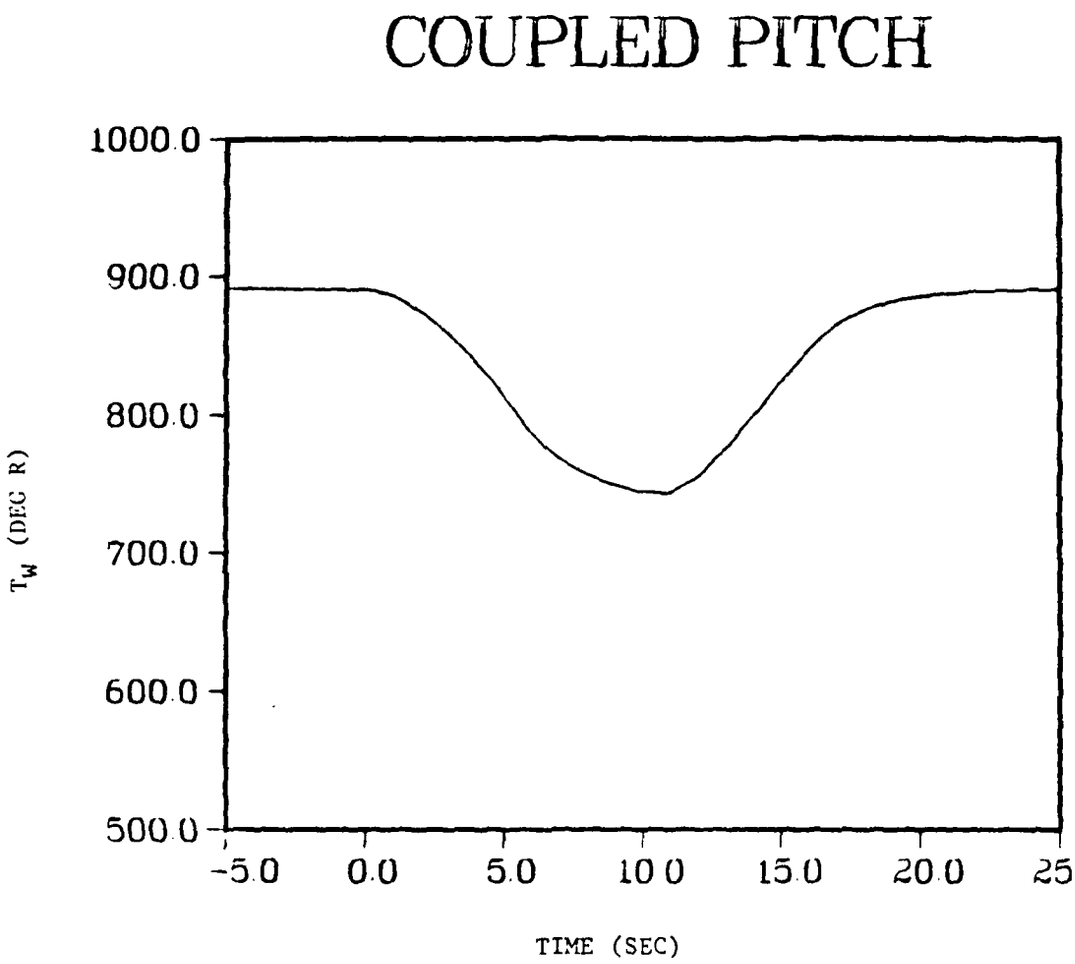

Figure 30 Wall Temperature Time History for x/L Location of .983333

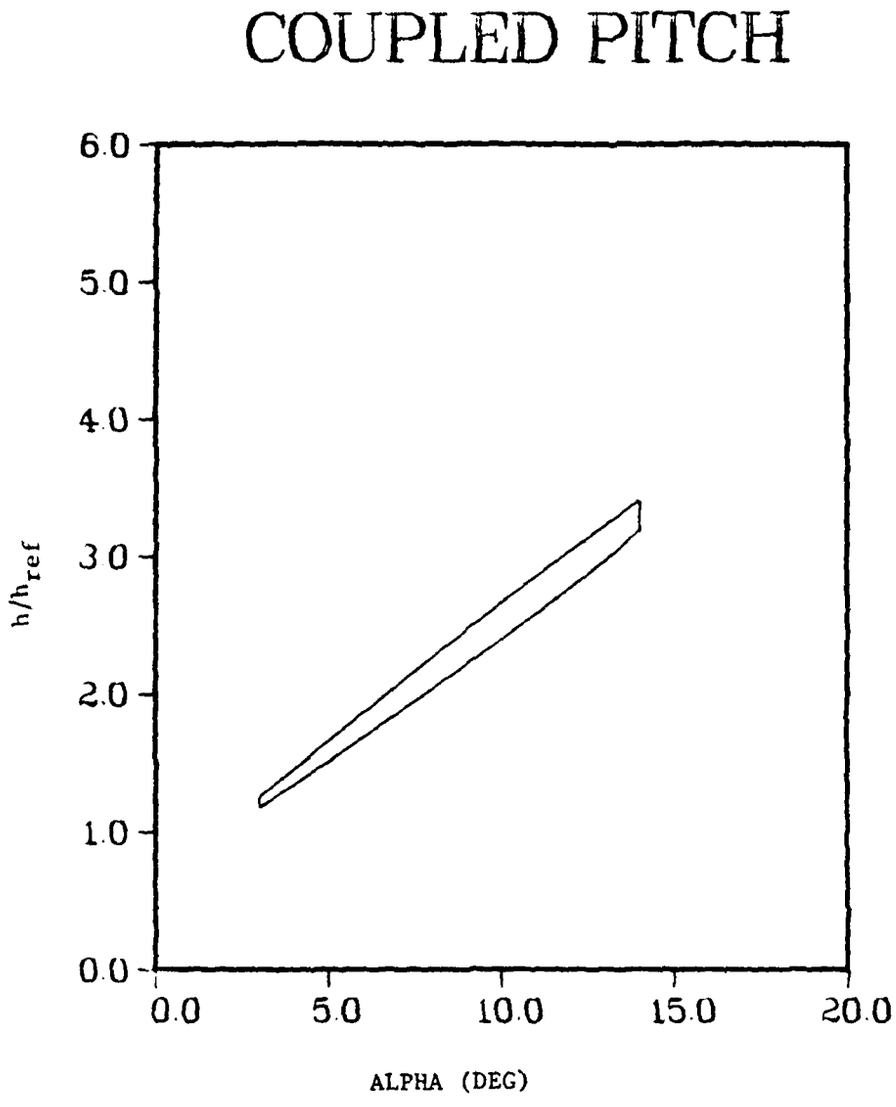

Figure 31 h/href versus Deflection Angle for x/L Location of .983333

V. Conclusions and Recommendations

Conclusions

The significant findings of this research can be put into two categories. One, the unique features of the code written to investigate nonisothermal wall effects, and two, the actual heat transfer results.

The code developed in this project solves the unsteady compressible boundary layer equations. In code development, the boundary layer equations are transformed using the Dorodnitsyn transformation. This is a unique feature because the equations can be solved much like the incompressible equations. These equations are then transformed to the computational plane and finite differenced. A three point upwind differencing scheme is used for the convective derivatives, a second order central difference is used for viscous terms, and the time terms use a first order backward difference. Finally, the momentum and energy equations are solved using optimized successive over-relaxation, and the continuity equation is solved for the V velocity by integration.

Another unique feature of this code is a generalized grid (as long as $X_\eta = 0$). This enables the program to handle various configurations. Although, if another grid is used, another method of handling the Y_ξ will have to be used because, at the present time, the analytical solution of Y_ξ based on the Blasius grid is used.

The grid used in the project is based on an optimized Blasius grid. When a compressible case is run, the grid must be adjusted by a grid factor to obtain enough points in the thermal boundary layer. Even with the adjustment, there are only 61 points in the streamwise direction and

30 points in the Y direction that go out a distance of 10 δ. This code has significantly fewer grid points than other schemes which will enable the code to run faster and less costly.

The boundary conditions also played an important part in this research. For the most complicated case, pitching a plate with a transient nonisothermal wall, both the edge conditions of the boundary layer and the wall temperature would change as the plate is pitched.

A final feature of this code is the way the leading edge start up is handled. When the code was first used for an isothermal case, error due to the leading edge was seen. A zero gradient is assumed at the leading edge and this greatly reduced the error. This similarity at the leading edge should be applicable to other problems if a small enough step is taken in the streamwise direction.

The code was used to solve for many cases, such as, an incompressible case, steady state isothermal and nonisothermal cases, transient wall temperature cases, and pitching plate cases, and the results are significant. The incompressible case and the isothermal cases were used as a program verification. The incompressible case compared well with the Blasius solution and the isothermal cases well with the approximate isothermal Eckert theory. From the isothermal cases it can be seen that the code solutions are very grid dependent. The nonisothermal cases followed the same trend as the approximate nonisothermal solution given by Eqn 32. It demonstrates the same dramatic decrease in the heat transfer coefficient just downstream of the temperature jump and the subsequent slow recovery. The transient nonisothermal wall displayed the same trend. In addition, the transient

cases both converged as time is marched. No lag due to change in wall temperature was evident but the time step may have been too big to see the small effect. An interesting outcome of the transient case with the wall temperature being a function of the heat rate is that the wall temperature is higher than wind tunnel wall temperature. Finally, the pitching plate cases were examined. The pitched plate with an isothermal wall temperature was used to investigate the error due to the first order time difference. Between .Ø5 and .Ø25 seconds, there was less than 2 percent change for a X/L location of .5 and an α of 12 degrees. The pitching plate with the wall temperature as a function of the heat rate yielded some very significant results. A significant hysteresis is not evident at the beginning of the plate and, after the interface a hysteresis due to nonisothermal effects does exist, more dramatically close to the interface than at the end of the plate.

This research has been significant in understanding the nonisothermal wall effects for the FRSI and HRSI used on the Shuttle. Other locations on the Shuttle can be identified where nonisothermal wall effects will impact. Even though this project was based on a Space Shuttle application, the code could and should be used in other applications.

Recommendations

The following is a list of recommendations set in an order of priority, even though, many of the items could be investigated independently.

1) The grid should be optimized for a nonisothermal wall.

2) A turbulence model should be added so the full boundary layer regime can be investigated.

3) Modify the equations for axisymmetric problems and, along the same lines, make the equations three dimensional.

4) Add the pressure gradient term to the momentum equation which was assumed to be zero in these applications.

5) Using the same Dorodnitsyn transformation and the similarity solution at the leading edge, investigate shock-fitting and shock capturing schemes for the parabolized Navier-Stokes Equations.

6) Investigate different finite difference solvers such as the tridiagonal solver.

7) Couple this program with a conduction model to allow conduction through the wedge.

Appendix A

Dorodnitsyn's Transformation of the boundary Layer Equations

This project is based on the solution of the boundary layer equations. The Dorodnitsyn transformation allowed the compressible unsteady boundary layer equations to be solved similar to the incompressible unsteady equations. The details of the transformation are included here for reference.

The unsteady compressible boundary layer equations are nondimensionalized by

$$x = \frac{x'}{L'} \qquad y = \frac{y'}{L'} \qquad t = \frac{t'}{L'/U'_\infty} \qquad u = \frac{u'}{U'_\infty} \qquad v = \frac{v'}{U'_\infty} \tag{A-1}$$

$$\mu = \frac{\mu'}{\mu'_\infty} \qquad \rho = \frac{\rho'}{\rho'_\infty} \qquad H = \frac{H'}{U'^2_\infty} \qquad T = C'_p T' \frac{}{U'^2_\infty} \qquad P = \frac{P'}{\rho'_\infty U'^2_\infty}$$

and become

continuity
$$\frac{\partial \rho}{\partial t} + \frac{\partial \rho u}{\partial x} + \frac{\partial \rho v}{\partial y} = 0 \tag{A-2}$$

x-momentum
$$\rho \frac{\partial u}{\partial t} + \rho u \frac{\partial u}{\partial x} + \rho v \frac{\partial u}{\partial y} = -\frac{\partial P}{\partial x} + \frac{\partial}{\partial y}\left(\frac{\mu}{Re} \frac{\partial u}{\partial y}\right) \tag{A-3}$$

energy
$$\rho \frac{\partial H}{\partial t} + \rho u \frac{\partial H}{\partial x} + \rho v \frac{\partial H}{\partial y} = \frac{\partial P}{\partial t} + \frac{\partial}{\partial y}\left(\frac{\mu}{RePr} \frac{\partial H}{\partial y}\right) +$$

$$\frac{\partial}{\partial y}\left(\frac{\mu(1-\frac{1}{Pr})}{Re} \frac{\partial U^2/2}{\partial y}\right) \tag{A-4}$$

in nonconservative form. The Reynolds number (Re) and Prandtl number (Pr) are defined as

$$Re = \frac{\rho'_\infty u'_\infty L'}{\mu'_\infty} \tag{A-5}$$

$$Pr = \frac{\mu' c_p'}{k'} \tag{A-6}$$

The Dorodnitsyn transformation (9:2-4)

$$X = x \qquad Y = \int_0^y \rho \, dy \qquad t'' = t$$

$$U = u \qquad V = \rho v + \frac{\partial Y}{\partial t} + u \frac{\partial Y}{\partial x} \tag{A-7}$$

is used to transform the equations, A-2 to A-4, into a form similar to the incompressible equations. Using the chain rule, $\frac{\partial u}{\partial x}$ can be defined as

$$\frac{\partial u}{\partial x} = \frac{\partial U}{\partial X}\frac{\partial X}{\partial x} + \frac{\partial U}{\partial Y}\frac{\partial Y}{\partial x} + \frac{\partial U}{\partial t''}\frac{\partial t''}{\partial x} \tag{A-8}$$

where $\frac{\partial X}{\partial x} = 1$ and $\frac{\partial t''}{\partial x} = 0$. Therefore,

$$\frac{\partial u}{\partial x} = \frac{\partial U}{\partial X} + \frac{\partial U}{\partial Y}\frac{\partial Y}{\partial x} \tag{A-9}$$

Similarly,

$$\frac{\partial u}{\partial y} = \rho \frac{\partial U}{\partial Y} \tag{A-10}$$

where $\frac{\partial Y}{\partial y} = \rho$ and $\frac{\partial t'}{\partial y} = \emptyset$.

Substituting these quantities into the continuity equation gives

$$\frac{\partial \rho}{\partial t} + \rho \frac{\partial U}{\partial X} + \frac{\partial U}{\partial Y}\frac{\partial Y}{\partial x} + u\frac{\partial \rho}{\partial x} + \frac{\partial V}{\partial y} - \frac{\partial^2 Y}{\partial y \partial t} - \frac{\partial u}{\partial y}\frac{\partial Y}{\partial x} - u\frac{\partial^2 Y}{\partial y \partial x} = \emptyset \quad \text{(A-11)}$$

allowing terms $\frac{\partial \rho}{\partial t}$, $u\frac{\partial \rho}{\partial x}$, and $\rho\frac{\partial U}{\partial Y}\frac{\partial Y}{\partial x}$ to cancel with terms $-\frac{\partial^2 Y}{\partial y \partial t}$, $-u\frac{\partial^2 Y}{\partial y \partial x}$, and $\frac{\partial u}{\partial y}\frac{\partial Y}{\partial x}$ respectively. This results in the continuity equation becoming like the incompressible form

$$\frac{\partial U}{\partial X} + \frac{\partial V}{\partial Y} = \emptyset \quad \text{(A-12)}$$

The same procedure is used for the momentum equation. Beginning with the nonconservative momentum equation, Eqn A-3, and again substituting and canceling terms, the equation becomes

$$\frac{\partial U}{\partial t'} + U\frac{\partial U}{\partial X} + V\frac{\partial U}{\partial Y} = -\frac{1}{\rho}\frac{\partial P}{\partial X} + \frac{\partial}{\partial Y}\left(\frac{\mu \rho}{Re}\frac{\partial U}{\partial Y}\right) \quad \text{(A-13)}$$

Taking a closer look at $\frac{\partial P}{\partial x}$,

$$\frac{\partial P}{\partial x} = \frac{\partial P}{\partial X}\frac{\partial X}{\partial x} + \frac{\partial P}{\partial y}\frac{\partial Y}{\partial x} + \frac{\partial P}{\partial t''}\frac{\partial t''}{\partial x} \quad \text{(A-14)}$$

Since $\frac{\partial P}{\partial Y} = \emptyset$ and $\frac{\partial t''}{\partial x} = \emptyset$,

$$\frac{\partial P}{\partial x} = \frac{\partial P}{\partial X} \quad \text{(A-15)}$$

This same procedure is used to show that $\frac{\partial P}{\partial t}$ is equal to $\frac{\partial P}{\partial t''}$ in the energy equation and that the energy equation becomes

$$\frac{\partial H}{\partial t''} + U\frac{\partial H}{\partial X} + V\frac{\partial H}{\partial Y} = \frac{1}{\rho}\frac{\partial P}{\partial t''} + \frac{\partial}{\partial Y}\left(\frac{\mu\rho}{RePr}\frac{\partial H}{\partial Y}\right) + \frac{\partial}{\partial Y}\left(\frac{\mu(1-\frac{1}{Pr})\rho}{Re}\frac{\partial}{\partial Y}U^2/2\right) \quad \text{(A-16)}$$

AD-A164 185 UNSTEADY SOLUTION OF THE BOUNDARY LAYER EQUATIONS WITH APPLICATION TO SPA..(U) AIR FORCE INST OF TECH WRIGHT-PATTERSON AFB OH SCHOOL OF ENGI.. K J LANGE 2/2

UNCLASSIFIED JUN 85 AFIT/GAE/ENY/84D-11 F/G 20/13 NL

END

FILMED

DTIC

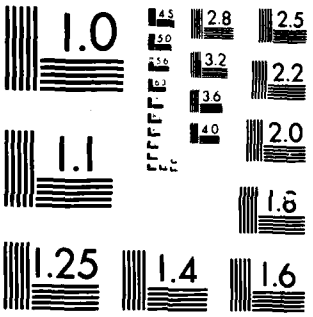

MICROCOPY RESOLUTION TEST CHART
NATIONAL BUREAU OF STANDARDS 1963 A

Appendix B

THESIS Computer Code

```
      PROGRAM THESIS(INPUT,OUTPUT,TAPE5=INPUT)
      COMMON/RESTRT/TIME,X(61),Y(61,30),U(61,0:31),V(61,30),
     &             H(61,0:31),W(30)
      DIMENSION A(10000)
      EQUIVALENCE (A,TIME)
      DIMENSION DX(61),DY(61,30),DYXI(61,30),DYB(61,30),DYF(61,30),
     &          ETAX(61,30),RHO(30),RM(30),T(30),DYRE(61,30),
     &          UNW1(61,30),HNW1(61,30),VNW1(61,30),UIM1(30),
     &          HIM1(30),UIM2(30),HIM2(30),QI(61),HWREF(61),TW(61),
     &          YP(61,30)
      REAL LAM,MU,MUINF,L,MINF,MUW
      INTEGER RST,CNT
      DATA IMAX,JMAX,NT,CNT,KT,NTW,RST/61,30,010,010,99,005,0/
      DATA MINF,UINF,RINF,TINF,TOINF/14.237,4848.,.6048E-5,48.3,2020./
      DATA DT,CP,L,PR,GAM,EPS/.1000,6008.,1.25,.72,1.4,.00001/
      ANGLE OF ATTACK (ALPHA)=14 DEG
      DATA UE,PE,TE,DPDT,TW1,TW2/4839.8,11.08,227.99,0.0,530.,530./
      OPEN(UNIT=8,FILE='RESTART',FORM='UNFORMATTED')
      OPEN(UNIT=9,FILE='PLT3D14')
      OPEN(UNIT=10,FILE='THSSOP')
      OPEN(UNIT=11,FILE='GRID')
      REWIND 11
C
C
CCCCCCCCCCCCCCCCCCCCCCCCCCCCCCCCCCCCCCCCCCCCCCCCCCCCCCCCCCCCCCCCCCCCCCC
C   THIS PROGRAM SOLVES THE UNSTEADY BOUNDARY LAYER EQUATIONS
C   ALSO IT SOLVES FOR THE HEAT RATE AT THE WALL AND DETERMINES
C   A HEAT TRANSFER COEFFICIENT
C
C
C     SYMBOLS
C     CNT             THE NUMBER OF TIME STEPS BETWEEN PRINTOUT
C     CP              COEFFICIENT OF HEAT
C     DX              DERIVATIVE OF X WRT XI
C     DY              DERIVATIVE OF Y WRT ETA
C     DYXI            DERIVATIVE OF Y WRT XI
C     DYB             Y DIFFERENCE BETWEEN J AND J-1
C     DYC             CENTRAL Y DIFFERENCE
C     DYF             Y DIFFERENCE BETWEEN J+1 AND J
C     DT              DELTA TIME
C     EPS             CONVERGENCE EPSILON
C     EMAX            MAX ERROR
C     GAM             RATIO OF SPECIFIC HEATS (GAMMA)
C     H               TOTAL ENTHALPY
C     HNW1            TOTAL ENTHALPY AT OLD TIME LEVEL
C     HIM1            ENTHALPY AT I-1 LOCATION
C     HIM2            ENTHALPY AT I-2 LOCATION
C     HC              HEAT COEFFICIENT
C     HREF            REFERENCE HEAT COEFFICIENT
C     I               COUNTER IN XI DIRECTION
C     IMAX            MAX NUMBER OF STEPS IN XI DIRECTION
C     J               COUNTER IN ETA DIRECTION
C     JMAX            MAX NUMBER OF STEPS IN ETA DIRECTION
C     K               COUNTER IN ITERATIONS
C     KT              MAX NUMBER OF ITERATIONS
C     L               LENGTH OF PLATE (FEET)
C     MINF            MACH AT INFINITY
C     MU              VISCOSITY, NONDIMENSIONAL
C     MUINF           VISCOSITY AT INITITY CONDITIONS
C     N               COUNTER IN TIME
C     NT              MAX NUMBER OF TIME STEPS
C     NTW             NUMBER OF TIME STEPS TO CALCULATE OMEGA
C     PRESS           NONDIMENSIONALIZED EDGE PRESSURE
C     PR              PRANDTL NUMBER
C     PE              PRESSURE AT THE EDGE OF THE BOUNDARY LAYER
C     Q               HEAT RATE AT THE WALL
```

```
C     RHO                 DENSITY
C     RM                  DENSITY TIMES VISCOSITY
C     RE                  REYNOLD'S NUMBER
C     RST                 RESTART INDICATOR
C     RINF                DENSITY AT INFINITY CONDITIONS (SLUG/FT**3)
C     T                   TEMPERATURE
C     TIME                TOTAL TIME ACCUMULATED
C     TW                  TEMPERATURE AT THE WALL
C     TE                  TEMPERATURE AT THE EDGE OF THE BOUNDARY LAYER
C     TINF                TEMPERATURE AT INFINITY (DEG RANKINE)
C     TOINF               TOTAL TEMPERATURE AT INFINITY (DEG RANKINE)
C     U                   VELOCITY IN X DIRECTION
C     UNM1                VELOCITY IN X DIRECTION AT OLD TIME LEVEL
C     UE                  VELOCITY AT THE EDGE OF THE BOUNDARY LAYER
C     UIM1                VELOCITY VECTOR AT I-1 LOCATION
C     UIM2                VELOCITY VECTOR AT I-2 LOCATION
C     UINF                VELOCITY AT INFINITY CONDITION (FT/SEC)
C     V                   VELOCITY IN Y DIRECTION
C     VNM1                VELOCITY IN Y DIRECTION AT OLD TIME LEVEL
C     W                   OPTIMIZATION OMEGA
CCCCCCCCCCCCCCCCCCCCCCCCCCCCCCCCCCCCCCCCCCCCCCCCCCCCCCCCCCCCCCCCCCCCCCCCCCC
C
      PRINT*,'NT,CNT,KT,RST='
      READ*,NT,CNT,KT,RST
      PRINT*,'DT,EPS='
      READ*,DT,EPS
      PRINT*,'FSOR='
      READ*,FSOR
      REWIND 10
      REWIND 9
      JMM1=JMAX-1
      GGM1=GAM/(GAM-1.)
      MUINF=(TINF**1.5*2.27E-8)/(TINF+198.6)
      COSJ=COS(3.14159/FLOAT(JMAX))*FSOR
      RE=RINF*UINF*L/MUINF
      PRESS=PE/(RINF*UINF**2.)
      TIME=0
      ALPHA=14.0
      HREF=.332*CP*SQRT(MUINF*RINF*UINF)/PR**(2./3.)
C
C     DA IS THE 2 DEG/SEC PITCH RATE NONDIMESIONALIZED TIME
      DA=2*L/UINF
C
C     TS IS THE NONDIMESIONAL TIME TO PITCH 11 DEG(14DEG-3DEG)
      TS=11/DA
      NTS=TS + 5*UINF/L
      NNTS=NTS + TS
C
C     DEFINE THE WALL TEMPERATURES-- IF TW1=TW2 NO TEMP STEP
C                                   IF TW1<TW2 TEMP STEP
C
      DO 11 I=1,IMAX
        IF(I.LE.28)THEN
        TW(I)=TW1
        ELSE
        TW(I)=TW2
        ENDIF
11    CONTINUE
C
C     GENERATE A GRID AND INITIAL CONDITIONS
C
      CALL FIRST(IMAX,JMAX,RE,CP,TW,TE,UE,UINF,PRESS,GGM1,X,Y,U,V,H,PR)
      DO 10 I=1,IMAX
        U(I,0)=0
        H(I,0)=0.0
```

```
        U(I,J)=0.0
        H(I,J)=0.0
10    CONTINUE
C
C     IF RESTARTING THE PROBLEM, READ THE INITIAL GUESS FROM TAPE 8
C
      REWIND 8
      IF(IRST.EQ.1)READ(8)A,TW
      PRINT*,'ALPHA,TIME='
      READ*,ALPHA,TIME
      PRINT*,'RC,DA='
      READ*,RC,DA
        CALL TERPO(ALPHA,UINF,RINF,CP,UE,PE,HE)
        DO 1888 I=1,IMAX
          U(I,JMAX)=UE
          H(I,JMAX)=HE
1888  CONTINUE
        PRESS=PE
      DA=DA*L/UINF
      RC=RC*UINF/L
      IF(ABS(DA).GT.1.E-10)THEN
         TS=11./DA
         NTS=TS+5.*UINF/L
         NNTS=NTS+TS
      END IF
C
C     CALCULATE DERIVATIVES XI WRT X, ETA WRT Y, AND ETA WRT X
C     XI WRT X EQUALS 1/DX, ETA WRT Y EQUALS 1/DY, AND
C     ETA WRT X EQUALS -DYXI/(DX*DY)
C
      DO 30 I=2,IMAX
        IM1=I-1
        IM2=I-2
        IP=I+1
        IF(I.EQ.IMAX)THEN
          DX(I)=X(I)-X(IM1)
        ELSE
          DX(I)=(X(IP)-X(IM1))/2.
        ENDIF
        DO 30 J=2,JMM1
          JP=J+1
          JM1=J-1
          JM2=J-2
            DY(I,J)=(Y(I,JP)-Y(I,JM1))/2.
          IF(I.EQ.IMAX)THEN
            DYXI(I,J)=Y(I,J)-Y(IM1,J)
          ELSE
            DYXI(I,J)=Y(I,J)*.5/(I-1)
          ENDIF
          DYB(I,J)=Y(I,J)-Y(I,JM1)
          DYC=(Y(I,JP)-Y(I,JM1))/2.
          DYF(I,J)=Y(I,JP)-Y(I,J)
          ETAX(I,J)=-DYXI(I,J)/(DX(I)*DY(I,J))
          DYRE(I,J)=1./(DYC*RE)
30    CONTINUE
C
C     PUT INFORMATION INTO THE OLD TIME LEVEL INITIALLY
C
      DO 40 I=1,IMAX
        DO 40 J=1,JMAX
          UNM1(I,J)=U(I,J)
          VNM1(I,J)=V(I,J)
          HNM1(I,J)=H(I,J)
          W(J)=1.0
40    CONTINUE
```

```
      DO 43 J=1,11
        W(J)=1.6-(J-1)*.06
43    CONTINUE
C
C     START THE TIME LOOP
C
      DO 500 N=1,NT
        TIME=TIME+DT
C
      IF(TIME.LE.0.)GO TO 2001
      IF(TIME.GT.(NNTS+DT))GO TO 2001
C     THIS SECTION PITCHES THE PLATE FROM 14 DEG TO 3 DEG AND BACK TO 14
C
        IF (TIME.LE.TS)ALPHA=ALPHA - DA*DT
C
        IF(ALPHA.LE.3.0)ALPHA=3.0
        IF(TIME.GT.TS.AND.TIME.LE.NTS)ALPHA=3.0
        IF(TIME.GT.NTS.AND.TIME.LE.NNTS)ALPHA=ALPHA + DA*DT
        IF(ALPHA.GE.14.)ALPHA=14.0
        IF(TIME.GT.NNTS)ALPHA=14.
        CALL TERPO(ALPHA,UINF,RINF,CP,UE,PE,HE)
        DO 2000 I=1,IMAX
          U(I,JMAX)=UE
          H(I,JMAX)=HE
2000  CONTINUE
        DPDT=(PRESS - PE)
        PRESS=PE

 2001 CONTINUE
      IF(N.EQ.1)GO TO 2003
      DO 2002 I=2,IMAX
      IF(X(I).GE..466667)THEN
      IF(Q(I).GT.0.)THEN
      TEQ=(Q(I)/(776.3*.85*4.761E-13))**.25
      ELSE
      TEQ=0.
      END IF
      DTRC=DT/RC
      IF(DTRC.GT.34.)DTRC=34.
      EXPRC=EXP(-DTRC)
      TW(I)=TW(I)*EXPRC+(1.-EXPRC)*TEQ
      HW=CP*TW(I)/UINF**2+U(I,1)**2/2.
      H(I,1)=HW
      END IF
 2002 CONTINUE
 2003 CONTINUE
C     START BACK AT BEGINNING OF GRID--REINITIALIZE VECTORS
C
        DO 510 J=1,JMAX
          UIM1(J)=0.0
          HIM1(J)=0.0
510   CONTINUE
C
C     CALCULATE THE OPTIMIZATION FACTOR OMEGA EVERY NTW TIME STEPS
C
        IF(N.EQ.(N/NTW)*NTW)THEN
          DO 520 I=2,IMAX
C
C     COMPUTE THE DENSITY TIMES VISCOSITY FOR EVERY J LOCATION
C
            DO 525 J=1,JMAX
              TEMP=H(I,J)-U(I,J)**2/2.
              DEN=GGM1*PRESS/TEMP
              TEMP=TEMP*UINF**2/CP
            MU=(2.32E-8*TEMP**.5)/(1.+220./(TEMP*10.**(8./TEMP))))/MUINF
```

```
                RM(J)=DEN*MU
                W(J)=1.85
525         CONTINUE
C
C       COMPUTE OMEGA
C
            DO 530 J=2,JMM1
              JP=J+1
              JM=J-1
              DIV=1./DT + 1.5*(U(I,J)/DX(I) + ABS(U(I,J)*ETAX(I,J) +
     &            V(I,J)/DY(I,J))) + DYRE(I,J)*.5*
     &            ((RM(JP)+RM(J))/DYF(I,J) + ((RM(J)+RM(JM))/DYB(I,J)))
              LAM=(-2.*SQRT(ABS((ETAX(I,J)*U(I,J) + V(I,J)/DY(I,J)) +
     &          .5*DYRE(I,J)*((RM(J)+RM(JM))/DYB(I,J))) *
     &            (.5*DYRE(I,J)*((RM(JP)+RM(J))/DYF(I,J))))))/DIV*COSJ
            IF(LAM.GT.0.97)LAM=0.97
              WN=2./(1.+SQRT(1.-LAM**2.))
              IF(WN.LT.W(J))W(J)=WN
530         CONTINUE
520       CONTINUE
          ENDIF
C
C       START I LOOP--MARCH IN XI DIRECTION
C
          DO 400 I=2,IMAX
C
            DELM=0.0
C       PUT NEW INFORMATION INTO THE VELOCITY AND ENTHALPY VECTORS AT THE
C       I-1 AND I-2 LOCATIONS
C
            DO 410 J=1,JMAX
              UIM2(J)=UIM1(J)
              UIM1(J)=U(I-1,J)
              HIM2(J)=HIM1(J)
              HIM1(J)=H(I-1,J)
410         CONTINUE
C
C       DEFINE CONSTANTS TO DETERMINE THE COEFFICIENTS FOR THE U AND V
C       VELOCITY EQUATIONS AND THE ENTHALPY EQUATION
C
            IF(I.EQ.2)THEN
              CIJ1=1.
              CIM1=1.
              CIM2=0.
              CVIJ=-.5
              CVIM1=.5
              CVIM2=0.
            ELSE
              CIJ1=1.5
              CIM1=2.0
              CIM2=-.5
              CVIJ=-.75
              CVIM1=1.
              CVIM2=-.25
            ENDIF
C
C       START THE ITERATION LOOP
C
            DO 300 K=1,KT
              EMAX=0.0
            EUMAX=0.
            EVMAX=0.
            EHMAX=0.
C
C       CALCULATE NEW VALUES FOR TEMPERATURE,DENSITY, AND VISCOSITY USING
```

```
C     THE NEW VALUES OF U, V, AND H (CALCAYED AT THE OLD ITERATION LEVEL)
C
        DO 310 J=1,JMAX
          T(J)=H(I,J)-U(I,J)**2/2
          TEMP=T(J)*UINF**2./CP
          RHO(J)=GGM1*PRESS/T(J)
          MU=TEMP** .5*2.32E-8/(1.+220./(TEMP*10.**(8./TEMP)))/MUINF
          RM(J)=RHO(J)*MU
310     CONTINUE
C
C     START J LOOP--MARCHING IN ETA DIRECTION
C
        DO 200 J=JMM1,2,-1
          JM1=J-1
          JM2=J-2
          JP=J+1
          UOLD=U(I,J)
          HOLD=H(I,J)
          IF(K.EQ.1)THEN
            WOPT=1.0
          ELSE
            WOPT=W(J)
          ENDIF
C
C     SETUP CONSTANTS TO DETERMINE COEFFICIENTS IN U, V, AND H EQUATIONS
C
C
C     SOLVE FOR U,V,AND H
C
          DRMF=(RM(JP)+RM(J))/DYF(I,J)*.5
          DRMB=(RM(J)+RM(JM1))/DYB(I,J)*.5
          CON=ETAX(I,J)*U(I,J) + V(I,J)/DY(I,J)
          IF(CON.LT.0.0)THEN
            IF(J.EQ.JMM1) THEN
            CIJ2=-1.0
            CJM1=-1.0
            CJM2=0.0
            ELSE
            CIJ2=-1.5
            CJM1=-2.0
            CJM2= .5
            ENDIF
            DRM1=DRMF
            DRM2=DRMB
            J1=JP
            J2=J+2
            J3=JM1
          ELSE
          IF(J.EQ.2)THEN
            CIJ2=1.
            CJM1=1.
            CJM2=0.
          ELSE
            CIJ2=1.5
            CJM1=2.0
            CJM2=-.5
          ENDIF
          DRM1=DRMB
          DRM2=DRMF
          J1=JM1
          J2=JM2
          J3=JP
          ENDIF
C       SOLVE FOR U VELOCITY
          CIJ=1. + CIJ1*DT/DX(I)*U(I,J) + CIJ2*DT*CON
```

```
     &        + DT*DYRE(I,J)*(DRMF+DRMB)
              CONJ1=CJM1*DT*CON + DT*DYRE(I,J)*DRM1
              CONJ2=CJM2*DT*CON
              CONIM=DT/DX(I)*U(I,J)
              CONVS=DT*DYRE(I,J)*DRM2
              US=(UMM1(I,J) + CIM1*CONIM*UIM1(J) + CIM2*CONIM*UIM2(J) +
     &           CONJ1*U(I,J1) + CONJ2*U(I,J2) + CONVS*U(I,J3))/CIJ
              U(I,J)=WOPT*US + (1.-WOPT)*U(I,J)
C         SOLVE FOR ENTHALPY
              CON=ETAX(I,J)*U(I,J) + V(I,J)/DY(I,J)
              IF(CON LT 0.0)THEN
                IF(J EQ JMM1) THEN
                CIJ2=-1.0
                CJM1=-1.0
                CJM2=0.0
                ELSE
                CIJ2=-1.5
                CJM1=-2.0
                CJM2=.5
                ENDIF
                DRM1=DRMF
                DRM2=DRMB
                J1=JP
                J2=J+2
                J3=JM1
              ELSE
              IF(J EQ.2)THEN
                CIJ2=1
                CJM1=1
                CJM2=0
              ELSE
                CIJ2=1.5
                CJM1=2.0
                CJM2=-.5
              ENDIF
              DRM1=DRMB
              DRM2=DRMF
              J1=JM1
              J2=JM2
              J3=JP
              ENDIF
              CIJ=1.  + CIJ1*DT/DX(I)*U(I,J) + CIJ2*DT*CON
     &           + DT*DYRE(I,J)*(DRMF+DRMB)/PR
              CONJ1=CJM1*DT*CON + DT*DYRE(I,J)*DRM1/PR
              CONJ2=CJM2*DT*CON
              CONIM=DT/DX(I)*U(I,J)
              CONVS=DT*DYRE(I,J)*DRM2/PR
              TCON=DYRE(I,J)*DT*((PR-1.)/PR)*.5
              HS=(HMM1(I,J) + CIM1*CONIM*HIM1(J) + CIM2*CONIM*HIM2(J) +
     &           CONJ1*H(I,J1) + CONJ2*H(I,J2) + CONVS*H(I,J3) +
     &           DPDT/RHO(J)+TCON*(DRMF*U(I,JP)**2-(DRMF+DRMB)*U(I,J)**2+
     &           DRMB*U(I,JM1)**2))/CIJ
              H(I,J)=WOPT*HS + (1.-WOPT)*H(I,J)
C
C         COMPUTE THE ERROR
C
              EU=ABS(U(I,J)-UOLD)
              EH=ABS(H(I,J)-HOLD)
              IF(EU.GE.EUMAX)EUMAX=EU
              IF(EH.GE.EHMAX)EHMAX=EH
            IF(EUMAX.GE.EMAX)EMAX=EUMAX
            IF(EHMAX.GE.EMAX)EMAX=EHMAX
C
C         END J LOOP
200       CONTINUE
```

```
C     CALCULATE V VELOCITY
      DO 250 J=2,JMM1
        JM1=J-1
        VOLD=V(I,J)
        D1=DY(I,J)/DX(I)
        D2=DYX(I,J)/DX(I)
        VCNIJ=CVIJ*D1 + D2
        VCNJ1=CVIJ*D1 - D2
        V(I,J)=V(I,JM1) + VCNIJ*U(I,J) + CVIM1*D1*UIM1(J) +
     &          CVIM2*D1*UIM2(J) + VCNJ1*U(I,JM1) + CVIM1*D1*UIM1(JM1)
     &          + CVIM2*D1*UIM2(JM1)
        EV=ABS(V(I,J)-VOLD)
        IF(EV.GE.EVMAX)EVMAX=EV
      IF(EVMAX.GE.EMAX)EMAX=EVMAX
250   CONTINUE
C
C     CHECK CONVERGENCE
C
        IF(EMAX.LE.EPS) GO TO 420
C       IF(K.EQ.KT)THEN
C         WRITE(10,6)
C       ENDIF
      DO 275 J=1,JMAX
        U(1,J)=U(2,J)
        H(1,J)=H(2,J)
        V(1,J)=V(2,J)
275   CONTINUE
C
C     END ITERATION LOOP
300   CONTINUE
420   CONTINUE
      DO 435 J=2,JMM1
      DEL=ABS(U(I,J) - UNM1(I,J))
      IF(DEL.GT.DELM)DELM=DEL
      DEL=ABS(H(I,J) - HNM1(I,J))
      IF(DEL.GT.DELM)DELM=DEL
435   CONTINUE
C     MOVE THE RESULTS INTO THE OLD TIME LEVEL
C
        DO 430 J=1,JMAX
          UNM1(I,J)=U(I,J)
          HNM1(I,J)=H(I,J)
          VNM1(I,J)=V(I,J)
430   CONTINUE
C
C     CALCULATE THE HEAT RATE AT THE WALL
C
        FDELY=(-3.*Y(I,1) + 4.*Y(I,2) - Y(I,3))/2.
        MUW=2.32E-8*TW(I)**.5/(1.+220./(TW(I)*10.**(9./TW(I))))
C     CONDUCTIVITY IS EQUAL TO MUW*CP/PR=K
        Q(I)=MUW/PR*RHO(1)/FDELY*(-3.*T(1) + 4.*T(2) - T(3))/2.*
     &          UINF**2/L
        HC=Q(I)/(.9*TOINF - TW(I))
        HHREF(I)=HC/HREF*SQRT(X(I)*L)
C
C     END I LOOP
400   CONTINUE
C
C     WRITE(*,*)DELM,K,EUMAX,EVMAX,EHMAX
C     WRITE(10,*)DELM,K,EUMAX,EVMAX,EHMAX
C     WRITE OUT SOLUTION AT A TIME STEP
C
      IF(N.EQ.(N/CNT)*CNT)THEN
      REWIND 8
      WRITE(8)A,TW
```

```
        WRITE(10,11)N,TIME
        DO 440 I=1,IMAX
          WRITE(10,2)I,X(I)
          WRITE(10,3)
          DO 450 J=1,JMAX
            T(J)=H(I,J)-U(I,J)**2/2.
            TEMP=T(J)*UINF**2/CP
C           WRITE(10,4)J,Y(I,J),U(I,J),H(I,J),T(J),TEMP,V(I,J)
450       CONTINUE
          WRITE(10,5)Q(I),HHREF(I)
          TIMEP=TIME*L/UINF
          WRITE(9,7)TIMEP,ALPHA,X(I),HHREF(I),TW(I)
440     CONTINUE
      ENDIF
C     END TIME LOOP
500   CONTINUE
C
C     COMPUTE PHYSICAL Y VALUES
      DO 1001 J=1,JMAX
        YP(1,J)=0.0
      WRITE(11,8)X(1),Y(1,J),YP(1,J)
1001  CONTINUE
      DO 650 I=2,IMAX
        DO 460 J=1,JMAX
          T(J)=H(I,J) - U(I,J)**2/2
          RHO(J)=GGM1*PRESS/T(J)
460     CONTINUE
C
        YP(I,1)=0.0
        WRITE(11,8)X(I),Y(I,1),YP(I,1)
        DO 470 J=2,JMAX
      YP(I,J)=YP(I,J-1) + (1/RHO(J) + 1/RHO(J-1))/2*(Y(I,J)-Y(I,J-1))
          WRITE(11,8)X(I),Y(I,J),YP(I,J)
470     CONTINUE
650   CONTINUE
8     FORMAT(3(2X,E13.5))
C
C     THIS SECTION FIGURES OUT THE THEORETICAL NONISOTHERMAL VALUES
C     FOR H/HREF
C
      PRINT*,'HISO='
      READ*,HISO
      DO 1000 I=1,IMAX
        HT=HISO
        IF(I.GE.29)THEN
          IF(I EQ 29)THEN
            DO 1002 J=1,4
              XX=X(I)+ DX(I)/FLOAT(5)*FLOAT(J)
          PHI=((1.9*TOINF-TW1)-(1.-(.466667/XX)**.75)**(-1./3 )*
     &          (TW2-TW1))/(1.9*TOINF-TW2)
          HT=HISO*PHI
          WRITE(9,8)XX,HT
1002        CONTINUE
          ELSE
            XX=X(I)
          PHI=((1.9*TOINF-TW1)-(1.-(.466667/XX)**.75)**(-1./3.)*
     &          (TW2-TW1))/(1.9*TOINF-TW2)
          HT=HISO*PHI
          WRITE(9,8)X(I),HT
          ENDIF
          ELSE
          WRITE(9,9)X(I),HT
          ENDIF
1000  CONTINUE
      REWIND 8
```

```
      WRITE(8,1) TW
1     FORMAT(///,2X,'N=',I6,5X,'TIME=',F15.6,1X,'SEC')
2     FORMAT(//,2X,'I=',I6,5X,'X LOCATION=',F15.6)
3     FORMAT(/,4X,'J',5X,'Y LOC',5X,'U',5X,'H',5X,'T',5X,'TEMP(R)',/)
4     FORMAT(2X,I4,6(2X,F18.9))
5     FORMAT(/,2X,'HEAT RATE (Q)=',F15.6,5X,'H/HREF=',F15.6)
6     FORMAT(/,'THIS SOLUTION HAS NOT CONVERGED WITH KT ITERATIONS',/)
7     FORMAT(5(2X,F15.6))
9     FORMAT(34X,2(2X,F15.6))
600   CONTINUE
      CLOSE(8)
      CLOSE(10)
      CLOSE(12)
      STOP
      END
      SUBROUTINE FIRST(IMAX,JMAX,RE,CP,TW,TE,UE,UINF,PRESS,GGM1,
     &                 X,Y,U,V,H,PR)
C     THIS SUBROUTINE TAKES THE BLASIUS SOLUTION, MODIFIES IT BY
C     THE DENSITY, AND FORMS A GRID   IT ALSO DETERMINES INITIAL
C     CONDITIONS
      DIMENSION X(61),Y(61,30),DY(61),U(61,0:31),H(61,0:31),RHO(30)
      DIMENSION V(61,30),YN(30),YOLD(30),TW(61)
C     THIS IS A BLASIUS PROFILE OPTIMIZED FOR RE=2 E6   THIS MUST
C     BE MODIFIED FOR MY REYNOLD'S NUMBER   ALSO, I AM BASING THIS
C     GRID ON THE THERMAL BOUNDARY LAYER THICKNESS SO MODIFY Y WITH
C     THE PRANDTL NUMBER
      DATA YOLD/0., 000248, 0005, 000756, 001024, 001318, .00168,
     &          002, 002872, 003402, 004342, 005548, 007099,
     &          009092, 01165, 014945, 019174, 024609, 031593,
     &          040568, 0521, 06692, 085963, 11043, 14187, 18228,
     &          .23414, .30078, 3862, .496/
      DX=1./(IMAX-1.)
      DO 100 I=1,IMAX
        X(I)=DX*(I-1)
        DO 120 J=1,JMAX
          Y(I,J)=YOLD(J)*SQRT(2.E6)/SQRT(RE)*SQRT(X(I))/PR
120     CONTINUE
100   CONTINUE
      HE=CP*TE/UINF**2. + (UE/UINF)**2./2.
      DO 150 I=2,IMAX
        HW=CP*TW(I)/UINF**2
        HSUB=HE - HW
        DO 130 J=1,JMAX
          DELTA=5.2/SQRT(RE)*SQRT(X(I))
          DELTAT=DELTA/PR
          IF(Y(I,J) LE DELTA)THEN
            U(I,J)=UE/UINF*(1.5*Y(I,J)/DELTA - .5*(Y(I,J)/DELTA)**3 )
          ELSE
          U(I,J)=UE/UINF
          ENDIF
          V(I,J)=0.0
          IF(Y(I,J) LE DELTAT)THEN
            H(I,J)=HW + HSUB*(1.5*Y(I,J)/DELTAT -  5*(Y(I,J)/DELTAT)**3)
          ELSE
            H(I,J)=HE
          ENDIF
          TEMP=H(I,J) - U(I,J)**2 /2.
          RHO(J)=GGM1*PRESS/TEMP
130     CONTINUE
      DO 145 J=2,JMAX
        Y(I,J)=Y(I,J)*1.0
145   CONTINUE
150   CONTINUE
      DO 180 J=1,JMAX
        U(1,J)=U(2,J)
```

```
        V(1,J)=0.0
        H(1,J)=H(2,J)
160   CONTINUE
      RETURN
      END
      SUBROUTINE TERPO(ALPHA,UINF,RINF,CP,UE,PE,HE)
C
C     THIS SUBROUTINE INTERPOLATES TO GET VELOCITY,PRESSURE,TEMPERATURE,
C     AND ENTHALPY AT A NEW ANGLE
C
      DIMENSION EVEL(14),ETEMP(14),EPRESS(14)
      DATA EVEL/0.,4843.7962,4843.7962,4834.5371,4823.7297,4811.1933,
     &          4796.8408,4780.5741,4762.3358,4742.0933,4719.6052,
     &          4695.4522,4669.00,4639.60/
      DATA ETEMP/0.,65.62,65.62,73.08,81.78,91.84,103.33,116.30,130.80,
     &          146.83,164.39,183.49,204.12,227.99/
      DATA EPRESS/0.,1.3063,1.3063,1.7262,2.2334,2.8322,3.5250,4.3135,
     &            5.1985,6.1801,7.2581,8.4319,9.7010,11.060/
C
      IALPH=INT(ALPHA)
      UE=EVEL(IALPH) + (ALPHA-IALPH) * (EVEL(IALPH+1) - EVEL(IALPH))
      UE=UE/UINF
      TE=ETEMP(IALPH) + (ALPHA-IALPH) * (ETEMP(IALPH+1) - ETEMP(IALPH))
      HE=CP*TE/UINF**2 + UE**2/2
      PE=EPRESS(IALPH)+(ALPHA-IALPH)*(EPRESS(IALPH+1) - EPRESS(IALPH))
      PE=PE/(RINF*UINF**2)
      RETURN
      END
```

Bibliography

1. Anderson, D. A., J. C. Tannehill, and R. H. Plecher. Computational Fluid Mechanics and Heat Transfer, New York, McGraw-Hill Book Company, 1984.

2. Cappelano, P. T. Heat Transfer/Boundary Layer Investigation of Heating Discrepancies in Wind Tunnel Testing of Orbiter Insulating Articles, Masters Thesis, Air Force Institute of Technology, December 1982.

3. Cebecci, T. and A. M. O. Smith. Analysis of Turbulent Boundary Layers, New York, Academic Press, 1974.

4. Eckert, E. R. G. "Survey of Boundary Layer Heat Transfer at High Velocities and High Temperatures", WADC Technical Report 59-624, WADC, April 1960.

5. Fiore, A. W. "Viscosity of Air," Journal of Spacecraft and Rockets, 3 (5): 756-758 (May 1966).

6. Hodge, J. K. "Implicit Methods for Model Equations", Notes.

7. Hodge, J. K., Y. K. Woo, and P. T. Cappelano. "Parameter Estimation for Imbedded Thermocouples in Space Shuttle Wind Tunnel Test Articles with a Nonisothermal Wall," AIAA 83-1533, June 1983.

8. Kays, W. M. and M. E. Crawford. Convective Heat and Mass Transfer, New. York, McGraw-Hill Book Company, 1980.

9. Kim, J. S. and K. S. Chang. "Calculation of Incompressible and Compressible Unsteady Boundary Layers by a Noniterative Finite Difference Method," AIAA 84-1639, June 1984.

10. Kuethe, A. M. and C. Y. Chow. Foundations of Aerodynamics, New York, John Wiley and Sons, 1976.

11. Liepmann, H. W. and A. Rosko. Elements of Gasdynamics, New York, John Wiley and Sons, 1957.

12. Nagumatsu, H. T. and R. E. Sheer, Jr. "Hypersonic Shock Wave Boundary Layer Interaction and Leading Edge Slip," ARS Journal, pp 454-462, May 1960.

13. Schlichting, H. Boundary-Layer Theory, New York, McGraw-Hill Book Company, 1979.

VITA

Karen J. Lange was born on 1 August 1956 in Minot, North Dakota. She graduated from Bartlett High School, Anchorage, Alaska in 1974 and attended the University of Alaska for two years. In 1976, she entered the United States Air Force Academy, graduating with Bachelor of Science degrees in Aeronautical Engineering and Mathematics in May 1980. Upon graduation, she was assigned to the Air Force Weapons Laboratory at Kirtland AFB, Albuquerque, New Mexico. She worked as an aeronautical engineer in the Chemical Laser Branch until June 1983 when she entered the School of Engineering at the Air Force Institute of Technology.

Permanent address: Box 5, Twenty Grand Rd
Eagle River, Alaska 99577

UNCLASSIFIED
SECURITY CLASSIFICATION OF THIS PAGE

AD-A164105

REPORT DOCUMENTATION PAGE

1a. REPORT SECURITY CLASSIFICATION: UNCLASSIFIED	1b. RESTRICTIVE MARKINGS
2a. SECURITY CLASSIFICATION AUTHORITY	3. DISTRIBUTION/AVAILABILITY OF REPORT: Approved for public release; distribution unlimited.
2b. DECLASSIFICATION/DOWNGRADING SCHEDULE	
4. PERFORMING ORGANIZATION REPORT NUMBER(S): AFIT/GAE/ENY/84D-11	5. MONITORING ORGANIZATION REPORT NUMBER(S)
6a. NAME OF PERFORMING ORGANIZATION: School of Engineering; 6b. OFFICE SYMBOL (If applicable): AFIT/ENY	7a. NAME OF MONITORING ORGANIZATION
6c. ADDRESS (City, State and ZIP Code): Air Force Institute of Technology, Wright-Patterson AFB, OH 45433	7b. ADDRESS (City, State and ZIP Code)
8a. NAME OF FUNDING/SPONSORING ORGANIZATION; 8b. OFFICE SYMBOL (If applicable)	9. PROCUREMENT INSTRUMENT IDENTIFICATION NUMBER
8c. ADDRESS (City, State and ZIP Code)	10. SOURCE OF FUNDING NOS. — PROGRAM ELEMENT NO. / PROJECT NO. / TASK NO. / WORK UNIT NO.
11. TITLE (Include Security Classification): See Box 19	
12. PERSONAL AUTHOR(S): KAREN J. LANGE, B.S., CAPT, USAF	
13a. TYPE OF REPORT: M.S. THESIS; 13b. TIME COVERED: FROM _____ TO _____; 14. DATE OF REPORT (Yr., Mo., Day): 1985 June; 15. PAGE COUNT: 110	
16. SUPPLEMENTARY NOTATION	
17. COSATI CODES — FIELD / GROUP / SUB. GR.	18. SUBJECT TERMS (Continue on reverse if necessary and identify by block number)

19. ABSTRACT (Continue on reverse if necessary and identify by block number)

Approved for public release: IAW AFR 190-1.
LYNN E. WOLAVER 16 JAN 86
Dean for Research and Professional Development
Air Force Institute of Technology (AFC)
Wright-Patterson AFB OH 45433

20. DISTRIBUTION/AVAILABILITY OF ABSTRACT: UNCLASSIFIED/UNLIMITED ☒ SAME AS RPT. ☐ DTIC USERS ☐	21. ABSTRACT SECURITY CLASSIFICATION: UNCLASSIFIED
22a. NAME OF RESPONSIBLE INDIVIDUAL: James K. Hodge, Major, USAF	22b. TELEPHONE NUMBER (Include Area Code): 513-255-3517; 22c. OFFICE SYMBOL: AFIT/ENY

DD FORM 1473, 83 APR — EDITION OF 1 JAN 73 IS OBSOLETE.

UNCLASSIFIED
SECURITY CLASSIFICATION OF THIS PAGE

Wind tunnel tests were conducted on Space Shuttle Orbiter insulating articles. The data was processed by a heat estimation program, revealing a large discrepancy in magnitude of the heat transfer coefficient over the Space Shuttle tile when compared to that yielded by flat plate theory and thin skin test results. An initial suggestion for the cause of this discrepancy was the nonisothermal wall effect. Understanding this effect was the main objective of this project.

In order to investigate these effects, an unsteady compressible boundary layer code, THESIS, was developed. First the boundary layer equations were transformed using the Dorodnitsyn transformation to allow the equations to be solved similar to incompressible equations. Then, the equations were then transformed to the computational plane and approximated by finite differences. Optimized successive over-relaxation is then used to solve the difference equations. The grid used for this program is optimized based on the Blasius solution, but the program is not limited to this because it has a generalized grid.

Upon running this program, leading edge startup problems arose. Therefore, a similarity solution is assumed at the leading edge which corrected the problem.

The program was verified with an incompressible case which was in good agreement with the Blasius solution, and a compressible case with an isothermal wall which agreed well with approximate theory. The isothermal case showed the solution was dependent on the grid. The steady state and transient nonisothermal wall cases displayed the same trend as the approximate nonisothermal solution. All cases had the same dramatic decrease in the heat transfer coefficient and the subsequent recovery in the streamwise direction. The most significant results came from pitching the plate with a nonisothermal wall. A large lag due to the nonisothermal wall effects exists. These results indicate that the nonisothermal wall effects may be affecting the wind tunnel results.

END

FILMED

3-86

DTIC